MECHANISTIC AND SPECTROSCOPIC INVESTIGATIONS OF PYRUVATE FORMATE-LYASE ACTIVATING ENZYME

by

Rachel Ann Udelhoven Hutcheson

A dissertation submitted in partial fulfillment
of the requirements for the degree

of

Doctor of Philosophy

in

Biochemistry

MONTANA STATE UNIVERSITY
Bozeman, Montana

November 2012

APPROVAL

of a dissertation submitted by

Rachel Ann Udelhoven Hutcheson

This dissertation has been read by each member of the dissertation committee and has been found to be satisfactory regarding content, English usage, format, citation, bibliographic style, and consistency and is ready for submission to The Graduate School.

Dr. Joan B. Broderick

Approved for the Department of Chemistry and Biochemistry

Dr. Mary J. Cloninger

Approved for The Graduate School

Dr. Ronald W. Larsen

STATEMENT OF PERMISSION TO USE

In presenting this dissertation in partial fulfillment of the requirements for a doctoral degree at Montana State University, I agree that the Library shall make it available to borrowers under rules of the Library. I further agree that copying of this dissertation is allowable only for scholarly purposes, consistent with "fair use" as prescribed in the U.S. Copyright Law. Requests for extensive copying or reproduction of this dissertation should be referred to ProQuest Information and Learning, 300 North Zeeb Road, Ann Arbor, Michigan 48106, to whom I have granted "the exclusive right to reproduce and distribute my dissertation in and from microform along with the non-exclusive right to reproduce and distribute my abstract in any format in whole or in part."

Rachel Ann Udelhoven Hutcheson

November 2012

DEDICATION

For my family and friends who have always given me unconditional love and support.

ACKNOWLEDGEMENTS

My utmost respect and gratitude go to my advisor, Dr. Joan Broderick, who has been a constant source of inspiration throughout my experiences here at Montana State University. Thank you for your valuable insight and wisdom that you were always willing to impart and your encouragement that kept me going. Thanks also go to my graduate committee for their efforts, advice, and guidance, Dr. Robert Szilagyi, Dr. John Peters, Dr. Brian Bothner, Dr. Martin Teintze, and Dr. Christa Merzdorf. I would like to additionally thank our collaborators Dr. J. Timothy Sage, Masaki Horitani, George Cutsail III, and Dr. Brian Hoffman. To the members of the Broderick group past and present, thank you for training me in the ways of anaerobic techniques, being an extra pair of helping hands when needed, and listening to all of my ideas be they crazy or not.

Life-long friends can be few and far in between, but thank you Emily, Heidi, Kaitlin, and Cassandra for being people that I can rely on, trust, and confide in. And last, but definitely not least, thank you to my family who has always been there to encourage me to push through the hard times, give exaltations during the good, and remind me to always believe in myself. Your love has been a true blessing. Mom, Dad, Adrienne, Amber, and Brandon you let me find my own way while still being there to give advice or a helping hand when I struggled. Kirk and Mary, Suzanne and Scott, Grandma Clara, Lisa, Sierra, and Aaron, you have become my family and made me one of your own. And thank you especially to my husband, Ryan, and son, Connor, for sticking with me and reminding me that life should be fun and full of messiness. Thank you all for helping me achieve my goals; you will always be remembered and appreciated!

TABLE OF CONTENTS

TABLE OF CONTENTS – CONTINUED

TABLE OF CONTENTS – CONTINUED

TABLE OF CONTENTS – CONTINUED

LIST OF TABLES

LIST OF FIGURES

LIST OF FIGURES – CONTINUED

LIST OF FIGURES – CONTINUED

LIST OF SCHEMES

LIST OF ABBREVIATIONS

AdoMet: *S*-adenosyl-L-methionine
aRNR: anaerobic ribonucleotide reductase
aRNR-AE: anaerobic ribonucleotide reductase activating enzyme
BioB: biotin synthase
dAdo: 5'-deoxyadenosine or 5'-deoxyadenosyl
DFT: density functional theory
ENDOR: electron nuclear double resonance
EPR: electron paramagnetic resonance
Fe-S cluster: iron-sulfur cluster
LAM: lysine 2,3-aminomutase
LipA: lipoate synthase
MTase: methyltransferase
MTTase: methylthiotransferase
NRVS: nuclear resonance vibrational spectroscopy
PFL: pyruvate formate-lyase
PFL-AE: pyruvate formate-lyase activating enzyme
RFQ: rapid freeze quench
SAM- *S*-adenosyl-L-methionine
SPL: spore photoproduct lyase
TIM: triosephosphate isomerase
XAS: X-ray absorption spectroscopy

ABSTRACT

Radical *S*-adenosylmethionine (SAM) enzymes are a large and rapidly growing superfamily composed of thousands of members catalyzing a wide diversity of reactions by utilizing a reduced $[4Fe\text{-}4S]^{1+}$ cluster and SAM to create a 5'-deoxyadenosyl radical capable of initiating controlled radical chemistry in important and difficult biochemical reactions. The prevalence of radical SAM enzymes in all kingdoms of life underscores the central role played by these enzymes. For the vast majority of putative radical SAM enzymes little is known regarding the reaction catalyzed or the mechanism of catalysis. Nevertheless, it is possible to gain insight into these enzymes from the radical SAM enzyme pyruvate formate-lyase activating enzyme (PFL-AE), which catalyzes the formation of a catalytically essential glycyl (G734) radical of pyruvate formate-lyase (PFL). The studies presented herein provide further understanding and characterization of PFL-AE as well as other radical SAM enzymes. The relevance and effect of the monovalent cation found in the active site of PFL-AE upon further analysis of the crystal structure was probed using coupled enzyme activity assays. Five different monovalent cations, Na^+, K^+, NH_4^+, Rb^+, and Cs^+, were investigated by calculating the specific activity of PFL-AE in the presence of each. PFL-AE was active in the presence of all tested cations, with specific activities correlating with cation size. Nuclear resonance vibrational spectroscopy performed on PFL-AE with an ^{57}Fe labeled cluster showed a enzyme stiffening around the cluster and elongation of Fe-S bonds upon substrate and substrate analog binding. Rapid freeze-quench was used to mix PFL-AE with PFL and SAM on a millisecond time scale. The resulting samples were analyzed by electron paramagnetic resonance, which revealed a newly observed radical intermediate. To attempt characterization of this radical intermediate, electron nuclear double resonance spectroscopy (ENDOR) was used with site-specifically labeled SAM. The ENDOR signal detected was too weak to be analyzed; however, other labeled SAM molecules will be used in the future. To help further expand knowledge of radical SAM enzymes, an initial characterization of a putative methylthiotransferase (a subclass of the radical SAM superfamily) was undertaken. Results indicated that the enzyme methylthiolated a ribosomal small protein and not tRNA.

CHAPTER 1

INTRODUCTION

Fe-S Clusters in Biology

Iron is the fourth most abundant element in the earth's crust [1], and as such it should come as no surprise that biology has incorporated it into proteins as iron-sulfur (Fe-S) clusters for a variety of functions including critical processes such as photosynthesis and respiration [2, 3]. Iron-sulfur clusters are ubiquitous in biology, however they remained undiscovered until the 1960s at which point they became well known for their roles in electron transfer, an understandable role resulting from at least two redox states that under normal biological conditions are readily accessible [4]. However, other functions that have broadened our understanding of the diverse nature of these clusters have surfaced, *vide infra*.

Cluster Forms

The major forms of Fe-S clusters in biology are [2Fe-2S], [3Fe-4S], and [4Fe-4S] (Figure 1.1). As there exists a preference for thiolate ligation of Fe-S clusters, proteins usually employ cysteinyl sulfurs to complete the tetrahedral coordination of each iron in the cluster. However, histidine, aspartate, serine, or backbone amide ligation at one of the Fe sites is occasionally found in clusters involved in electron transfer, and they are thought to be involved in modifying redox potential [5], gating electron transport [6], or coupling proton and electron transport [7].

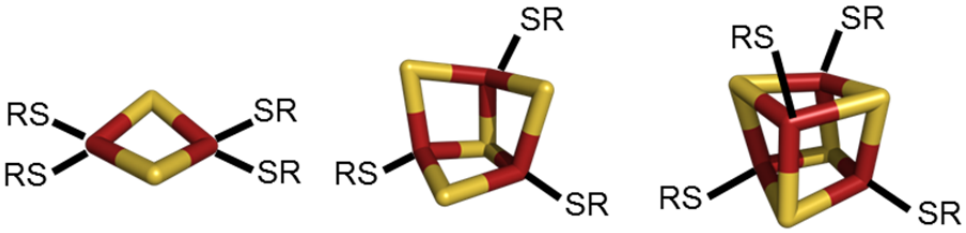

Figure 1.1. Major Fe-S cluster forms found in biology. The [2Fe-2S] cluster (left) is present in certain ferredoxins (others contain a [4Fe-4S] cluster) and Rieske proteins, while the [3Fe-4S] cluster (center) is less common and can be found in arsenite oxidase. [4Fe-4S] clusters (right) are located in high-potential iron proteins (HiPIP) as well as aconitase and members of the radical SAM superfamily (although one Fe remains uncoordinated by the protein).

While the simple Fe-S clusters are the most prevalent, more complex metallo-cofactors exist that function in enzymes such as Mo-nitrogenase (M-cluster) and [FeFe]-hydrogenase (H-cluster) (Figure 1.2), and not only are the structures of the clusters unique, but the ligation is as well requiring maturation enzymes catalyzing distinct transformations [8, 9]. The M-cluster consists of a Mo-7Fe-9S cluster and can be viewed as $[MoFe_3S_4]$ and $[Fe_4S_3]$ subclusters bridged by three sulfides as well as the recently identified carbide at the center of the metal-sulfur core [10]. It is coordinated to the MoFe protein through one cysteine thiolate ligand at a terminal Fe and a histidine imidazole at the Mo, and also contains the non-protein ligand homocitrate attached to the Mo. The H-cluster is more easily envisioned as a [4Fe-4S] cluster bound to the protein through four cysteine thiolates, while one of those cysteines bridges it to a 2Fe subcluster. Besides the contact with one cysteine, the 2Fe subcluster contains no other protein ligands, and the irons exist in hexacoordinated environments with two cyanides, three

carbon monoxides, and a five membered dithiolate ligand (although the identity of the bridgehead atom still remains unresolved).

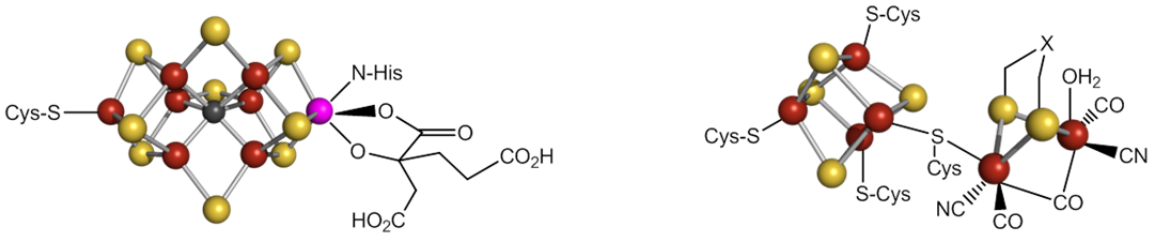

Figure 1.2. The M-cluster of Mo-nitrogenase (left) with Fe shown in red, S in yellow, Mo in green, and C in dark gray. The cluster is ligates to the protein by one Cys and one His residue, and is also coordinated in a bidentate fashion by homocitrate. The H-cluster of [FeFe]-hydrogenase consists of a [4Fe-4S] (Fe shown in red and S in yellow) ligated to the protein by four Cys residues, one of which connects it to the 2Fe subcluster. The 2Fe subcluster's unique ligation environment consists of two cyanide and three carbon monoxide molecules as well as a dithiolate linker whose bridgehead atom identity is unknown. Figure is from [9].

Cluster Functions

As stated earlier the first recognized and most familiar function of Fe-S clusters is electron transfer and these types of clusters can be found in ferredoxins, photosystem I, and three of the protein complexes, I, II, and III, in the mitochondria electron-transfer chain. The flexibility of Fe-S cluster electron transfer stems from the delocalization of the electron density over the Fe atoms of the cluster [2] as well as proteins modulating the reduction potentials of the cluster through changes in cluster ligation and the protein environment [2, 5, 11]. Remarkably, the range of reduction potentials for Fe-S clusters afforded by these changes spans from approximately -700 to +400 mV [2, 11].

While this wide range makes Fe-S clusters ideal electron transfer agents, they can also provide structural stability to enzymes as appears to be the case in endonuclease III

[12] and MutY[13]. In both of these enzymes the Fe-S cluster stabilizes a fold involved in positioning of positively charged residues for DNA binding [13, 14]. Other Fe-S cluster containing proteins regulate gene expression by turning genes on and off in response to certain stimuli. FNR is a global regulator controlling the expression of more than 100 genes in response to oxygen [15, 16]. Under anaerobic conditions FNR contains a $[4Fe\text{-}4S]^{2+}$ cluster and is capable of DNA binding, but upon exposure to oxygen, the cluster is degraded to a $[2Fe\text{-}2S]^{2+}$ cluster and is no longer capable of binding DNA [17, 18]. SoxR, the first Fe-S cluster containing transcription factor identified, requires a [2Fe-2S] cluster in order to sense superoxide and NO stress [19, 20]. Two other regulators, IscR and IRP, are involved in sensing iron and Fe-S clusters. IscR regulates the Isc Fe-S cluster assembly proteins by repressing the *isc* operon, and is active when Fe-S cluster assembly is not needed [21]. The iron-responsive protein (IRP) regulates the expression of ferritin (an iron storage protein) and transferrin (responsible for iron transport and its mRNA is easily degraded). The IRP is capable of coordinating a [4Fe-4S] or [3Fe-4S] cluster produced by Fe-S cluster biosynthesis machinery, although the presence of a cluster inhibits its ability to bind mRNA [22]. Under high iron conditions IRP contains an Fe-S cluster, and as a result no mRNA is bound allowing for the transcription of ferritin, needed to store the excess iron, and transferrin mRNA is degraded preventing the import of more iron into the cell [22-24]. However, in iron limiting conditions, the IRP no longer contains a cluster and binds the 5' end of ferritin mRNA preventing transcription and thus storage of iron needing to be accessible [22-24].

Alternatively, the binding of IRP to the 3' end of transferrin mRNA stabilizes it allowing for increased production and import of iron [22-24].

Interestingly a related protein to IRP, aconitase a [4Fe-4S] containing enzyme, has a function involved in substrate binding and catalysis in the mitochondria as part of the citric acid cycle. Although not its major function, IRP containing a [4Fe-4S] cluster also has aconitase activity [24]. Aconitase, which catalyzes the isomerization of citrate and isocitrate, can bind both citrate and isocitrate at a unique Fe of its cluster that is not ligated by a cysteine [25]; upon substrate binding the cluster catalyzes the reaction by acting as a Lewis acid. Enzymes belonging to the radical *S*-adenosylmethionine (SAM) superfamily also utilize a [4Fe-4S] cluster for substrate binding and catalysis. Similar to aconitase, radical SAM enzymes contain a site-differentiated cluster that they use to bind SAM. This family of enzymes functions to activate C-H bonds through H atom abstraction and catalyzes diverse and otherwise difficult reactions.

Radical SAM Enzymes

Studies performed on lysine 2,3-aminomutase (LAM),which catalyzes the interconversion of L-lysine and L-β-lysine, biotin synthase (BioB), which catalyzes the biosynthesis of biotin from dethiobiotin, and pyruvate formate-lyase activating enzyme (PFL-AE) and anaerobic ribonucleotide reductase activating enzyme (aRNR-AE), which both activate their substrates (PFL and aRNR respectively) through the generation of a glycyl radical, revealed a common requirement for a [4Fe-4S] cluster and SAM. It was also postulated that these enzymes utilized these common elements in the creation of a

putative highly reactive 5'-deoxyadenosyl radical intermediate, which functions to initiate catalysis by abstraction of a substrate hydrogen atom. Other probable enzymes utilizing the same chemistry were identified based on similarities in sequences, especially in the Fe-S cluster binding region, and in some cases the reactions catalyzed [26].

A bioinformatics analysis of these proteins led to the identification of hundreds of enzymes that were also likely to employ a [4Fe-4S] cluster and SAM in the initiation of their reactions and termed the radical SAM superfamily [27]. While this study added many new enzymes and a diverse set of reactions to the family, new radical SAM enzymes are currently emerging at a rapid pace, and the superfamily is now thought to consist of thousands instead of hundreds of enzymes.

Radical SAM Superfamily Characteristics

As previously mentioned, radical SAM enzymes were noted to contain a common cysteine motif, CX_3CX_2C, whose thiolates function to coordinate three irons of a [4Fe-4S] cluster; the cysteines in this motif are absolutely conserved and occur at the N-terminal end of the radical SAM domain. Although this remains the case for the majority of radical SAM enzymes, variations have been noted. ThiC, which catalyzes the conversion of 5-aminoimidazole ribonucleotide to 4-amino-5-hydroxymethyl-2-methyl-pyrimidine phosphate (HMP-P), includes a CX_2CX_4C motif at the C-terminal end of the enzyme [28]. Elp3 (a component of the elongator complex), although not a confirmed radical SAM enzyme, does appear to bind small quantities of iron, approximately 1.3 Fe atoms per protein, and SAM [29]. The cysteine motif in archael Elp3 is CX_4CX_2C [29].

Finally, HmdB, which appears to be involved in the synthesis of the Hmd cofactor of HmdA, contains a CX_5CX_2C motif [30].

Other sequence motifs shared by members of the radical SAM superfamily include two used in SAM binding. The glycine-rich GGE motif is thought to be important in the correct conformation of the loop directly after the β_2 strand; a specific orientation is needed for hydrogen bonding with the nitrogen atom of the methionine moiety of SAM [31]. The second is a $GXIXGX_2E$ motif involved in interactions with the adenosine portion of SAM. The isoleucine, or other large hydrophobic residue, is appropriate for stacking with the adenine moiety, and the following glycine and glutamate (or aspartate) appear to be important in maintaining the structure of the SAM binding site through interactions between the glutamate and a backbone nitrogen of the glycine [31].

A vital commonality among the radical SAM enzymes is the presence of an oxygen sensitive and labile [4Fe-4S] cluster ligated by the cysteine triad motif discussed above. This motif suggested the presence of a site-differentiated cluster similar to aconitase in which one of the iron sites remains uncoordinated by a cysteinyl sulfur. Also like aconitase, it was determined that the unique iron was able to bind its co-substrate, SAM (Figure 1.3). One of the early indications that this was the case came from striking changes in the electron paramagnetic resonance (EPR) signal of the $[4Fe\text{-}4S]^{1+}$ cluster (whose role in catalysis is described below), with the addition of SAM [32, 33]. The nature of the interaction between SAM and the cluster was eventually confirmed with PFL-AE through the use of electron-nuclear double resonance (ENDOR) with site-

specifically labeled SAM molecules [33, 34] and Mössbauer spectroscopy with only the unique iron labeled with ^{57}Fe [35]. The SAM was found to coordinate the unique iron through its carboxy and amino moieties with the cluster aiding in anchoring and positioning it for catalysis (Figure 1.3) [34]. However, the ligand in the absence of SAM is still unknown.

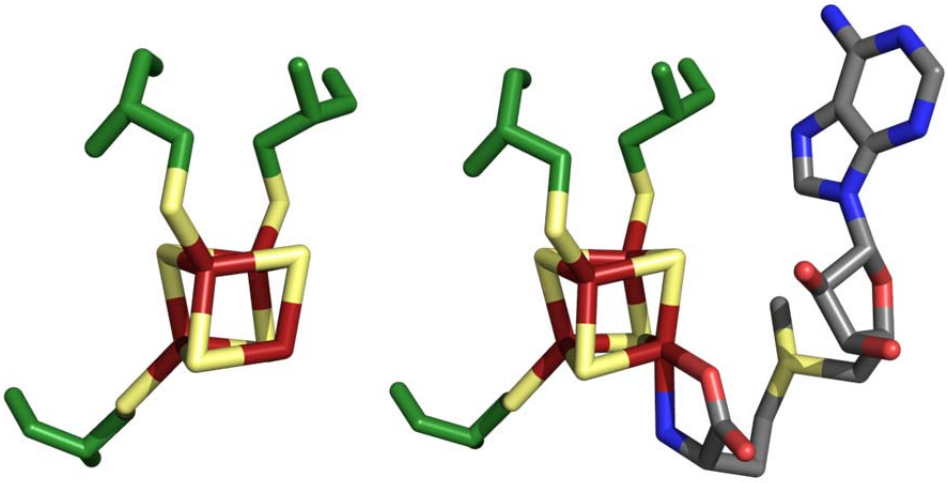

Figure 1.3. A site-differentiated [4Fe-4S] (Fe shown in dark red and S in yellow) cluster shown without substrate bound (left) or with SAM (shown in gray) bound to the unique iron of the cluster (right) by the carboxy and amino moieties. The three cysteinyl sulfur ligands from the protein are shown in green. Structures were built from PFL-AE (PDB ID 3CB8) [36].

More recently, as multiple structures for radical SAM enzymes have become available, a structural commonality among the superfamily has been exposed. The radical SAM superfamily shares a conserved core domain consisting of a triosephosphate isomerase (TIM) barrel, which in the majority of cases is a partial $(\alpha/\beta)_6$ barrel but can also consist of a full $(\alpha/\beta)_8$ barrel [37, 38]. The variance in completeness as well as the openness of the barrel is directly related to the substrate size with the less complete and more open barrels present in the enzymes acting upon larger substrates (Figure 1.4). The

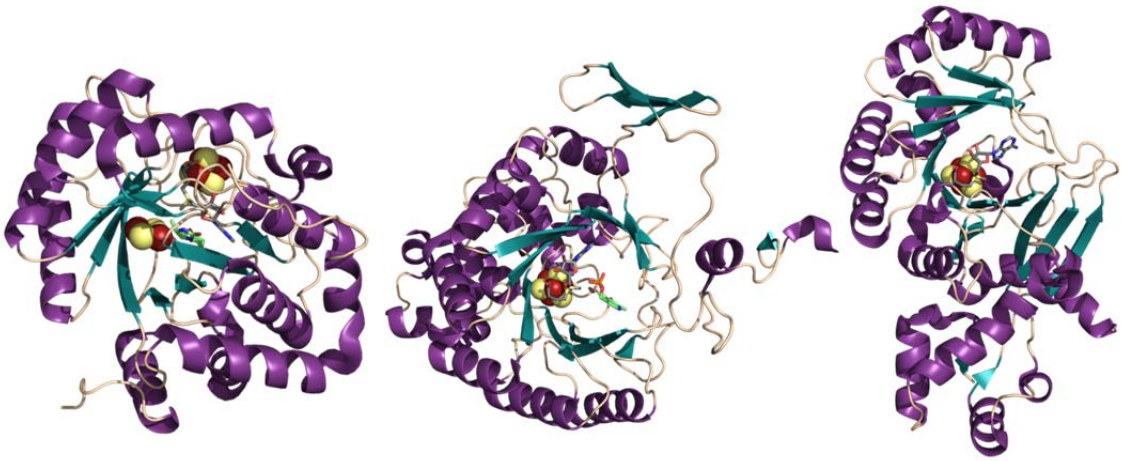

Figure 1.4. Crystal structures of three radical SAM enzymes. Left: BioB (PDB ID 1R30) [39] catalyzes the conversion of dethiobiotin to biotin through sulfur insertion. BioB contains a full, closed TIM barrel. Center: LAM (PDB ID 2A5H) [40] catalyzes the interconversion of L-lysine to L-β-lysine and contains a partial and more open TIM barrel. Right: RlmN (PDB ID 3RFA) [41] modifies A2503 in 23S rRNA by adding a methylating C2. RlmN has a very open, partial TIM barrel.

[4Fe-4S] cluster is located within the barrel on the loop containing the CX_3CX_2C motif at one end of the barrel with the unique iron positioned toward the center of the barrel facing the active site opening. In all of the structures with SAM bound, the unique iron is bound by SAM through the carboxy and amino moieties confirming the coordination determined previously by ENDOR with PFL-AE. This coordination aids in the protection of the oxygen sensitive, labile cluster by shielding it from solvent exposure. SAM is also held in position by a series of conserved residues as mentioned previously. The interactions between the residues and SAM include electrostatic, H-bonding, hydrophobic, as well as π-stacking interactions. Besides SAM binding, the opening of the barrel, which provides the substrate access to the active site, can be closed off by other protein elements, the substrate, or a combination of both, which allows the radical chemistry that occurs to be contained preventing deleterious side reactions from taking

place due to the reactive nature of the intermediate species. To aid in the accomplishment of this, radical SAM enzyme substrates bind in the lateral opining of the TIM barrel, and this binding not only helps to seal the opening, but it also positions the hydrogen atom to be abstracted in close proximity to the 5'-C of SAM; for structures with substrate bound the distance between the 5'-C and hydrogen abstracted is approximately 3.8 to 4.1 Å [38].

Mechanistic Commonalities

Radical SAM enzymes utilize their [4Fe-4S] cluster bound by a cysteine triad motif for catalysis, and this cluster can transition between an oxidized +2 state, which is diamagnetic and EPR silent, and a reduced +1 state, which is paramagnetic and EPR active. Initial evidence for the $[4Fe\text{-}4S]^{1+}$ cluster as the catalytically active state came from aRNR-AE, LAM, and PFL-AE. For aRNR-AE in the absence of its substrate aRNR, the $[4Fe\text{-}4S]^{1+}$ cluster was shown to interact with SAM and generate methionine (one of the cleavage products of SAM) along with oxidation of the cluster to the 2+ state [42]. Additionally, enzyme assays of LAM combined with EPR spectroscopy showed that in the presence of SAM the $[4Fe\text{-}4S]^{1+}$ LAM cluster was catalytically active [43]. However, the most direct evidence came when PFL-AE was photoreduced with 5-deazariboflavin to the $[4Fe\text{-}4S]^{1+}$ state with SAM (PFL-AE has an unappreciable cleavage rate of SAM in the absence of its substrate, PFL) and monitored by EPR spectroscopy, which showed an increasing amount of 1+ cluster with increasing times of photoreduction [44]. In corresponding samples to which PFL was added, the EPR spectra showed an increasing amount of glycyl radical with increasing reduction times;

spin quantitation of the EPR signals showed a 1:1 stoichiometry of $[4Fe\text{-}4S]^{1+}$ cluster formed to glycyl radical produced [44]. Further, the loss of the $[4Fe\text{-}4S]^{1+}$ cluster signal indicated it was oxidized to the 2+ state, and it was proposed that the reduced cluster provided the electron required for SAM cleavage to generate methionine and the 5'-deoxyadenosyl (dAdo) radical intermediate [44].

The 5'-dexoyadenosyl radical has not been directly observed as it is highly reactive. An allylically stabilized dAdo radical analog, however, has been detected when LAM was assayed with the SAM analog *S*-3', 4'-anhydroadenosylmethionine (anSAM) [45, 46]. Further experimental evidence observed in several radical SAM enzymes for the participation of the dAdo radical includes the stoichiometric production of deoxyadenosine and methionine from SAM cleavage and the transfer of a substrate based label to deoxyadenosine [47-58].

The currently accepted mechanistic model for radical SAM enzyme catalysis resulting from these observations is shown in Scheme 1.1. In the first step the $[4Fe\text{-}4S]^{2+}$ cluster is bound at the site-differentiated iron by the amino and carboxy moieties of SAM [34]. The $[4Fe\text{-}4S]^{2+}$ cluster then undergoes a single electron reduction to the $[4Fe\text{-}4S]^{1+}$ catalytically active state [44]; in many cases it is thought that flavodoxin acts as the natural reductant *in vivo*. The $[4Fe\text{-}4S]^{1+}$ cluster reductively cleaves the bound SAM molecule through an inner-sphere electron transfer forming methionine and the dAdo radical. The dAdo radical activates a specific C-H bond of the substrate through direct H atom abstraction generating a substrate based radical at which point the specific reaction catalyzed by the enzymes diverge [48]. In some instances, as is the case with the glycyl

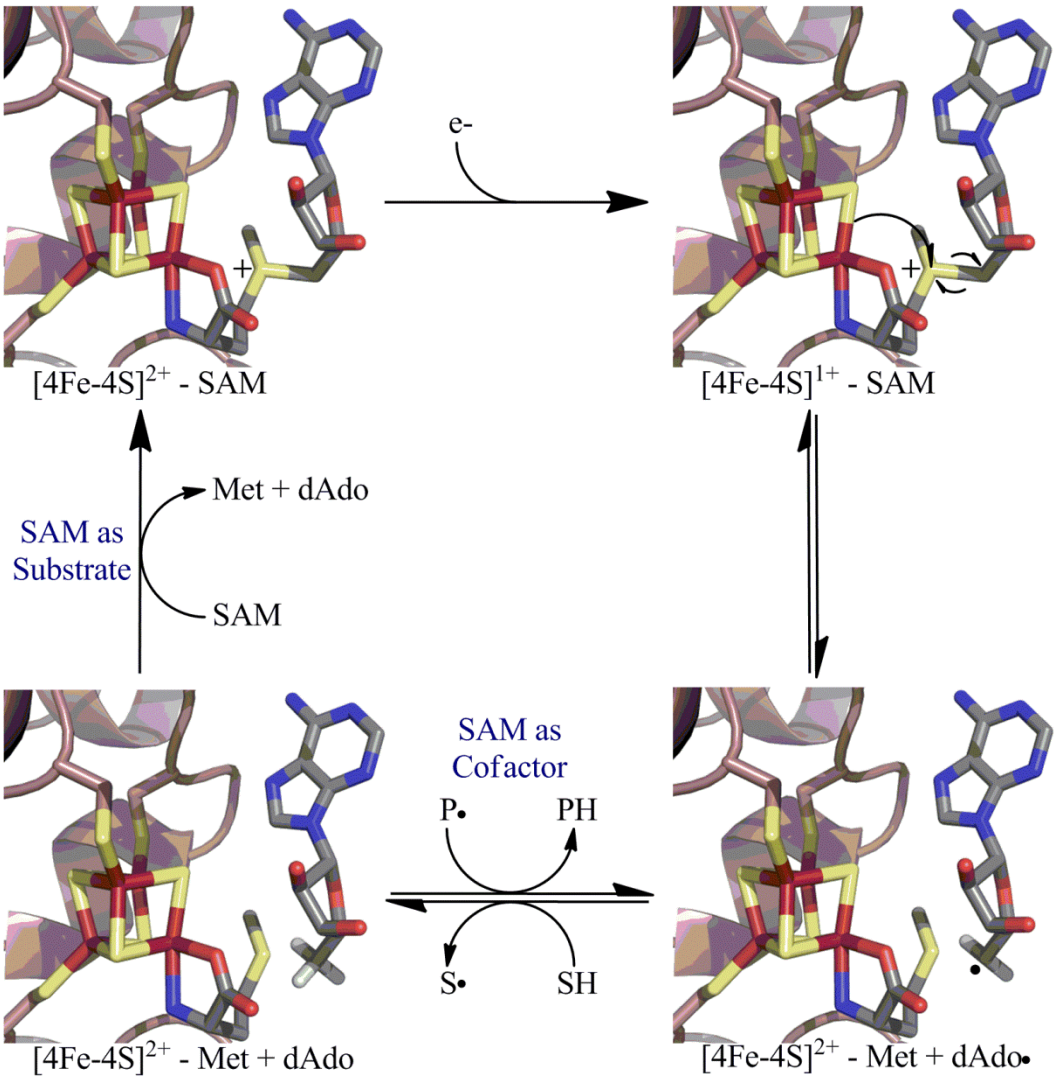

Scheme 1.1. Common mechanistic steps of radical SAM enzymes. SH refers to the enzyme substrate and the specific hydrogen atom abstracted by the dAdo radical. P• represents a product radical formed after direct hydrogen atom abstraction. If SAM is used as a cofactor, a hydrogen is reabstracted from the 5'-C of dAdo and SAM is reformed for another round of catalysis; if SAM is used as a co-substrate, Met and dAdo as the cleavage products are replaced by a new SAM molecule beginning the process anew.

radical enzyme-activating enzymes like PFL-AE and aRNR-AE, the substrate radical is the final product, but for many others the substrate radical can be the beginning of often complex and intriguing biochemical transformations.

Another consideration in radical SAM catalyzed reactions is whether SAM is used as a cofactor or a co-substrate. In a minority of the characterized radical SAM enzymes such as LAM and spore photoproduct lyase (SPL), SAM is used as a cofactor [48, 59-61]; the substrate radical undergoes turnover and the last product radical reabstracts a hydrogen atom from the 5'-carbon of deoxyadenosine. This regenerates the deoxyadenosine radical, which could then recombine with methionine along with simultaneous cluster reduction beginning a new round of catalysis. Alternatively, SAM is used as a co-substrate in PFL-AE, aRNR-AE, BioB, and the majority of other characterized radical SAM enzymes [50, 60]. In these enzymes after the 5'-deoxyadenosyl radical produces a substrate radical, the resulting methionine and 5'-deoxyadenosine must be replaced in the active site by a new molecule of SAM in order for a second cycle of catalysis to occur.

One of the most important aspects in the mechanism of radical SAM reactions is the control of the radical chemistry performed by these enzymes. In fact, in radical SAM enzymes the redox potentials for the $[4Fe\text{-}4S]^{2+/1+}$ couple are rather negative falling in the range of approximately -450 mV, which for physiological electron donors such as flavodoxin is inaccessible [62, 63]. However, binding of SAM to the cluster increases the reduction potential to a point where biological reductants are capable of donating an electron to the [4Fe-4S] cluster [62]. In contrast, bringing the cluster potential within range of *in vivo* reductants also moves SAM, estimated at approximately -1.8 V [64-66], further away, and the reductive cleavage of SAM is now ~1.4 V (or ~32 kcal mol^{-1}) uphill. So, how then are radical SAM enzymes able to catalyze the formation of the 5'-

deoxyadenosyl radical? An understanding of how this superfamily is able to overcome the large barrier has come from studies of LAM by Wang and Frey [67]. They found that the binding of SAM to the [4Fe-4S] cluster contributes 19 kcal mol^{-1} towards the lowering of the energy barrier, and subsequent binding of lysine in the active site of LAM contributes an additional 4 kcal mol^{-1} [67]. Combined, these two effects lower the energy barrier of SAM cleavage to 9 kcal mol^{-1} [67]. The remaining gap may be bridged through the act of electron transfer; the transfer of an electron from the $[4Fe\text{-}4S]^{1+}$ cluster to the sulfonium of SAM converts the coordination of the unique iron from pentacoordinate to the more favorable hexacoordinate [67]. This change in coordination was supported by the X-ray crystal structures of HydE with SAM bound (at 1.62 Å resolution) as well as HydE with Met and 5'-dAdo (at 1.25 Å resolution) [68]. In both structures the unique iron is coordinated by three sulfides from the [4Fe-4S] cluster; in the SAM bound structure the unique iron is also coordinated by the amino and carboxy

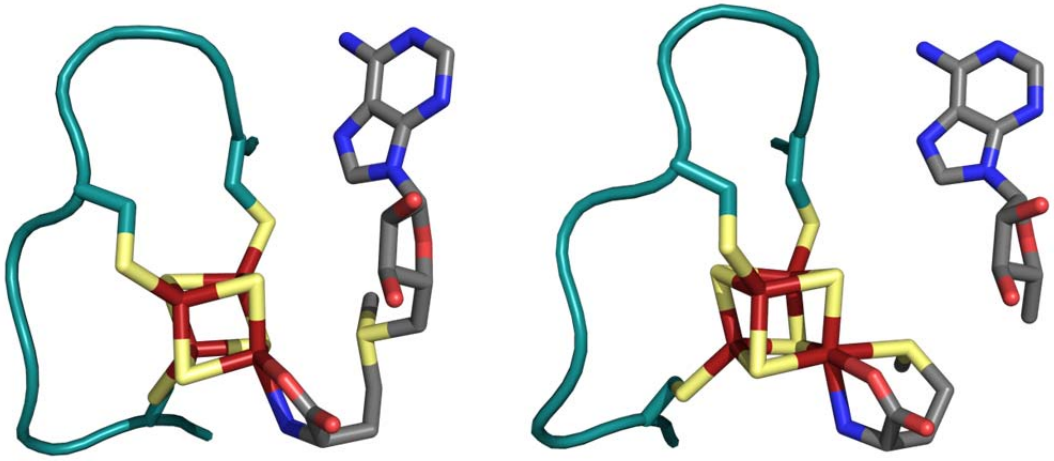

Figure 1.5. Left: HydE [4Fe-4S] cluster bound by SAM with the unique iron pentacoordinated (PDB ID 3IIZ) [68]. Right: HydE [4Fe-4S] cluster bound by Met with the unique iron hexacoordinated (PDB ID 3IIX) [68]. In both figures the protein backbone is shown in teal, the Fe-S cluster in dark red and yellow, and SAM or the cleavage products Met and dAdo in gray.

moieties of SAM giving it a total of five ligands while in the structure with Met and 5'dAdo the unique iron gains an additional ligand from the Met sulfur for a total of six (Figure 1.5) [68].

Reaction Diversity

In radical SAM enzymes, elements such as a $[4Fe\text{-}4S]^{1+}$ cluster and SAM are used to catalyze the formation of the reactive 5'-deoxyadenosyl radical for hydrogen atom abstraction, which results in activation of otherwise inert C-H bonds. That this common activation is followed by a diverse array of reactions is astounding (Table 1.1). The reactions catalyzed include sulfur insertion, viral inhibition, DNA repair, complex cofactor assembly, methylation and methylthiolation (see Chapter 7 for a detailed discussion), and numerous others.

Sulfur Insertion One group of radical SAM enzymes, catalyzing the insertion of one or more sulfur atoms into their substrate, includes biotin synthase (BioB), which synthesizes biotin from dethiobiotin through the addition of a sulfur atom [69, 70], and lipoate synthase (LipA), which catalyzes the addition of two sulfur atoms on octanoyl-acyl carrier protein transforming it into lipoyl-acyl carrier protein [71, 72]. These enzymes contain a second Fe-S cluster ([2Fe-2S] for BioB [63, 73] and [4Fe-4S] for LipA[74]) that is generally accepted to be the source of the inserted sulfur atoms. Recent evidence that suggests the cluster is indeed the source of sulfur comes from BioB; during turnover the production of the reaction intermediate 9-mercaptodethiobiotin was accompanied by the reduction of the [2Fe-2S] cluster [75].

Table 1.1. Examples of some of the varied reactions catalyzed by radical SAM enzymes. The table indicates the enzyme, the reaction catalyzed by that enzyme, and whether SAM is used by the enzyme as a substrate or cofactor.

Enzyme	Reaction Catalyzed	Role of SAM
Activating enzymes	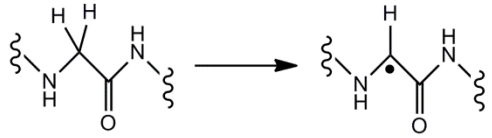	Substrate
LAM	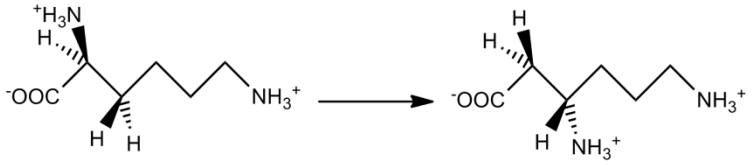	Cofactor
MoaA	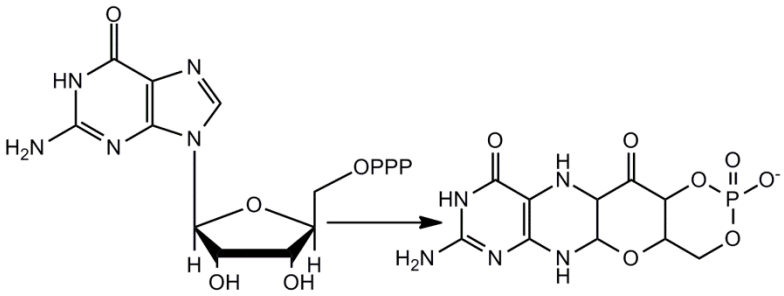	Substrate
ThiC	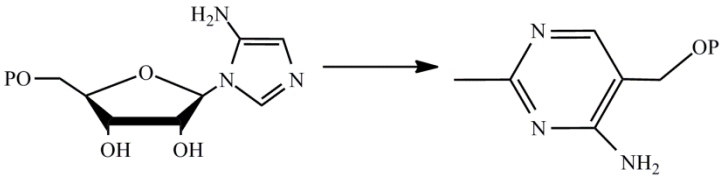	Substrate
ThiH	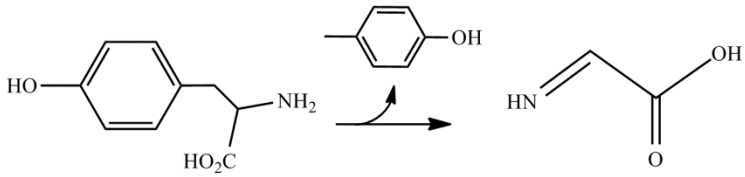	Substrate
SPL	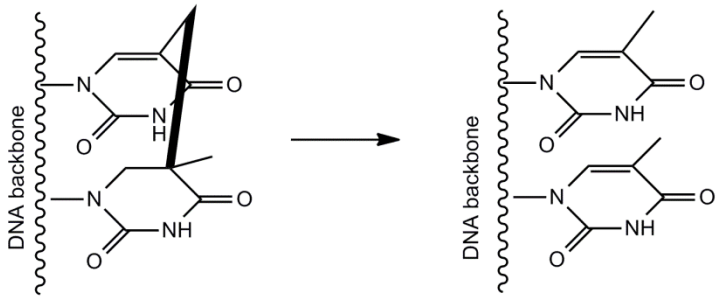	Cofactor

Table 1.1 Continued. Examples of some of the varied reactions catalyzed by radical SAM enzymes. The table indicates the enzyme, the reaction catalyzed by that enzyme, and whether SAM is used by the enzyme as a substrate or cofactor.

Enzyme	Reaction Catalyzed	Role of SAM
BioB	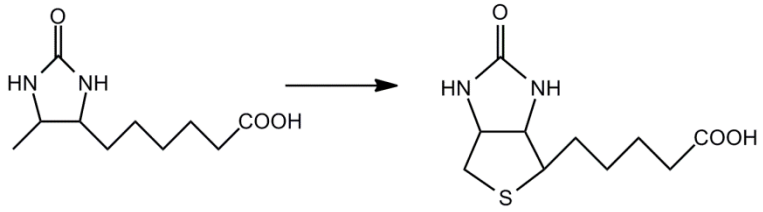	Substrate
LipA	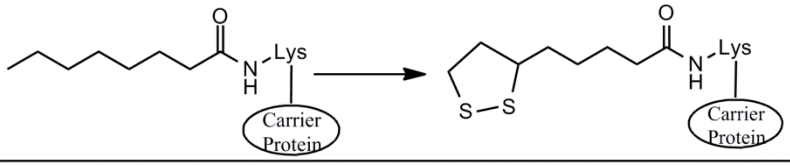	Substrate
MiaB	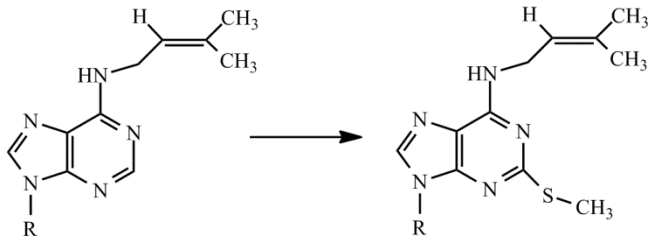	Substrate
TWY1	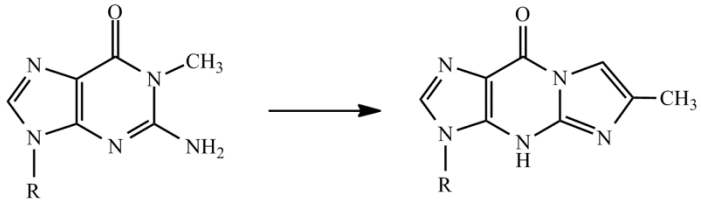	Substrate
HemN	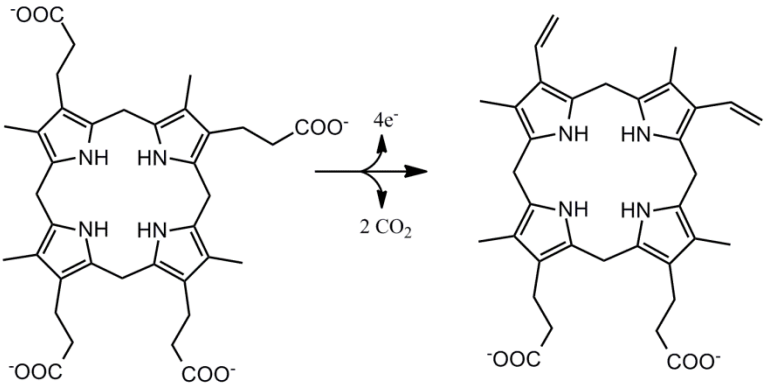	Substrate
AtsB	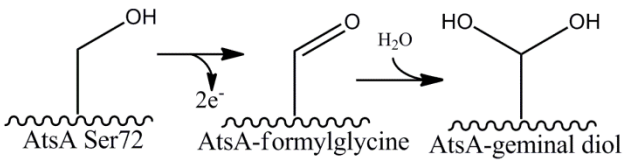	Substrate

Complex Cofactor Assembly The active site of [FeFe] hydrogenase contains a complex metallocofactor, designated the H-cluster (see above), which requires three maturase enzymes for construction of the 2Fe subcluster (the [4Fe-4S] cluster is assembled and inserted through general cell machinery [76]). Of the three maturases (HydE, HydF, and HydG), *two* are radical SAM enzymes [77], while the third, HydF, is a scaffold for the assembly [78]. The two radical SAM enzymes, HydE and HydG, are responsible for the synthesis of the unique carbon monoxide, cyanide, and dithiolate ligands. HydG has been shown to catalyze the formation of carbon monoxide [79] and cyanide [80] through the degradation of tyrosine, and it is generally accepted that HydE is involved in production of the ditholate ligand possibly utilizing chemistry similar to BioB and LipA [8, 9].

Modification of Large Biomolecules Many radical SAM enzymes are responsible for the modification of large biomolecules such as DNA, RNA, and other proteins. Spore photoproduct lyase (SPL) catalyzes the repair of spore photoproduct, a thymine dimer, in spore-forming bacterial DNA. The 5'-dAdo radical abstracts the C-6 hydrogen atom initiating β-scission leading to the monomeric products [48]. Certain other enzymes modify biomolecules involved in the translational machinery (see Chapter 7). Methylthiotransferases, such as MiaB and MtaB, add a methylthio modification to tRNA whereas RimO adds one to a small ribosomal subunit protein. RlmN and Cfr methyltransferases methylate ribosomal 23S RNA. Others including the glycyl radical enzyme (GRE) activating enzymes, for example aRNR-AE and PFL-AE, as mentioned

previously act upon another protein (aRNR and PFL respectively) by abstracting a hydrogen atom from a glycine forming a catalytically essential glycyl radical.

Pyruvate Formate-Lyase Activating Enzyme

Mechanistic and Structural Characterization of PFL

Pyruvate formate-lyase (PFL), the 170 kDa homodimer substrate of pyruvate formate-lyase activating enzyme (PFL-AE), is a central enzyme in anaerobic glucose metabolism and is the anaerobic counterpart to the pyruvate dehydrogenase complex;

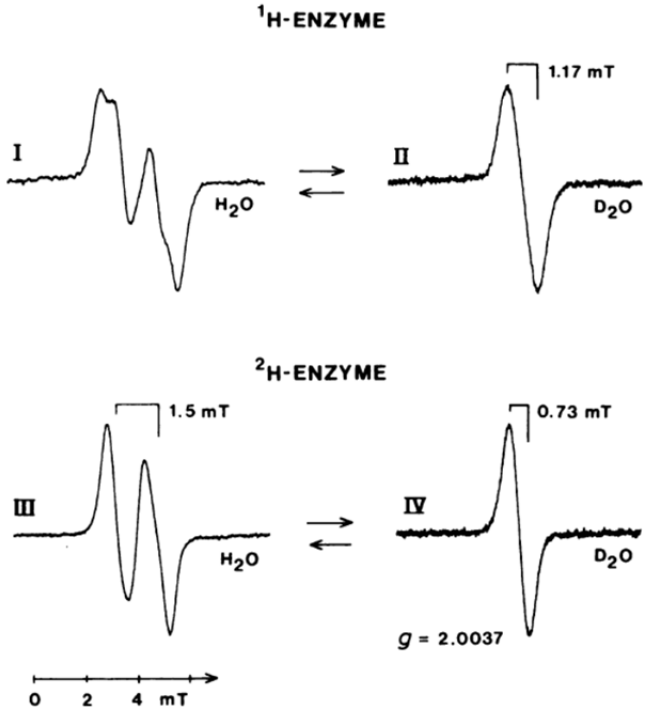

Figure 1.6. EPR spectra of the glycyl radical on PFL Gly734 [81]. Spectra I and II are PFL containing ^{1}H, and samples were prepared in either H_2O (I) or D_2O (II). Spectra III and IV are PFL containing ^{2}H, and samples were prepared in either H_2O (III) or D_2O (IV). Spectra I and III show splitting of the radical EPR signal by the remaining hydrogen on Cα of Gly734 while spectra II and IV show an unsplit signal due to the deuterium, which is exchanged on Cα of Gly734.

PFL catalyzes the conversion of pyruvate and coenzyme A (CoA) to formate and acetyl-CoA. The homodimer of PFL shows half-sites reactivity meaning that only one monomer is activated at any given time [82]. The first step in initiating the reaction of PFL is the PFL-AE catalyzed generation, through abstraction of the pro-*S* hydrogen atom, of a Gly734 glycyl radical (Figure 1.6) [81], whose exchange with solvent is mediated by the catalytically essential Cys419 [83]. Cys419 transfers this radical to Cys418, the other catalytically necessary residue, generating a thiyl radical, which is transferred to the other catalytically necessary residue Cys418 [84-87] (Scheme 1.2). The Cys418 thiyl radical is then proposed to attack the carbonyl carbon on pyruvate breaking the carbon-carbon bond [84, 85] resulting in a formate anion radical, which abstracts a hydrogen atom from

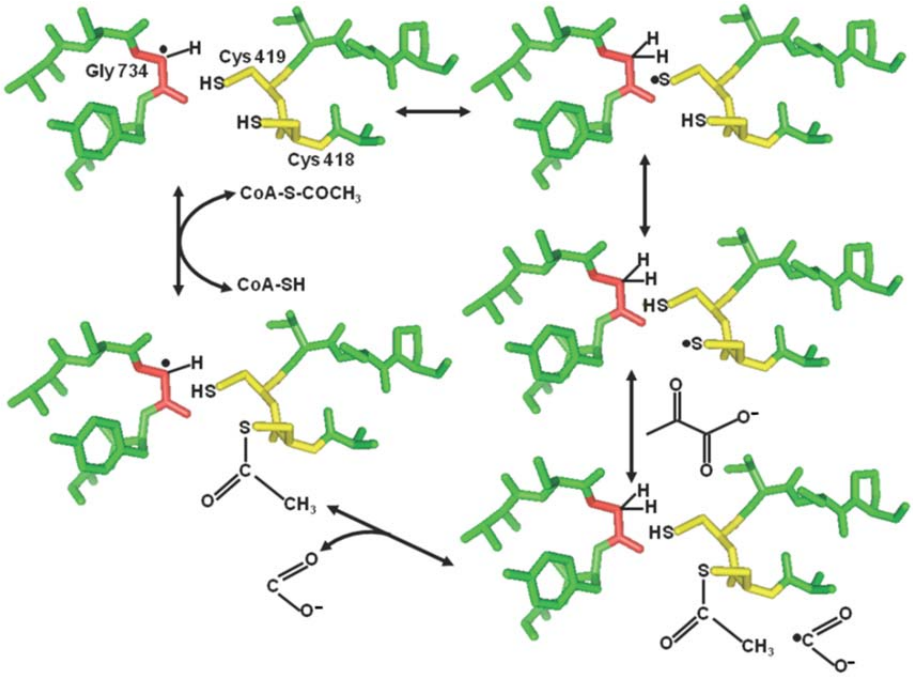

Scheme 1.2. Proposed mechanism for PFL catalyzed conversion of pyruvate and CoA to formate and acetyl-CoA. The catalytic residues are shown in red for Gly734 and yellow for Cys418 and Cys419. Figure from [88] using the PFL crystal structure, PDB ID 2PFL.

Gly734 reforming the glycyl radical, and attaching the acetyl moiety to Cys418, which reacts with CoA to form acetyl-CoA [87, 89-91]. The role of the Cys419 in this ping-pong mechanism is as a radical transporter between Gly734 and Cys418 [84, 87], hence its role in mediating solvent exchange with the glycyl radical, which is the resting state of the enzyme. In the absence of oxygen the glycyl radical is incredibly stable; however exposure of the radical to oxygen quickly results in PFL inactivation by cleavage at Gly734 into 82 kDa and 3 kDa fragments [55]. The activity of the large PFL core fragment corresponding to residues 1-733 of PFL can be recovered by a small 14 kDa protein, YfiD, showing high sequence similarity to the C-terminal portion of PFL [92]. In fact, the identity of 22 of the residues around the radical bearing glycine is strictly conserved (Figure 1.7). In order to perform PFL catalytic function, the YfiD protein

```
                :** . .:.: *    .**:* :     :. . ** *
PFL         RDQKGAVASLTSVAKLPFAYAKDGISYTFSIVPNALGKDD
YfiD        --EKGEARCIVAKA----GYAEDEV-----VAVSKLG-DI

                * *:. :       .: *. :**********:.** * **
PFL         EVRKTNLAGLMDGYFHHEASIEGGQHLNVNVMNREMLLDA
YfiD        EYREVPVE------VKPEVRVEGGQHLNVNVLRRETLEDA

                :::*******************  ***:***:****:*
PFL         MENPEKYPQLTIRVSGYAVRFNSLTKEQQQDVITRTFTQS
YfiD        VKHPEKYPQLTIRVSGYAVRFNSLTPEQQRDVIARTFTES
```

Figure 1.7. ClustalX alignment of YfiD and the C-terminal end of PFL. The 22 amino acids around the glycine, Gly734 boxed in red, where the glycyl radical is formed are strictly conserved.

associates with the PFL core protein and a glycyl radical at Gly102 is generated by PFL-AE [92]. It is proposed that YfiD functions as a "spare part" for cells that have

undergone oxidative stress as a means to quickly recovery the generation of ATP through PFL activity and the production of acetyl-CoA [92].

The crystal structure of PFL (Figure 1.8) has revealed how the three catalytic residues are able to interact to perform the transfer of the radical. Each monomer of PFL consists of a 10-stranded α/β barrel constructed in an antiparallel fashion from two parallel five-stranded β-sheets with the active site residing in close proximity to the center of the barrel [84]. The catalytic residues, Gly734 and Cys418/Cys419, are located on opposing finger loops within the active site; the Gly734 Cα and Cys419 Sγ are at a distance of 3.7 Å [84]. The Gly734 is also buried 8 Å from the protein surface protecting it and the active site from excessive solvent exposure The two monomers of the overall

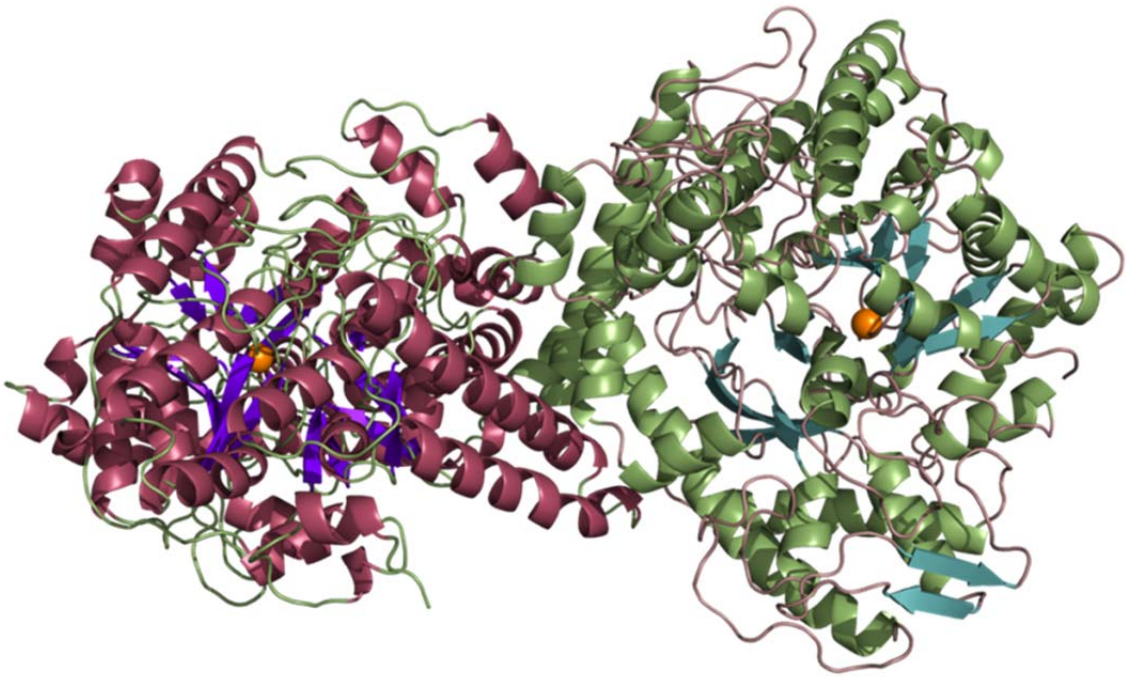

Figure 1.8 The crystal structure of PFL (PDB ID 2PFL) showing the PFL dimer with one monomer shown in purples and one in greens. Glycine residue 734 is shown as an orange sphere.

dimer structure are related by an almost perfect two-fold rotation, and the surface of interaction mainly involves helical regions found at the N-terminal ends of PFL before the beginning of the barrel formation; this tight contact creates a buried surface area of 2,052 $Å^2$ [84].

Mechanistic and Structural Characterization of PFL-AE

Pyruvate formate-lyase activating enzyme, a 28 kDa monomer, was identified as an essential enzyme in the activation of pyruvate formate-lyase in the late 1960s and was known to be dependent on ferrous iron and *S*-adenosylmethionine [93]. The role of the iron and SAM, however, were unclear, and it was suggested that SAM, as it was converted into methionine and 5'-deoxyadenosine, was used for transient adenosylation of PFL-AE [94] and that the iron was a mononuclear Fe(II) site [95]. It wasn't until 1994

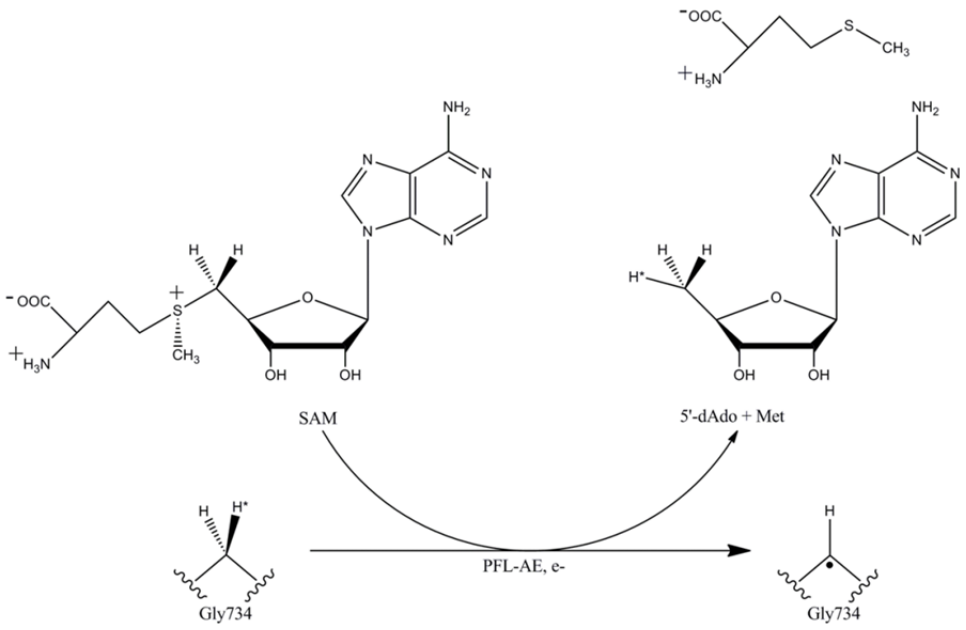

Scheme 1.3. PFL-AE generation of the glycyl radical. PFL-AE generation of the 5'deoxyadenosyl radical causes glycyl radical formation by H-atom abstraction. The labeled hydrogen from Gly734 can be found in the resulting 5'-deoxyadenosine.

that the role of SAM in abstracting the glycine hydrogen atom was understood; through the use of [2-^{2}H]glycine-labeled PFL, the deuterium was observed to be stoichiometrically transferred to 5'-deoxyadenosine implicating a 5'-deoxyadenosyl radical in the generation of the glycyl radical (Scheme 1.3) [96].

The anaerobic purification of PFL-AE by Broderick et al. gave the first indication that the iron was part of an iron-sulfur cluster [97]. Using resonance Raman and EPR spectroscopy, they were able to detect the presence of a mixture of $[2Fe\text{-}2S]^{2+}$ and $[4Fe\text{-}4S]^{2+}$ clusters that were converted to $[4Fe\text{-}4S]^{2+}$ when reduced with sodium dithionite; the presence of SAM allowed the cluster to be further reduced to the $[4Fe\text{-}4S]^{1+}$ state [97]. Later Mössbauer spectroscopy and improved purification techniques under strict anaerobic conditions allowed PFL-AE to be isolated with a mixture of $[2Fe\text{-}2S]^{1+}$, $[3Fe\text{-}4S]^{1+}$, and $[4Fe\text{-}4S]^{2+}$ clusters that could be reduced to $[4Fe\text{-}4S]^{2+}$ and $[4Fe\text{-}4S]^{1+}$ clusters without SAM [98, 99]. Knappe et al. were also able to reconstitute a [4Fe-4S] cluster in PFL-AE purified in the apo state and showed through individual site-directed mutagenesis of the six cysteines in PFL-AE followed by reconstitution that it was the CX_3CX_2C motif (as discussed previously) involved in binding the cluster [100]. Additional experimental support was obtained when none of the reconstituted mutants of the CX_3CX_2C motif showed enzymatic activity [100].

Catalytic Cluster The occurrence of multiple Fe-S cluster forms in PFL-AE made it necessary to determine which was catalytically active. As discussed with other radical SAM enzymes, it was determined through controlled and quantified EPR spectroscopy (Figure 1.9) that the active cluster of PFL-AE is the $[4Fe\text{-}4S]^{1+}$ state. The PFL-AE

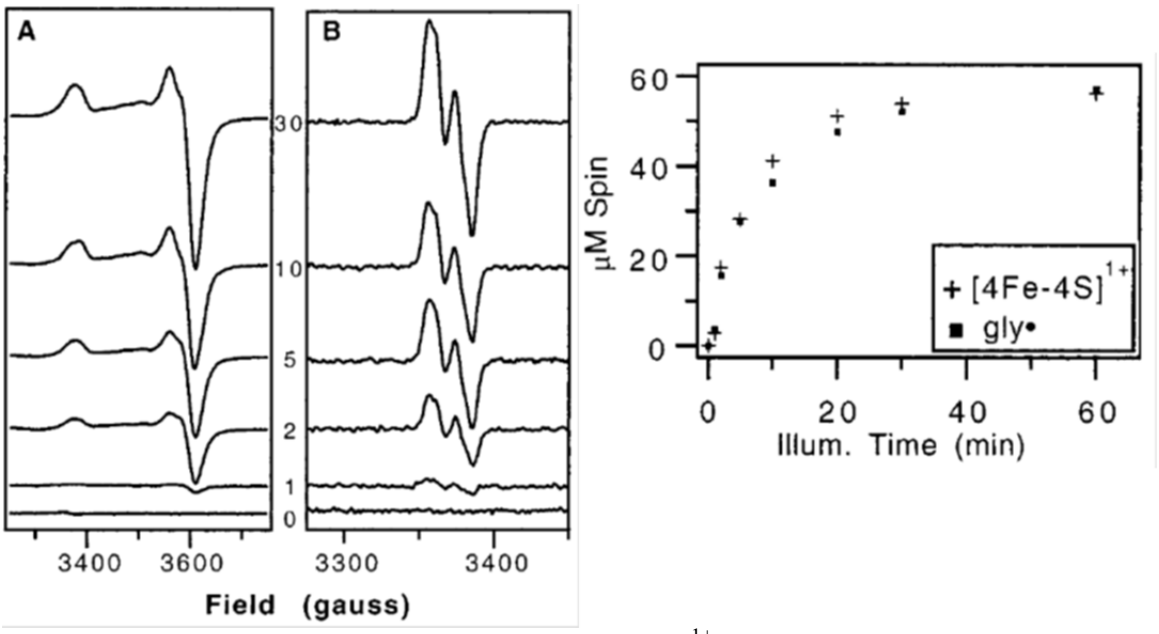

Figure 1.9. Left: EPR spectra of the reduced $[4Fe\text{-}4S]^{1+}$ cluster of SAM (A) showing a nearly axial signal whose intensity increases with longer photoreduction times (in minutes) as indicated to the right of each spectra. The increase in intensity indicates an increase in the amount of $[4Fe\text{-}4S]^{1+}$ cluster produced. The EPR spectra in (B) is of PFL-AE with PFL added showing a split signal indicative of the glycyl radical formed on PFL. The signal intensity also increases with time as more glycyl radical is produced. Right: Spin quantitation of the EPR spectra on the left show a 1:1 correlation between the amount of $[4Fe\text{-}4S]^{1+}$ cluster and the amount of glycyl radical produced implicating the $[4Fe\text{-}4S]^{1+}$ cluster as the catalytically active form. Figures are from [44].

cluster was reduced by photoreduction with 5-deazariboflavin at varying illumination times, SAM was added in excess, and the sample was split in two; to one of the halves PFL was added in a 1:1 stoichiometry with PFL-AE, and both samples were analyzed by EPR spectroscopy [44]. The samples containing no PFL showed a nearly axial signal indicative of a $[4Fe\text{-}4S]^{1+}$ cluster, and the signal intensity increased with increasing illumination times signifying production of more 1+ cluster [44]. Those containing PFL showed a split isotropic signal suggestive of a glycyl radical whose signal intensity also increased with longer illumination times; furthermore these samples no longer showed a signal corresponding to the $[4Fe\text{-}4S]^{1+}$ cluster demonstrating that production of the glycyl

radical was likely concomitant with cluster oxidation [44]. When the signals were spin quantitated a stoichiometry of 1:1 $[4Fe\text{-}4S]^{1+}$ cluster to glycyl radical was observed; these results strongly suggested that, as the generation of the glycyl radical is stoichiometric to SAM cleavage and requires a source of electrons, the $[4Fe\text{-}4S]^{1+}$ cluster was the electron source and was subsequently converted to the oxidized and EPR silent $[4Fe\text{-}4S]^{2+}$ cluster [44]. Additionally, the samples containing oxidized cluster could be reilluminated forming the $[4Fe\text{-}4S]^{1+}$ cluster indicating its ability to cycle between the two redox states [44].

The Unique Fe and SAM Binding The presence of a cysteine triad motif conserved among the radical SAM enzymes suggested that, like aconitase, PFL-AE likely contained a site-differentiated [4Fe-4S] cluster. Presumably a unique iron would be more labile due to its lack of cysteine coordination, so naturally abundant (^{56}Fe) PFL-AE was grown and anaerobically purified after which it was briefly exposed to oxygen to form a $[3Fe\text{-}4S]^{1+}$ cluster and gel filtered to remove unbound iron [35]. For Mössbauer spectroscopy the $[3Fe\text{-}4S]^{1+}$ containing PFL-AE was reconstituted with ^{57}Fe and DTT to label the unique site, which produced a $[4Fe\text{-}4S]^{2+}$ cluster [35]. The Mössbauer spectra (Figure 1.10) demonstrated that the unique iron was indeed labeled forming the $[3(^{56}Fe)(^{57}Fe)\text{-}4S]^{2+}$ cluster; additionally, upon the addition of a 10 fold excess of SAM a new quadrupole doublet with a large isomer shift was formed while the original doublet from the unique site ^{57}Fe decreased in intensity indicating an interaction between SAM and the unique site, more specifically ionic ligands from SAM [35]. While this data demonstrated an interaction between SAM and the unique iron, it did not indicate the

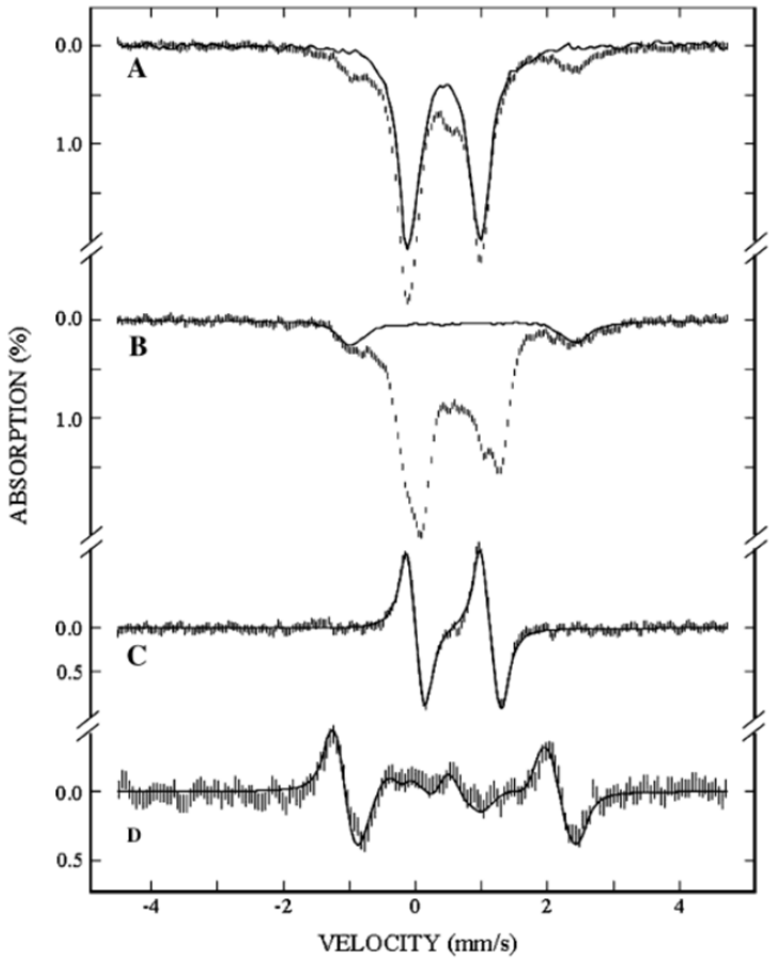

Figure 1.10. Mössbauer spectra of PFL-AE with unique site of the [4Fe-4S] cluster labeled with ^{57}Fe. PFL-AE alone (A) shows a quadrupole doublet that is affected by the addition of SAM (B). The addition of SAM displays a new quadrupole doublet and the original shows a decrease in intensity. Spectra C and D are the difference spectra of (A-B) at 50 mT (C) and 8 T (D). In A the solid line is the experimental spectrum of the $[4Fe\text{-}4S]^{2+}$ cluster in PFL-AE, and in B the solid line is the control containing the reconstitution ingredients and SAM without PFL-AE present. The solid lines in C and D are the difference spectra of theoretical simulations of a unique iron site with and without SAM. Figure is from [35].

specific nature of the interaction, which was established through the use of ENDOR and SAM isotopically labeled with ^{17}O or ^{13}C on the carboxyl group or ^{15}N on the amino group [34]. Anaerobically purified PFL-AE was photoreduced to the $[4Fe\text{-}4S]^{1+}$ state and a two-fold excess of the labeled SAM was added; upon ENDOR analysis, coupling

between the $[4Fe\text{-}4S]^{1+}$ cluster and each of the labeled SAM molecules was seen establishing that the coordination of SAM to the unique iron was through an oxygen from the carboxyl group and the nitrogen of the amino group as is shown in Figure 1.3 [34].

PFL-AE Structure The coordination of SAM to the unique iron through its carboxy and amino moieties was also observed upon the solving the PFL-AE crystal structure with SAM bound to the cluster [36]. As has been seen with other radical SAM enzymes, PFL-AE displays a partial $(\alpha/\beta)_6$ TIM barrel fold with a wide lateral opening capable of accepting its large substrate, PFL. The iron-sulfur cluster is located at the top

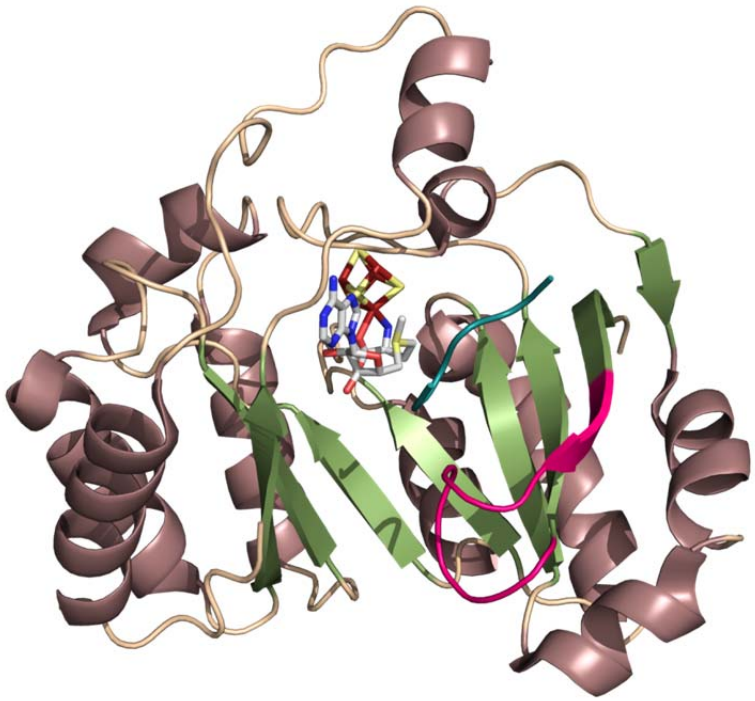

Figure 1.11. Structure of PFL-AE generated from PDB ID 3CB8 [36]. PFL-AE contains a partial $(\alpha/\beta)_6$ TIM barrel with a wide opening to accommodate the large protein substrate, PFL. SAM shown in light grey is bound to the cluster through its carboxy and amino moieties. The PFL peptide is shown as a deep teal loop. Loop A which undergoes the largest conformational change upon peptide binding is colored magenta.

of the barrel and the bound SAM shows interactions with the SAM binding motifs discussed earlier, specifically the GGE motif (PFL-AE residues G^{77}, G^{78}, and E^{79}) as well as the $GXIXGX_2E$ motif (V^{168}, V^{170}, G^{172}, and E^{175} of PFL-AE). Additionally two completely conserved residues in PFL-AE, D^{104} and R^{166}, are in close proximity to the 5'-C of SAM and may play a role in catalysis, although no direct interactions are made with SAM. A second PFL-AE structure with both SAM and a 7-mer peptide containing the glycine 734 and sequence surrounding it from PFL bound in the active site was also solved (Figure 1.11) [36]. In this structure the peptide is bound across the lateral opening of the barrel with the glycine projecting in towards the active site placing the Cα 4.1 Å from the 5'-C of SAM in an ideal location for hydrogen atom abstraction by the 5'-deoxyadenosyl radical. Interactions between the peptide and PFL-AE are made mainly by backbone atoms in the peptide and side chains in PFL-AE, which are highly conserved and include a DGXGXR ($D^{16}G^{17}XG^{19}XR^{21}$ in PFL-AE) motif on loop A, which undergoes a large conformational change upon peptide binding by swinging up to make these contacts.

PFL and PFL-AE Interactions

The crystal structures of PFL and PFL-AE raise an interesting dilemma in the mechanism of activation of PFL. In the PFL crystal structure Gly734 is buried 8 Å within the protein; however, the hydrogen atom abstraction by the 5'-dAdo radical forming the glycyl radical is direct and stereospecific [96]. The PFL-AE structure with peptide bound showing the glycine within the active site in close proximity to the 5'-C of SAM provides an interesting solution. To allow PFL-AE access to the catalytic glycine,

PFL would have to undergo a dramatic conformational change. Evidence for this conformational change has been obtained by Peng et al. and shows that, in the presence of PFL-AE, PFL can adopt a closed conformation in which the Gly734 is buried or an open conformation in which the loop containing Gly734 is exposed (Figure 1.12) [88].

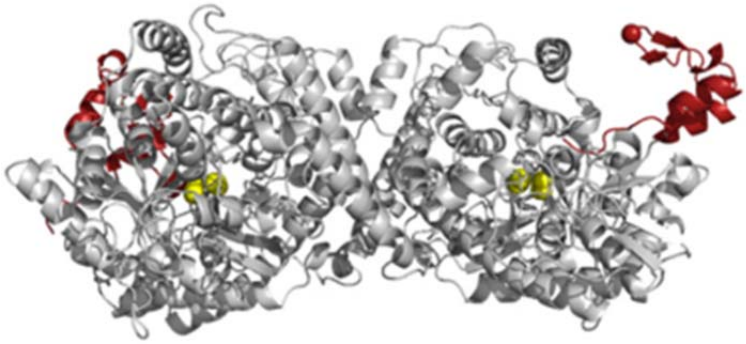

Figure 1.12. This image showing the proposed open conformation of PFL from [88] was generated in PyMol by manual rotation of the radical domain, which is connected to the barrel by a flexible loop that is thought to allow the radical domain freedom to adopt the more open conformation predicted in the presence of PFL-AE. The radical domain is displayed in red with Gly734 shown as a red sphere. The catalytic residues Cys418 and Cys419 are shown as yellow spheres.

The open conformation of PFL is favored in the presence of PFL-AE; consequences of the open conformation include a decreased T_m of PFL, lowered catalytic activity of the activated enzyme , and a less stable glycyl radical which undergoes less H/D exchange with solvent [88]. The lower melting temperature seen in the open conformation of PFL is understandable as the open conformation represents the removal of a core domain from the PFL structure. A decrease in the catalytic activity of PFL is likely a direct result of the reduced glycyl radical stability as the loss of the radical would preclude the conversion of pyruvate to formate and acetyl-CoA; the loss in radical stability was attributed to nondestructive quenching (PFL that had lost its glycyl radical could be

reactivated) by the high concentrations of DTT used in the buffer as the radical was less likely to be reinserted into the PFL core thus protecting it. As for the decrease in H/D exchange at Gly734, it is Cys419 that mediates this exchange, and the open conformation eliminates the close proximity necessary between the two for the transfer to occur [88]. The validation of this more open conformation of PFL provides a direct route of access to the glycine by PFL-AE for direct hydrogen atom abstraction.

Research Goals

While PFL-AE remains one of the best characterized radical SAM enzymes, there is still much that has been left unanswered as to the mechanism by which PFL-AE activates PFL. The crystal structure of PFL-AE and further analysis of the open conformation of PFL provided insight into the interaction necessary for PFL-AE to access the glycine from which it abstracts a hydrogen atom. However, when the crystal structure of PFL-AE was solved, the presence of a monovalent cation in the active site was revealed. Many enzymes are activated by cations, although the role in PFL-AE was unclear as buffers containing either NaCl or KCl have consistently been used to control ionic strength. The cation was found in close proximity to SAM, and an interaction with the unbound carbonyl oxygen of SAM's carboxy moiety was discovered. The location of the cation within the active site also puts it near the Fe-S cluster. To determine the most likely cation found in the active site *in vivo* as well as the effect of the cation on the electronic structure of the active site and on PFL-AE activity, EPR spectroscopy and

activity assays were performed in the presence of five different cations: Na^+, K^+, NH_4^+, Rb^+, and Cs^+.

Another unresolved question from the crystal structures of PFL-AE is how the binding of SAM affects PFL-AE; to date there is no crystal structure of SAM alone. In order to analyze the effects of SAM binding nuclear resonance vibrational spectroscopy (NRVS), a relatively new technique as applied to metalloproteins, was employed. NRVS utilizes Mössbauer active isotopes such as ^{57}Fe, which in the case of PFL-AE presents a unique opportunity to specifically target the effects of SAM binding on the [4Fe-4S] cluster. To this end, the PFL-AE cluster was labeled by supplementing the PFL-AE with ^{57}Fe during overexpression. NRVS measurements were completed at Argonne National Laboratories, and two force constants were calculated, stiffness and resilience, which determine the rigidity of the protein around the cluster and the change in lengths of the Fe-S bonds.

The third goal of this research was to identify and characterize the intermediates in the generation of the glycyl radical created from hydrogen atom abstraction by the 5'-deoxyadenosyl radical. As these putative SAM radical intermediates are short lived, rapid freeze quench (RFQ) was used to isolate one. PFL-AE was mixed with PFL and SAM on a millisecond time scale and analyzed by EPR. An intermediate of the reaction was trapped and detected by EPR spectroscopy. As the intermediate is paramagnetic, which was demonstrated by the EPR signal obtained, ENDOR was also attempted with site-specifically labeled SAM in an effort to identify and characterize it based on coupling between the label and the paramagnetic center.

References

1. Tan L, and Chi-lung Y (1970) Int. Geol. Rev. 12: 778-786.

2. Beinert H (2000) J. Biol. Inorg. Chem. 5: 2-15.

3. Beinert H, Holm RH, and Münck E (1997) Science 277: 653-659.

4. Broderick JB. (2003) In Comprehensive Coordination Chemistry II: From Biology to Nanotechnology (McCleverty J, and Meyer T, Eds.), pp 739-757, Elsevier Science.

5. Link TA (1999) Adv. Inorg. Chem. 47: 83-157.

6. Calzolai L, Zhou ZH, Adams MWW, and LaMar GN (1996) J. Am. Chem. Soc. 118: 2513-2514.

7. Hunsicker-Wang LM, Heine A, Chen Y, Luna EP, Todaro T, Zhang YM, Williams PA, McRee DE, Hirst J, Stout CD, and Fee JA (2003) Biochemistry 42: 7303-7317.

8. Shepard EM, Boyd ES, Broderick JB, and Peters JW (2011) Curr. Opin. Chem. Biol. 15: 319-327.

9. Peters JW, and Broderick JB (2012) Annu. Rev. Biochem. 81: 429-450.

10. Wiig JA, Hu Y, Lee CC, and Ribbe MW (2012) Science 337: 1672-1675.

11. Meyer J (2008) J. Biol. Inorg. Chem. 13: 157-170.

12. Fu W, O'Handley S, Cunningham RP, and Johnson MK (1992) J. Biol. Chem. 267: 16135-16137.

13. Lukianova OA, and David SS (2005) Curr. Opin. Chem. Biol. 9: 145-151.

14. Thayer MM, Ahern H, Xing D, Cunningham RP, and Tainer JA (1995) EMBO J. 14: 4108-4120.

15. Green J, Scott C, and Guest JR (2001) Adv. Microb. Physiol. 44: 1-34.

16. Kiley PJ, and Beinert H (1998) FEMS Microbiol. Rev. 22: 341-352.

17. Popescu CV, Bates DM, Beinert H, Munck E, and Kiley PJ (1998) Proc. Natl. Acad. Sci. U.S.A. 95: 13431-13435.

18. Khoroshilova N, Popescu C, Munck E, Beinert H, and Kiley PJ (1997) Proc. Natl. Acad. Sci. U.S.A. 94: 6087-6092.

19. Demple B, Ding H, and Jorgensen M (2002) Methods Enzymol. 348: 355-364.

20. Ding H, and Demple B (2000) Proc. Natl. Acad. Sci. U.S.A. 97: 5146-5150.

21. Schwartz CJ, Giel JL, Patschkowski T, Luther C, Ruzicka FJ, Beinert H, and Kiley PJ (2001) Proc. Natl. Acad. Sci. U.S.A. 98: 14895-14900.

22. Haile DJ, Rouault TA, Harford JB, Kennedy MC, Blondin GA, Beinert H, and Klausner RD (1992) Proc. Natl. Acad. Sci. U.S.A. 89: 11735-11739.

23. Rouault TA, Haile DJ, Downey WE, Philpott CC, Tang C, Samaniego F, Chin J, Paul I, Orloff D, Harford JB, and Klausner RD (1992) Biometals 5: 131-140.

24. Haile DJ, Rouault TA, Tang CK, Chin J, Harford JB, and Klausner RD (1992) Proc. Natl. Acad. Sci. U.S.A. 89: 7536-7540.

25. Kennedy MC, Werst M, Telser J, Emptage MH, Beinert H, and Hoffman BM (1987) Proc. Natl. Acad. Sci. U.S.A. 84: 8854-8858.

26. Cheek J, and Broderick JB (2001) J. Biol. Inorg. Chem. 6: 209-226.

27. Sofia HJ, Chen G, Hetzler BG, Reyes-Spindola JF, and Miller NE (2001) Nucleic Acids Res. 29: 1097-1106.

28. Chatterjee A, Li Y, Zhang Y, Grove TL, Lee M, Krebs C, Booker SJ, Begley TP, and Ealick SE (2008) Nat. Chem. Biol. 4: 758-765.

29. Paraskevopoulou C, Fairhurst SA, Lowe DJ, Brick P, and Onesti S (2006) Mol. Microbiol. 59: 795-806.

30. McGlynn SE, Boyd ES, Shepard EM, Lange RK, Gerlach R, Broderick JB, and Peters JW (2010) J. Bacteriol. 192: 595-598.

31. Nicolet Y, and Drennan CL (2004) Nucleic Acids Res. 32: 4015-4025.

32. Liu A, and Graslund A (2000) J. Biol. Chem. 275: 12367-12373.

33. Walsby CJ, Hong W, Broderick WE, Cheek J, Ortillo D, Broderick JB, and Hoffman BM (2002) J. Am. Chem. Soc. 124: 3143-3151.

34. Walsby CJ, Ortillo D, Broderick WE, Broderick JB, and Hoffman BM (2002) J. Am. Chem. Soc. 124: 11270-11271.

35. Krebs C, Broderick WE, Henshaw TF, Broderick JB, and Huynh BH (2002) J. Am. Chem. Soc. 124: 912-913.

36. Vey JL, Yang J, Li M, Broderick WE, Broderick JB, and Drennan CL (2008) Proc. Natl. Acad. Sci. U.S.A. 105: 16137-16141.

37. Dowling DP, Vey JL, Croft AK, and Drennan CL (2012) Biochim. Biophys. Acta.: 1178-1195.

38. Vey JL, and Drennan CL (2011) Chem. Rev. 111: 2487-2506.

39. Berkovitch F, Nicolet Y, Wan JT, Jarrett JT, and Drennan CL (2004) Science 303: 76-79.

40. Lepore BW, Ruzicka FJ, Frey PA, and Ringe D (2005) Proc. Natl. Acad. Sci. U.S.A. 102: 13819-13824.

41. Boal AK, Grove TL, McLaughlin MI, Yennawar NH, Booker SJ, and Rosenzweig AC (2011) Science: 1089-1092.

42. Ollagnier S, Mulliez E, Schmidt PP, Eliasson R, Gaillard J, Deronzier C, Bergman T, Graslund A, Reichard P, and Fontecave M (1997) J. Biol. Chem. 272: 24216-24223.

43. Lieder KW, Booker S, Ruzicka FJ, Beinert H, Reed GH, and Frey PA (1998) Biochemistry 37: 2578-2585.

44. Henshaw TF, Cheek J, and Broderick JB (2000) J. Am. Chem. Soc. 122: 8331-8332.

45. Magnusson OT, Reed GH, and Frey PA (1999) J. Am. Chem. Soc. 121: 9764-9765.

46. Magnusson OT, Reed GH, and Frey PA (2001) Biochemistry 40: 7773-7782.

47. Benjdia A, Leprince J, Sandström C, Vaudry H, and Berteau O (2009) J. Am. Chem. Soc. 131: 8348-8349.

48. Cheek J, and Broderick JB (2002) J. Am. Chem. Soc. 124: 2860-2861.

49. Escalettes F, Florentin D, Bui BTS, Lesage D, and Marquet A (1999) J. Am. Chem. Soc. 121: 3571-3578.

50. Frey PA, Rothe M, Wagner AFV, and Knappe J (1994) J. Biol. Chem. 269: 12432-12437.

51. Gambarelli S, Luttringer F, Padovani D, Mulliez E, and Fontecave M (2005) Chembiochem : a European journal of chemical biology 6: 1960-1962.

52. Grove TL, Benner JS, Radle MI, Ahlum JH, Landgraf BJ, Krebs C, and Booker SJ (2011) Science 332: 604-607.

53. Guianvarc'h D, Florentin D, Bui BTS, Nunzi F, and Marquet A (1997) Biochem. Biophys. Res. Commun. 236: 402-406.

54. Kilgore JL, and Aberhart DJ (1991) J. Chem. Soc., Perkin Trans. 1: 79-84.

55. Knappe J, Neugebauer FA, Blaschkowski HP, and Gänzler M (1984) Proc. Natl. Acad. Sci. U.S.A. 81: 1332-1335.

56. Ruszczycky MW, Choi S-h, and Liu H-w (2010) J. Am. Chem. Soc. 132: 2359-2369.

57. Yan F, and Fujimori DG (2011) Proc. Natl. Acad. Sci. U.S.A. 108: 3930-3934.

58. Yokoyama K, Numakura M, Kudo F, Ohmori D, and Eguchi T (2007) J. Am. Chem. Soc. 129: 15147-15155.

59. Chen D, Walsby C, Hoffman BM, and Frey PA (2003) J. Am. Chem. Soc. 125: 11788-11789.

60. Frey PA, Hegeman AD, and Ruzicka FJ (2008) Crit. Rev. Biochem. Mol. Biol. 43: 63-88.

61. Marsh EN, Patterson DP, and Li L (2010) Chembiochem : a European journal of chemical biology 11: 604-621.

62. Hinckley GT, and Frey PA (2006) Biochemistry 45: 3219-3225.

63. Ugulava NB, Gibney BR, and Jarrett JT (2001) Biochemistry 40: 8343-8351.

64. Colichman EL, and Love DL (1953) J. Org. Chem. 18: 40-46.

65. Grimshaw J. (1981) In The Chemistry of the Sulphonium Group (Stirling CJM, and Patai S, Eds.), pp 141-155, Wiley & Sons Ltd.

66. Saeva FD, and Morgan BP (1984) J. Am. Chem. Soc. 106: 4121-4125.

67. Wang SC, and Frey PA (2007) Biochemistry 46: 12889-12895.

68. Nicolet Y, Amara P, Mouesca J-M, and Fontecilla-Camps JC (2009) Proc. Natl. Acad. Sci. U.S.A. 106: 14867-14871.

69. Sanyal I, Cohen G, and Flint DH (1994) Biochemistry 33: 3625-3631.

70. Ifuku O, Kishimoto J, Haze S, Yanagi M, and Fukushima S (1992) Biosci. Biotechnol. Biochem. 56: 1780-1785.

71. Miller JR, Busby RW, Jordan SW, Cheek J, Henshaw TF, Ashley GW, Broderick JB, Cronan JE, Jr., and Marletta MA (2000) Biochemistry 39: 15166-15178.

72. Cicchillo RM, Iwig DF, Jones AD, Nesbitt NM, Baleanu-Gogonea C, Souder MG, Tu L, and Booker SJ (2004) Biochemistry 43: 6378-6386.

73. Ugulava NB, Surerus KK, and Jarrett JT (2002) J. Am. Chem. Soc. 124: 9050-9051.

74. Cicchillo RM, Lee KH, Baleanu-Gogonea C, Nesbitt NM, Krebs C, and Booker SJ (2004) Biochemistry 43: 11770-11781.

75. Taylor AM, Stoll S, Britt RD, and Jarrett JT (2011) Biochemistry 50: 7953-7963.

76. Mulder DW, Boyd ES, Sarma R, Lange RK, Endrizzi JA, Broderick JB, and Peters JW (2010) Nature 465: 248-251.

77. Posewitz MC, King PW, Smolinski SL, Zhang L, Seibert M, and Ghirardi ML (2004) J. Biol. Chem. 279: 25711-25720.

78. Shepard EM, McGlynn SE, Bueling AL, Grady-Smith CS, George SJ, Winslow MA, Cramer SP, Peters JW, and Broderick JB (2010) Proc. Natl. Acad. Sci. U.S.A. 107: 10448-10453.

79. Shepard EM, Duffus BR, George SJ, McGlynn SE, Challand MR, Swanson KD, Roach PL, Cramer SP, Peters JW, and Broderick JB (2010) J. Am. Chem. Soc. 132: 9247-9249.

80. Driesener RC, Challand MR, McGlynn SE, Shepard EM, Boyd ES, Broderick JB, Peters JW, and Roach PL (2010) Angewandte Chemie 49: 1687-1690.

81. Wagner AFV, Frey M, Neugebauer FA, Schafer W, and Knappe J (1992) Proc. Natl. Acad. Sci. U.S.A. 89: 996-1000.

82. Unkrig V, Neugebauer FA, and Knappe J (1989) Eur. J. Biochem. 184: 723-728.

83. Parast CV, Wong KK, Lewisch SA, Kozarich JW, Peisach J, and Magliozzo RS (1995) Biochemistry 34: 2393-2399.

84. Becker A, Fritz-Wolf K, Kabsch W, Knappe J, Schultz S, and Volker Wagner AF (1999) Nat. Struct. Biol. 6: 969-975.

85. Becker A, and Kabsch W (2002) J. Biol. Chem. 277: 40036-40042.

86. Knappe J, and Sawers G (1990) FEMS Microbiol. Rev. 6: 383-398.

87. Plaga W, Vielhaber G, Wallach J, and Knappe J (2000) FEBS Lett. 466: 45-48.

88. Peng Y, Veneziano SE, Gillispie GD, and Broderick JB (2010) J. Biol. Chem. 285: 27224-27231.

89. Plaga W, Frank R, and Knappe J (1988) Eur. J. Biochem. 178: 445-450.

90. Parast CV, Wong KK, Kozarich JW, Peisach J, and Magliozzo RS (1995) J. Am. Chem. Soc. 117: 10601-10602.

91. Lehtiö L, Leppänen VM, Kozarich JW, and Goldman A (2002) Acta Crystallogr. Sect. D 58: 2209-2212.

92. Wagner AFV, Schultz S, Bomke J, Pils T, Lehmann WD, and Knappe J (2001) Biochem. Biophys. Res. Commun. 285: 456-462.

93. Knappe J, Schacht J, Mockel W, Hopner T, Vetter H, Jr., and Edenharder R (1969) Eur. J. Biochem. 11: 316-327.

94. Knappe J, and Schmitt T (1976) Biochem. Biophys. Res. Commun. 71: 1110-1117.

95. Wong KK, Murray BW, Lewisch SA, Baxter MK, Ridky TW, Ulissi-DeMario L, and Kozarich JW (1993) Biochemistry 32: 14102-14110.

96. Frey M, Rothe M, Wagner AF, and Knappe J (1994) J. Biol. Chem. 269: 12432-12437.

97. Broderick JB, Duderstadt RE, Fernandez DC, Wojtuszewski K, Henshaw TF, and Johnson MK (1997) J. Am. Chem. Soc. 119: 7396-7397.

98. Broderick JB, Henshaw TF, Cheek J, Wojtuszewski K, Smith SR, Trojan MR, McGhan RM, Kopf A, Kibbey M, and Broderick WE (2000) Biochem. Biophys. Res. Commun. 269: 451-456.

99. Krebs C, Henshaw TF, Cheek J, Huynh BH, and Broderick JB (2000) J. Am. Chem. Soc. 122: 12497-12506.

100. Külzer R, Pils T, Kappl R, Huttermann J, and Knappe J (1998) J. Biol. Chem. 273: 4897-4903.

CHAPTER 2

GENERAL METHODS

Growth and Purification of PFL

The pKK223-3 vector containing the *Escherichia coli pflB* gene was transformed into *Escherichia coli* BL21(DE3)pLysS for PFL expression. Fifty mL of LB media with 50 μg/mL of ampicillin was inoculated with one colony of the PFL expressing *E. coli* and grown overnight at 37°C with shaking at 250 rpm. The overnight culture was added to 10 L of LB media with 50 μg/mL of ampicillin and incubated at 37°C in a 10 L New Brunswick benchtop fermentor with 250 rpm stirring. Compressed air was purged through the fermentor at a flow rate of 5 L/min. When the cells reached early log phase at an OD_{600} of approximately 0.6-0.8, isopropyl-β-D-thiogalactopyranoside (IPTG) was added to a final concentration of 1 mM to induce protein expression. The growth was allowed to continue for an additional 3 hours at which point the cells were harvested by centrifugation at 6,000 rpm for 10 minutes at 4°C, frozen with liquid nitrogen and stored at -80°C. Average cell yields are 3.5 mg/L.

Cells were thawed and suspended, at an approximate ratio of 2 mL lysis buffer per 1 g of cell paste, in 20 mM Tris, pH 7.2, 1% Triton X-100, 5% (w/v) glycerol, 10 mM $MgCl_2$, 8 mg lysozyme (per 50 mL buffer), 1 mM phenylmethylsulfonyl fluoride (PMSF), and trace amounts of RNase A and DNase I (approximately 0.1 mg each per 50 mL buffer). The suspension was stirred at 4°C and homogenized by agitation with a 30 mL syringe and 18 gauge needle for 1 hour. The lysed cells were centrifuged at 18,000

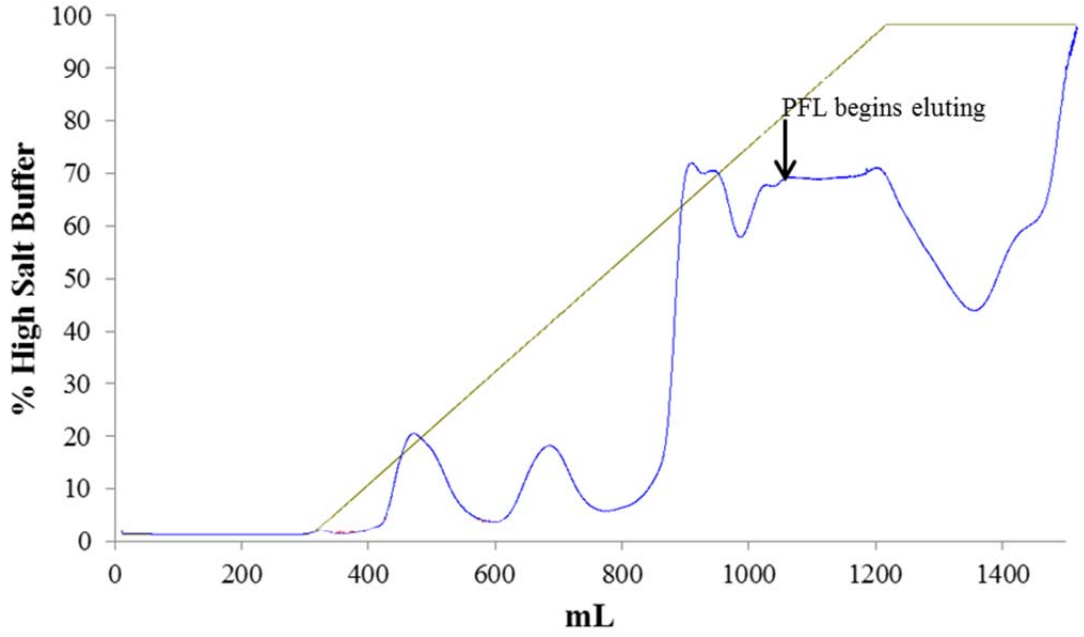

Figure 2.1. Representative chromatogram of PFL purification on the Waters AP-5 300 mm column containing Accell Plus QMA resin. Buffers utilized were No Salt Buffer (20 mM Tris, pH 7.2, 1 mM DTT) and High Salt Buffer (20 mM Tris, pH 7.2, 200 mM NaCl, 1 mM DTT). PFL elutes with approximately 170 mM NaCl which is indicated by the arrow in this chromatogram.

rpm for 30 minutes at 4°C at which point the lysate was decanted and centrifuged for an additional 30 minutes. The lysate was decanted and either directly purified or flash-frozen with liquid nitrogen and stored at -80°C. Approximately 30 mL of lysate was loaded onto a Waters AP-5 300 mm column containing Accell Plus QMA resin equilibrated with No Salt Buffer (20 mM Tris, pH 7.2, 1 mM DTT). No Salt Buffer was used to wash the column with 300 mL after which a gradient from No Salt Buffer to High Salt Buffer (20 mM Tris, pH 7.2, 200 mM NaCl, 1 mM DTT) was run over 900 mL followed by another wash of High Salt Buffer for 300 mL. Using these conditions PFL elutes with approximately 170 mM NaCl (Figure 2.1). Fractions containing ≥50% pure PFL as judged by SDS-PAGE were combined, concentrated using a Millipore Amicon

Ultra centrifugal device with a 30K MWCO filter to 10 mL or less, and buffer exchanged into Buffer B (20 mM Tris, pH 7.2, 1 M $(NH_4)_2SO_4$, 1 mM DTT). This protein solution was then loaded onto a HighLoad High Performance 16/10 phenyl sepharose column equilibrated with Buffer B. A column wash with Buffer B was performed with 50 mL followed by a 50 mL gradient to Buffer A (20 mM Tris, pH 7.2, 1 mM DTT). A final Buffer A step was completed with 50 mL. PFL elutes at the beginning of the final Buffer A step (Figure 2.2), and fractions containing ≥95% pure PFL as judged by SDS-PAGE (Figure 2.3) were pooled, concentrated using a Millipore Amicon Ultra centrifugal device with a 10K MWCO filter, flash-frozen, and stored at -80°C. Average protein yields are 27 mg per 1 L of growth.

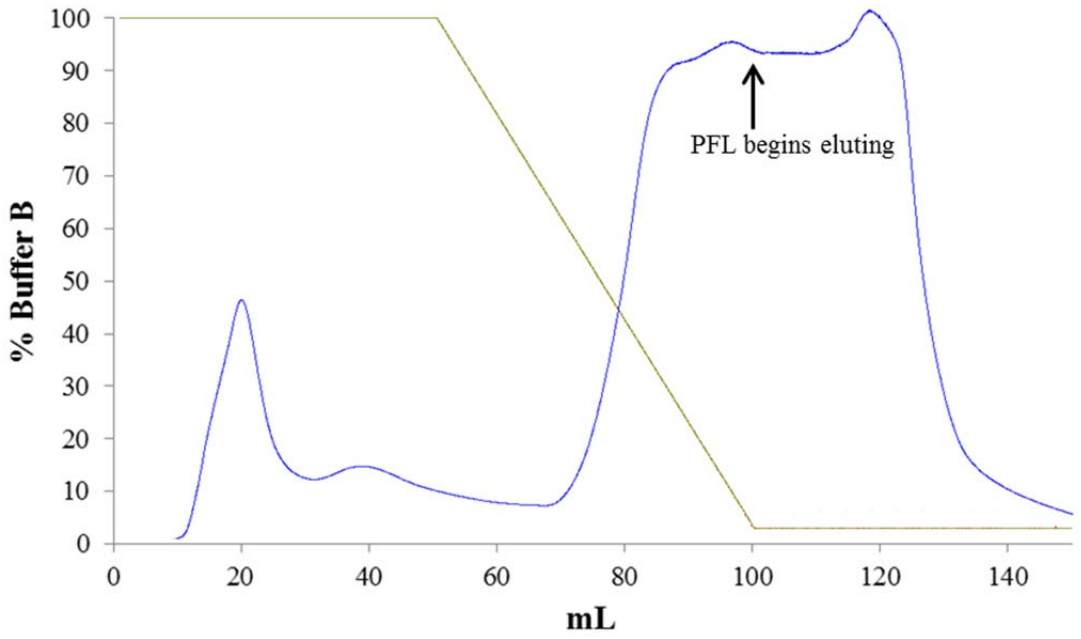

Figure 2.2. Representative chromatogram of PFL purification on the HighLoad High Performance 16/10 phenyl sepharose column. Buffers used were Buffer B (20 mM Tris, pH 7.2, 1 M $(NH_4)_2SO_4$, 1 mM DTT) and Buffer A (20 mM Tris, pH 7.2, 1 mM DTT). PFL elutes with 100% Buffer A as indicated by the arrow in this chromatogram.

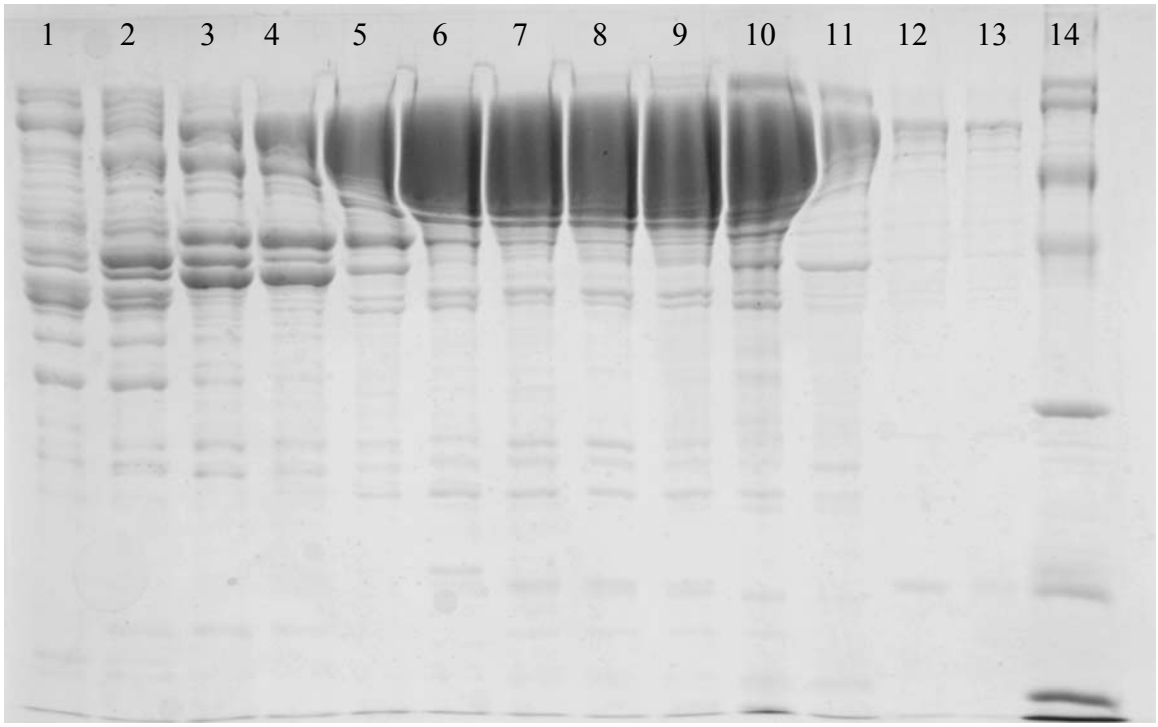

Figure 2.3. Representative SDS-PAGE gel from PFL purification after the HighLoad High Performance 16/10 phenyl sepharose column. Lanes 1-13 are Fractions 1, 3, 5, 6, 8, 10, 12, 14, 15, 17, 19, 21, and 23 respectively from Figure 2.2. Lane 14 is a molecular weight marker.

Purified PFL was degassed on a Schlenk line using the freeze-pump-thaw method. PFL was placed in a round bottom flask fitted with a schlenk line compatible top and frozen in a thin layer around the bottom and sides of the flask. A vacuum was pulled on the flask for 10-20 minutes (depending on sample size). The flask was then filled with nitrogen gas, and the protein was allowed to thaw. This cycle was repeated for a total of three times. The protein was then brought into an MBraun Unilab anaerobic glovebox containing ≤1 ppm oxygen to be aliquoted in screw top vials containing an o-ring. The protein samples were then flash-frozen and stored at -80°C.

Growth and Purification of PFL-AE

The pCAL-nEK vector containing the *Escherichia coli pflA* gene was transformed into *Escherichia coli* BL21(DE3)pLysS for PFL-AE expression. 50 mL of LB media with 50 μg/mL of ampicillin and 34 μg/mL chloramphenicol was inoculated with one colony of the PFL-AE expressing *E. coli* and grown overnight at 37°C with shaking at 250 rpm. The overnight culture was added to 9.8 L of minimal media with 50 μg/mL of ampicillin, 34 μg/mL chloramphenicol, glucose solution, and vitamins. Minimal media consists of 100g Casamino acids, 84.2g MOPS, 8.0g Tricine, 14.7g NaCl, 16.0g KOH, and 5.1g NH_4Cl in 9.8 L of H_2O; the glucose solution contains 50g glucose in 200mL H_2O, 25mL "O" solution (0.1 g $FeCl_2 \cdot 4H_2O$ dissolved in 10 mL of 12 M HCl with 1 mL "T" solution [18.4 mg $CaCl_2 \cdot 2H_2O$, 64 mg H_3BO_3, 40 mg $MnCl_2 \cdot 4H_2O$, 18 mg $CoCl_2 \cdot 6H_2O$, 4 mg $CuCl_2 \cdot 2H_2O$, 340 mg $ZnCl_2$, and 605 mg $Na_2MoO_4 \cdot 2H_2O$ diluted to 100 mL with H_2O] and 2.68 g $MgCl_2 \cdot 6H_2O$ brought up to a final volume of 50 mL with H_2O), 25mL 1M KH_2PO_4, 12.5mL 276mM K_2SO_4, and 62.5mL 0.1M $CaCl_2$; vitamins are 10mg each of biotin, pantothenic acid, vitamin B12, thiamine, folic acid, riboflavin, niacinamide, thioctic acid, and pyridoxine. The growth was incubated at 37°C in a 10 L New Brunswick benchtop fermentor with 250 rpm stirring, and compressed air was purged through the fermentor at a flow rate of 5 L/min. When the cells reached an OD_{600} of approximately 0.5, isopropyl-β-D-thiogalactopyranoside (IPTG) was added to a final concentration of 0.5 mM to induce protein expression, and the media was supplemented with 750 mg of $Fe(NH_4)_2(SO_4) \cdot 6H_2O$. The growth was allowed to continue for an additional 2 hours at which point it was cooled. When the temperature reached 30°C, the

fermentor was purged with nitrogen gas, and at 20°C it was moved to a 4°C fridge where sparging with nitrogen gas continued overnight and 750 mg of $Fe(NH_4)_2(SO_4)•6H_2O$ was again added. Cells were harvested by centrifugation at 6,000 rpm for 10 minutes at 4°C, frozen with liquid nitrogen and stored at -80°C. Average cell yields are 5 g/L.

Purification was carried out under anaerobic conditions in a Coy anaerobic chamber (Coy Laboratories, Grass Lake, MI) for all following steps. Cells were thawed and suspended, at an approximate ratio of 2 mL lysis buffer per 1 g cell paste, in 50 mM Tris, pH 7.5, 200 mM NaCl, 1% (w/v) Triton X-100, 5% (w/v) glycerol, 10 mM $MgCl_2$, 1 mM DTT, 1 mM PMSF, 16 mg lysozyme (per 100 mL buffer), and trace amounts of DNase I and RNase A (approximately 0.2 mg each). The suspension was gently stirred for 15 minutes and then stirred on ice for an additional 45 minutes. A 30 mL syringe and 18 gauge needle were also used to homogenize the solution. The lysed cells were centrifuged at 18,000 rpm for 30 min at 4°C at which point the lysate was decanted and centrifuged for a second time. The lysate was decanted and loaded onto a Waters AP-5 600 mm column containing preparatory grade Superdex 75 resin which was first washed with 1 mM dithionite to help eliminate residual oxygen and then equilibrated with Gel Filtration Buffer (50 mM Tris, pH 7.5, 200 mM NaCl, 1 mM DTT). The Gel Filtration Buffer was washed over the column for a total of 900 mL, and PFL-AE begins to elute between 550 and 600 mL of filtrate (Figure 2.4). Fractions containing a dark brown color and an absorbance at 426 nm were pooled and concentrated using a Millipore Amicon Ultra centrifugal device with a 10K MWCO filter to 10 mL or less, flash-frozen, and stored at -80°C overnight. The following day, the stored protein was loaded back onto

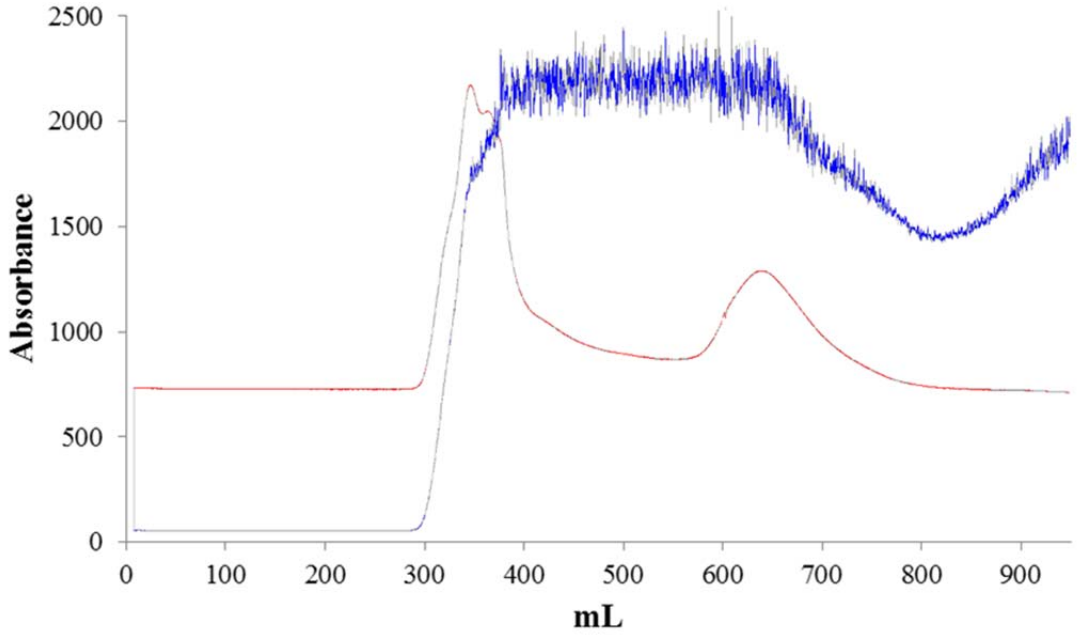

Figure 2.4. Representative chromatogram from the first Superdex 75 column of PFL-AE purification using Gel Filtration Buffer (50 mM Tris, pH 7.5, 200 mM NaCl, 1 mM DTT). The blue trace represents the absorbance at 280 nm and the red at 426 nm (split in trace results from an auto-zeroing). PFL-AE begins to elute between 550 and 600 mL of filtrate. Fractions containing a dark brown color and an absorbance at 426 nm are kept.

the superdex 75 resin, which was reequilibrated with Gel Filtration Buffer, and gel fitrated with Gel Filtration Buffer. PFL-AE began to elute after 600 mL of filtrate (Figure 2.5). The ratio of the absorbance at 426 nm to 280 nm was obtained using a Thermo Scientrific Evolution 60 spectrophotometer, and fractions with the highest ratio were pooled and concentrated using a Millipore Amicon Ultra centrifugal device with a 10K MWCO filter, aliquoted into screw cap vials with o-rings, flash-frozen, and stored at -80°C. Average protein yields are 13.5 mg protein per 1 L of growth.

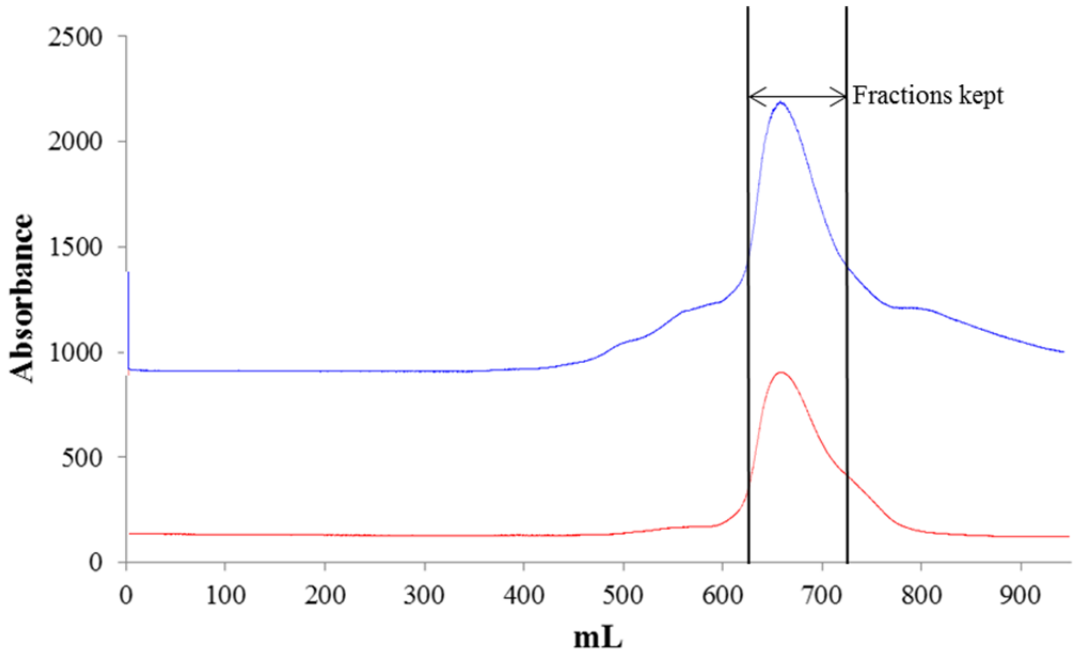

Figure 2.5. Representative chromatogram from the second Superdex 75 column of PFL-AE purification using Gel Filtration Buffer (50 mM Tris, pH 7.5, 200 mM NaCl, 1 mM DTT). The blue trace represents the absorbance at 280 nm and the red at 426 nm (split in trace results from an auto-zeroing). PFL-AE begins to elute after 600 mL of filtrate. Fractions containing the highest ratio of the absorbance at 426 nm to 280 nm were kept.

Protein and Iron Quantification

Protein concentration was determined by the method of Bradford [1] using a dye kit from Bio-Rad and bovine serum albumin (BSA) as a standard. For PFL-AE, a correction factor for the Bradford assays was determined by amino acid hydrolysis of the purified enzyme, completed at the MBC Core Facility, University of Massachusetts, Amherst [2]. Briefly, 0.1 mg/mL BSA was added to a total of 800 µL H_2O in differing amounts (usually to a final amount of 1, 2, 3, 4, 5, and 6 µg BSA in each standard) to which 200 µL of Bradford dye was added. The samples were incubated at room temperature for approximately 30 minutes, and then the absorbance at 595 nm was

recorded using a Thermo Scientrific Evolution 60 spectrophotometer to create a standard curve. Protein samples were made (by substituting protein for BSA) such that the absorbance fell within the standard curve range.

Iron assays were performed according to the method of Beinert [3]. An iron standard of 10 μg/mL was used to create a standard curve by adding differing amounts (usually to a final amount of 0.4, 0.8, 1.2, 1.6, and 2.0 μg Fe in each standard) to a final volume of 1 mL. Protein samples were made (by substituting protein for Fe standard) such that the absorbance fell within the standard curve range. To each of the samples 500 μL of 1:1 1.2 M HCL: 4.5% $KMnO_4$ was added, and they were then incubated for 2 hours in a 65°C water bath. After the incubation, 100 μL of Reagent B (4.90 g ammonium acetate and 4.4 g ascorbic acid were dissolved in 5 mL H_2O; 40 mg each of neocuproine and ferrozine were added, and the volume was brought up to 12.5 mL with H_2O) was added to each. The samples were vortexed for approximately 5 seconds every 10 minutes for a total of 30 minutes at room temperature. The absorbance at 562 nm was recorded using a Thermo Scientrific Evolution 60 spectrophotometer.

Synthesis and Purification of SAM

In a small vial, 8.275 mL of 100 mM Tris HCl, pH 8, 37 mg KCl, 53 mg $MgCl_2$, 18 μL 0.5 M EDTA, 73 mg ATP, 18 mg L-methionine, 800 μL βME (β-mercaptoethanol), 5 μL inorganic phosphatase, and 1 mL SAM synthetase crude lysate, were added together and gently stirred for 15-16 hours at room temperature. The reaction was quenched with 1 mL of 1 M HCl and centrifuged at 18,000 rpm and 4°C for 30

minutes. The supernatant was decanted in equal portions into two falcon tubes and stored at 4°C until purification. For the SAM synthetase crude lysate SAM synthetase overproducing strain DM22 (pK8) was stored in 50% glycerol at –80°C. A single colony of transformed cells was used to inoculate 50 mL LB media containing 30 μg/mL oxytetracycline (LB/Tet). This culture was grown for 12-14 hours to saturation and then used to inoculate 700 mL LB/Tet in each of 4 x 2800 mL Fernbach culture flasks. The culture was grown at 37°C with vigorous shaking for 12-14 hours before harvesting by centrifugation at 8,000 rpm for 10 min. The supernatant was decanted and the cells stored at -80°C. Cell paste was suspended in 100 mM Tris-HCl, pH 8.0 containing 1 mM EDTA (3–3.5 mL/g cells). Lysozyme was added at 50 μg/mL phenylmethylsulfonyl fluoride (PMSF) at a final concentration of 0.1 mM plus trace amounts of RNase and DNase. The suspension was incubated at 4˚C for 1.5 hours with stirring. The suspension was centrifuged at 15,000 rpm for 20 min. The supernatant was decanted and stored unpurified at –80˚C in 1 mL Eppendorf tubes until needed.

Approximately 5 mL of the SAM synthesis reaction was loaded onto an HR 10/10 column containing Source 15S resin equilibrated with Buffer A (H_2O). The column was washed with 30 mL of Buffer A, and then a gradient to 10% Buffer B (1 M HCl) was applied over 15 mL. 10% Buffer B was run for another 15 mL before a gradient to 100% Buffer B was achieved over 100 mL. Buffer B was used to wash for 20 mL and a gradient to Buffer A was accomplished over 10 mL. A final 40 mL wash of Buffer A

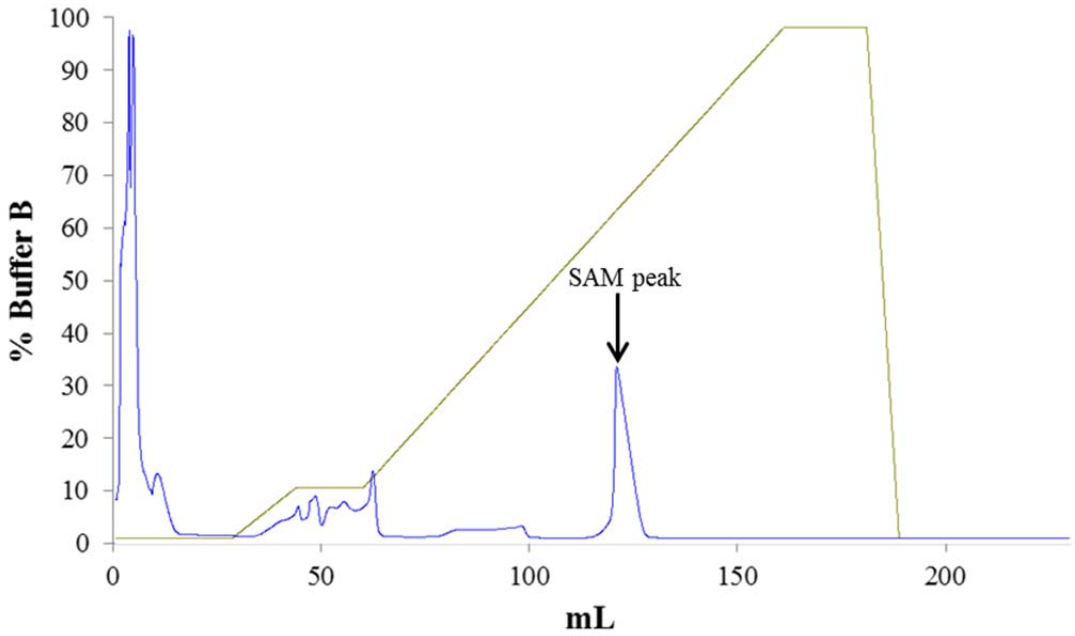

Figure 2.6. Representative chromatogram from SAM purification on the Source 15S column using Buffer A (H_2O) and Buffer B (1 M HCl). SAM elutes at approximately 0.6 M HCl or 120 mL in this chromatogram.

was performed before the second half of the SAM synthesis was loaded for purification as above. SAM elutes at approximately 0.6 M HCl (Figure 2.6). Purified SAM was lyophilized overnight and brought into an MBraun Unilab anaerobic glovebox containing ≤1 ppm oxygen for reconstitution. SAM was dissolved in 100 mM Tris and the pH was adjusted to approximately 7.0 to 7.5 after which the final Tris concentration was brought to 50 mM with additional water. SAM was aliquoted into screw cap vials with o-rings, flash-frozen, and stored at -80°C. SAM concentration was calculated by determining the absorbance at 260 nm and using 16,000 M^{-1} cm^{-1} as the extinction coefficient for SAM at 260 nm.

References

1. Bradford MM (1976) Anal. Biochem. 72: 248-254.

2. Broderick JB, Duderstadt RE, Fernandez DC, Wojtuszewski K, Henshaw TF, and Johnson MK (1997) J. Am. Chem. Soc. 119: 7396-7397.

3. Beinert H (1978) Methods Enzymol. 54: 435-445.

CHAPTER 3

THE ACTIVATION OF PYRUVATE FORMATE-LYASE ACTIVATING ENZYME IS STIMULATEDBY K^+

Contribution of Authors and Co-Authors

Manuscripts in Chapters 3, 4, and 7

Author: Rachel U. Hutcheson

Contributions: Performed activity assays in the presence of Na^+, K^+, NH_4^+, Rb^+, and Cs^+ as well as differing K^+ concentrations and prepared and ran PFL-AE EPR samples in the presence of Na^+, K^+, NH_4^+, Rb^+, and Cs^+. Generated figures and wrote the manuscript in preparation for submission.

Co-author: Kaitlin S. Duschene

Contributions: Aided in the acquisition of UV-Vis data from PFL-AE activity assays in the presence of Na^+, K^+, NH_4^+, Rb^+, and Cs^+ as well as differing K^+ concentrations.

Co-author: Adam V. Crain

Contributions: Performed PFL-AE activity assays with choline chloride.

Co-author: Ashley Rasmussen

Contributions: Aided in the acquisition of UV-Vis data from initial PFL-AE activity assays in the presence of Na^+, K^+, NH_4^+, Rb^+, and Cs^+.

Co-author: Jian Yang

Contributions: Prepared PFL-AE EPR samples in the presence of varying K^+ concentrations for the determination of the K_D of K^+ binding.

Co-author: Jessica L. Vey

Contributions: Collected X-ray data and solved PFL-AE structures in the presence of SAM as well as SAM and the 7-mer peptide.

Co-author: Catherine L. Drennan

Contributions: Assisted with X-ray data analysis and interpretation of data.

Co-author: Joan B. Broderick

Contributions: Provided important insight and overview of the activity assays, preparation of the EPR samples, interpretation of results, and aided in the preparation of the manuscript and figures.

Manuscript Information Page

Rachel U. Hutcheson, Kaitlin S. Duschene, Adam V. Crain, Ashley Rasmussen, Jian Yang, Jessica L. Vey, Catherine L. Drennan, Joan B. Broderick
Biochemistry
Status of the manuscript:
__X__Prepared for submission to a peer-reviewed journal
____ Officially submitted to a peer-reviewed journal
____ Accepted by a peer-reviewed journal
_____Published in a peer-reviewed journal

Published by the American Chemical Society

THE ACTIVATION OF PYRUVATE FORMATE-LYASE ACTIVATING ENZYME IS STIMULATED BY K^+

The following work is currently in progress to be submitted for publication

Rachel U. Hutcheson[1], Kaitlin S. Duschene[1], Adam V. Crain[1], Ashley Rasmussen[1], Jian Yang[1], Jessica L. Vey[2], Catherine L. Drennan[2], Joan B. Broderick[1]

1. *Department of Chemistry and Biochemistry and the Astrobiology Biogeocatalysis Research Center, Montana State University, Bozeman, MT 59717*
2. *Departments of Chemistry and Biology, Massachusetts Institute of Technology, Cambridge, MA 02139*

Abstract

Pyruvate formate-lyase activating enzyme (PFL-AE), which activates pyruvate formate-lyase (PFL) by generating a catalytically essential glycyl radical on PFL, is one of the earliest known members of the radical SAM superfamily. This family of enzymes utilizes a [4Fe-4S] cluster to reductively cleave SAM (*S*-adenosylmethionine) to produce a 5'-deoxyadenosyl (dAdo) radical intermediate. These enzymes also share a common structural core composed of either a full $(\alpha/\beta)_8$, or partial $(\alpha/\beta)_6$, TIM barrel fold. The crystal structure of PFL-AE reveals the presence of a monovalent cation, modeled as Na^+. The significance of this cation in PFL-AE function has been explored by using activity assays as well as EPR spectroscopic studies of PFL-AE with and without SAM bound. Of the five monovalent cations tested (Na^+, K^+, NH_4^+, Rb^+, and Cs^+), PFL-AE is active in the presence of all of them. Additionaly, an apparent binding constant of approximately 6.5 mM as estimated by EPR spectroscopy was determined for K^+. The activity of PFL-AE is also dependent on the concentration of potassium ion in the assay, with an increase in activity correlated with an increase in cation concentration. The EPR signal associated

with the $[4Fe\text{-}4S]^{+}$ cluster in reduced PFL-AE is significantly affected by the presence of the different cations, pointing to effects on the electronic structure as would be expected from the cation's location within the active site.

Introduction

Pyruvate formate-lyase activating enzyme (PFL-AE) is a member of the radical *S*-adenosylmethionine (SAM) superfamily [1], which is involved in reactions across the phylogenic kingdom including enzyme activation, DNA repair, viral inhibition, cofactor maturation, large biomolecule modification, as well as numerous others [2, 3]. Radical SAM enzymes share a common CX_3CX_2C motif, or variation thereof, that coordinates a site-differentiated [4Fe-4S] cluster, and the unique iron of the cluster is ligated by the amino and carboxy moieties of SAM [4, 5]. The reduced $[4Fe\text{-}4S]^{1+}$ cluster reductively cleaves SAM forming methionine and a 5'-deoxyadensyl (dAdo) radical [6]. This radical then abstracts a hydrogen atom from the substrate beginning the different reactions catalyzed by these enzymes. In the case of PFL-AE the dAdo radical abstracts a hydrogen atom from glycine 734 of pyruvate formate-lyase (PFL), a 170 kDa homodimer [7, 8]. PFL is a central enzyme involved in anaerobic glucose metabolism, and is responsible for conversion of pyruvate and coenzyme A (CoA) to formate and acetyl-CoA under anaerobic conditions [7, 8].

Two crystal structures of PFL-AE have been solved: one with PFL-AE in complex with SAM and the other with PFL-AE in complex with SAM and a 7-mer PFL peptide substrate analog containing the catalytic glycine (Figure 3.1) [9]. The

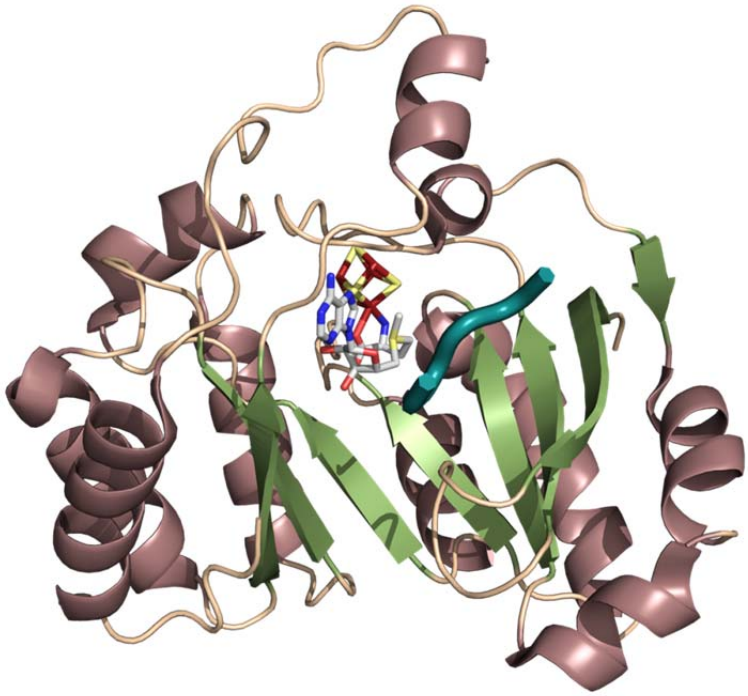

Figure 3.1. Crystal structure of PFL-AE with SAM (light grey sticks) and PFL peptide (thick teal loop) bound. SAM is bound to the Fe-S cluster (red and yellow cube) through its amino and carboxy moieties. The 7-mer PFL peptide corresponds to the PFL radical loop containing Gly734 where the glycyl radical is formed. PFL-AE displays a partial $(\alpha/\beta)_6$ TIM barrel with a large opening capable of accommodating its large 170 kDa substrate PFL.

combination of these two structures has given insight into the mechanism of PFL-AE activity. As with other radical SAM enzymes, the PFL-AE structure is composed of a triosephosphate isomerase (TIM) barrel. In PFL-AE it is a partial $(\alpha/\beta)_6$ barrel with a wide opening able to accommodate the large substrate PFL. These structures confirm the binding of SAM through the amino and carboxy moieties to the unique iron of the cluster as was first indicated by results obtained from ENDOR spectroscopy [5]. Two motifs present in PFL-AE, which are conserved in the radical SAM superfamily, show interactions with SAM. The GGE motif (PFL-AE residues G^{77}, G^{78}, and E^{79}) directly binds the methionine portion of SAM The GXIXGXXE motif (V^{168}, V^{170}, G^{172}, and E^{175}

in PFL-AE) stabilizes the adenine moiety binding site; the adenine ring of SAM is also packed against two histidines (H^{37} and H^{202}). In addition, the PFL-AE structure containing the PFL peptide shows substrate binding across the lateral opening of the barrel. Interactions between PFL-AE and the peptide are mainly between the peptide backbone and PFL-AE side chains. One of the interactions from PFL-AE includes the highly conserved DGXGXR motif located on loop A (residues 10-20), and upon peptide binding this loop undergoes a large conformation change by swinging up into the active site to establish these interactions. The movement of this loop is thought to be essential to the activation of PFL possibly through orienting the glycine loop of PFL in the active site. The positioning of the peptide in the active site of PFL-AE is an interesting observation as in the PFL crystal structure (Figure 3.2) the glycine from which a hydrogen atom is abstracted is buried approximately 8 Å from the surface [10].

PFL is a homodimer with each monomer constructed as a 10 stranded α/β barrel and the active site located at the center. Also within the active site are two catalytically essential cysteine residues, Cys418 and Cys419. In order for turnover of pyruvate by PFL to occur the radical must be transferred from Gly734 to Cys419 necessitating the positioning of the glycyl radical in the active site [10, 11]. However, the formation of the glycyl radical by PFL-AE occurs through a site-specific abstraction of the pro-*S* hydrogen of Gly734 [12]. Combined with the structure of PFL-AE with peptide bound, this suggests that a conformational change by PFL is required for the glycine containing loop to be accessible to the active site of PFL-AE. In fact, recent data suggest that PFL assumes a more open conformation in the presence of PFL-AE including a decrease in

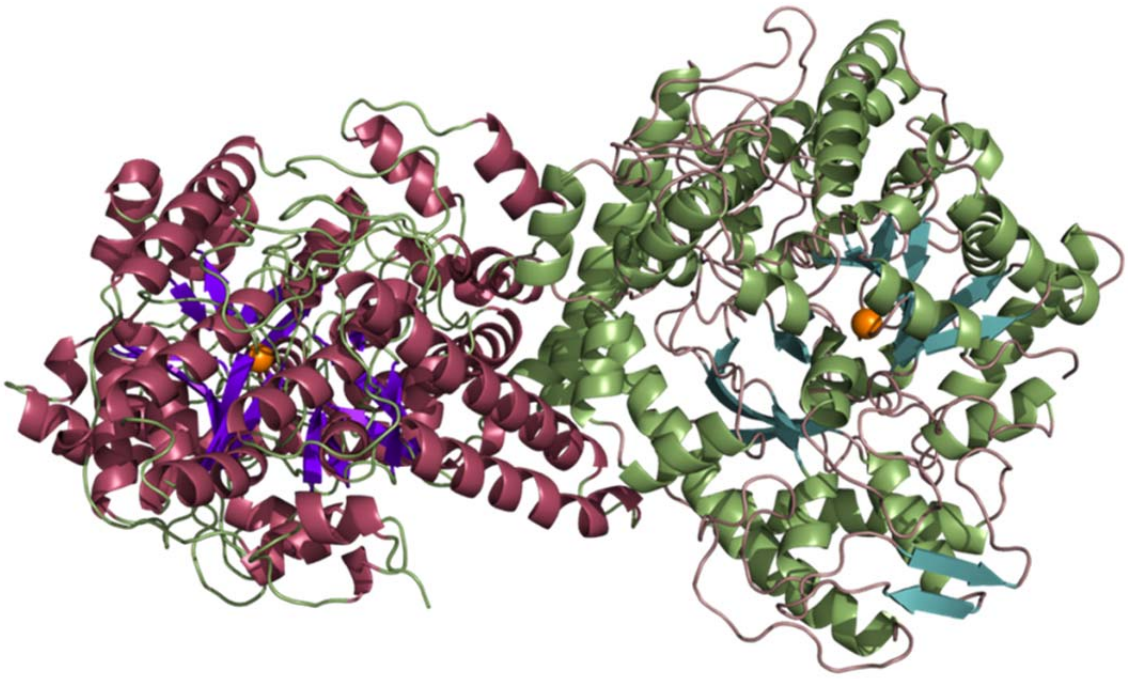

Figure 3.2. The PFL crystal structure with one monomer is shown in purple and the other in green. Glycine 734, which harbors the glycyl radical, is shown as an orange sphere and is buried within the active site near the center of the 10 stranded α/β barrel. Also in the active site near Gly734 on an opposing finger loop are the two catalytic cysteine residues, Cys418 and Cys419. The distance between Gly734 Cα and Cys419 Sγ is 3.7 Å.

the T_m of PFL, lower PFL activity, and a less stable glycyl radical that experiences less H/D exchange [13]. In the proposed open conformation of PFL the radical loop containing Gly-734 flips out of the protein so that it can be accessed by PFL-AE [13].

After publication of the PFL-AE crystal structures, further analysis revealed the presence of a monovalent cation, M^+, (modeled as a sodium ion in the structure) in the active site. The two most likely and biologically relevant cations are Na^+ and K^+, but determining which cation it is in a crystal structure can be difficult; Na^+ has the same number of electrons as a water molecule and K^+ has an ionic radius almost identical to a water molecule [14]. However, some insight can be gained from the distances between

M^+ and the atoms with which it interacts: an average of ~2.4 Å for Na^+ and ~2.8 Å for K^+ [15]. As shown by this study, the most likely candidate is K^+, an essential element required for the catalysis of a number of enzymes such as diol dehydratase, glycerol dehydratase, GroEL, and pyruvate kinase [14, 16-20].

Activation of an enzyme by M^+ is not accomplished through regulation as concentrations of Na^+ and K^+ are both tightly controlled within a cell [21]. Instead the M^+ cation assists in binding of substrate and catalysis through lowering of the energy barriers in the ground and/or transition states [14]. This can occur when the M^+ ion is used to directly interact with the substrate or when M^+ binding to the enzyme triggers conformation changes. These two different effects are used to separate enzymes activated by M^+ (such as Na^+ or K^+) into two types, type I and type II [14]. In type I enzymes the M^+ is cofactor-like and helps to anchor the substrate in the active site. It is also absolutely required for enzyme activity. Type II enzymes use M^+ as an allosteric effector. Upon M^+ binding (and no direct substrate contact), conformational changes are elicited which enhance enzyme activity; however the M^+ is not absolutely required for activity. For example in the type I enzyme diol dehydratase, a coenzyme B_{12}-dependent enzyme, the absolute requirement of K^+ [22] is explained by the crystal structure of the enzyme bound to propanediol. The K^+, coordinated by five protein ligands, draws in the substrate through interactions with two of its hydroxyl oxygens, and so the absence of K^+ would preclude substrate binding [19]. Aminoimidazole riboside kinase is a type II activated enzyme, and the binding of K^+ is proposed to alter the conformation of the backbone residues 252-255 [23]. The alteration would position the catalytic Asp255 in a

manner that would allow it to interact with the phosphate moiety of the nucleotide thus enabling phosphorylation of the substrate aminoimidazole riboside [23]. For M^+ activated enzymes, those activated by K^+ can also be activated by NH_4^+ and Rb^+ but are not activated as well by the smaller Na^+ or the larger Cs^+ cations, while Na^+ activated enzymes are not activated as well by any of the larger cations (K^+, Rb^+, and Cs^+) nor the smaller Li^+ cation [24]. In this work, we demonstrate that PFL-AE activity is highest in and stimulated by the presence of K^+. In the presence of NH_4^+ and Rb^+ PFL-AE also shows a high activity while the presence of Na^+ or Cs^+ results in a slightly lower activity.

Materials and Methods

PFL and PFL-AE Growth and Purification

PFL and PFL-AE were both grown and purified as previously described [6, 25-27]. Briefly, the *Escherichia coli* genes *pflA* (PFL-AE) and *pflB* (PFL) were individually expressed in *Escherichia coli* BL21(DE3)pLysS. PFL-AE was anaerobically purified using a Waters AP-5 600 mm column containing preparatory grade Superdex 75 resin. PFL was aerobically purified first on a Waters AP-5 300 mm column containing Accell Plus QMA resin followed by a HighLoad High Performance 16/10 phenyl sepharose column. PFL was degassed on a Schlenk line prior to use.

Protein and Fe Quantitation

Protein concentration was determined by the method of Bradford [28] using dye reagent from Biorad. A correction factor, determined by acid hydrolysis [25] was utilized in the final calculations of PFL-AE concentration. Iron content was determined

using the method of Beinert [29]. PFL-AE contained between 3 and 4 Fe per protein for the following experiments unless otherwise indicated.

PFL-AE Activity Assays

PFL-AE activity was assayed in a Unilab MBraun anaerobic chamber containing $\leq$ 1 ppm O_2 using a modified version of the coupled enzyme assays as previously published [25, 30, 31]. An activation solution containing 0.05 μM PFL-AE, 5 μM PFL, 0.1 mM SAM, 10 mM oxamate, 8 mM DTT, 30 μM 5-deazariboflavin (added last in the dark), 0.1 M Tris, pH 7.6, and 0.1 M of one of the following: NaCl, KCl, NH_4Cl, RbCl, or CsCl was mixed. This mix was photoreduced by illumination with a 300 W halogen lamp at 25°C ± 1°C for a specified amount of time (usually 0, 2, 4, 5, 10, or 15 minutes) and then covered with foil to prevent further reduction. The coupling solution used in conjunction with the activation solution contained 3 mM NAD+, 55 μM coenzymeA, 0.1 mg/mL BSA, 10 mM pyruvate, 10 mM malate, 2 U/mL citrate synthase, 30 U/mL malic dehydrogenase, 10 mM DTT, and 0.1 M Tris, pH 8.1 and was kept at room temperature. All solutions were degassed on a Schlenk line and solids were brought into the chamber prior to mixing. (For the determination of the dependence of PFL-AE activity on the concentration of K^+, the concentration of K^+ in the activation solution was changed to either 50 mM, 25 mM, 10 mM, or 0 mM. The ionic strength was maintained by adding choline chloride and PFL-AE was exchanged into a choline chloride buffer to remove Na^+ present from purification. However, this did cause a loss of iron and PFL-AE in these assays contained approximately 2.5 Fe per protein)

To assay the activity 5 µL of the activation solution was placed on a lid of an anaerobic cuvette containing 895 µL of coupling solution prior to its removal from the chamber. The two solutions were mixed just prior to placing in a thermostatted (at 30°C) Cary 6000i UV-Vis spectrophotometer. The absorbance at 340 nm was recorded for 90 seconds. One unit of PFL activity corresponds to the production of one µmole of pyruvate per minute, and 35 units of PFL is equivalent to 1 nmole of PFL active sites [32]. The definition of one unit of PFL-AE activity is the amount that catalyzes the production of 1 nmole of active PFL per minute [25].

Determination of K_D for K^+

A mixture containing 200 µM PFL-AE, 2 mM SAM, 200 µM 5-deazariboflavin (added last in the dark), 1 mM DTT, 50 mM Tris, pH 8.5, and either 0, 1, 2, 5, 10, 20 50, 100, or 200 mM KCl (total ionic strength was maintained at 200 mM with NaCl). The mixture was then placed in an EPR tube and photoreduced by illumination with a 300 W halogen lamp in an ice bath for one hour. The samples were then frozen with liquid nitrogen.

EPR Sample Preparation

In an Mbruan anaerobic chamber with ≤1 ppm O_2 200 µM PFL-AE, 200 µM 5-deazariboflavin (added last in the dark), 5 mM DTT, 100 mM Tris, pH 7.6, and 200 mM of one of the following: NaCl, KCl, NH_4Cl, RbCl, or CsCl was placed in an EPR tube. Photoreduction was accomplished by illumination with a 300 W halogen lamp in an ice bath for one hour, and samples without SAM were frozen with liquid nitrogen. For

samples with SAM the solution was removed; SAM was added to a final concentration of 2 mM and allowed to incubate for 5-10 minutes before freezing in liquid nitrogen.

EPR Spectroscopy

EPR spectra were recorded on a Bruker EMX X-band spectrometer equipped with a liquid helium cryostat and temperature controller from Oxford Instruments. Typical experiment parameters were 12 K and 9.37 GHz, with 1.83 mW microwave power, 100 kHz modulation frequency, and 10 G modulation amplitude. Each spectrum is the average of two scans.

Results

A Monovalent Cation is in the Active Site of PFL-AE

Further analysis of the PFL-AE crystal structure with SAM and PFL peptide bound indicated the presence of a monovalent cation located in the active site (Figure 3.3), but was not detected in the structure with only SAM bound. Many interactions between proteins and an M^+ ion occur through carbonyl oxygen atoms. In the PFL-AE structure the monovalent cation interacts with four amino acid oxygens as well as one SAM oxygen. The cation interactions with the four amino acids include two with backbone carbonyl oxygens from Thr105 and Met127 as well as two with side chain residue carbonyl oxygens from Asp104 and Asp129 (Figure 3.4 A). All of these interactions are within 3 Å of the cation, and all four of the amino acids appear to be strictly conserved in PFL-AE. Like diol dehydratase, the interaction between the cation and SAM also involve an oxygen atom (Figure 3.4 B). This interaction at 2.4 Å is from

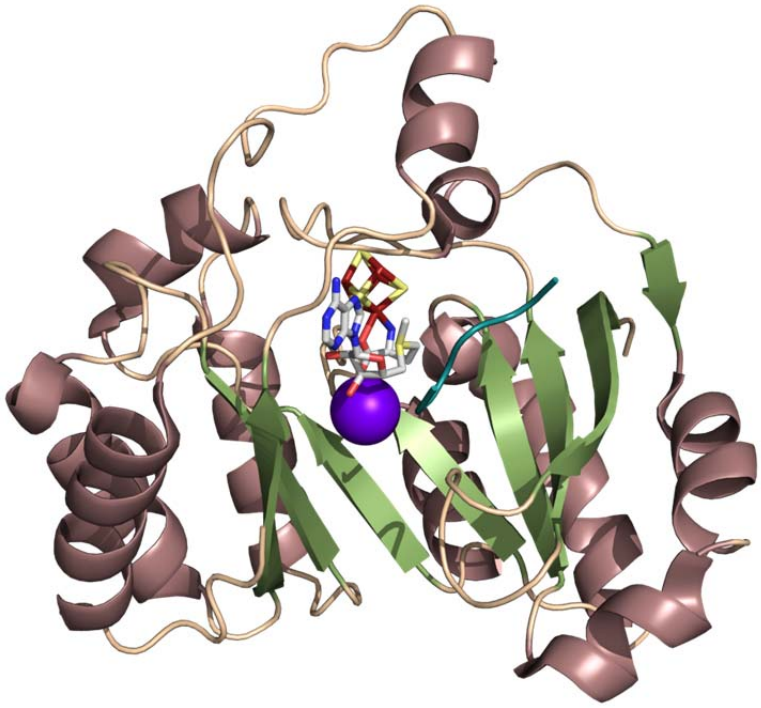

Figure 3.3. Structure of PFL-AE in which the monovalent cation is shown as a purple sphere. The cation is located in the active site in close proximity to the Fe-S cluster and appears to have interactions with SAM through one carboxy and one ribose oxygen atom.

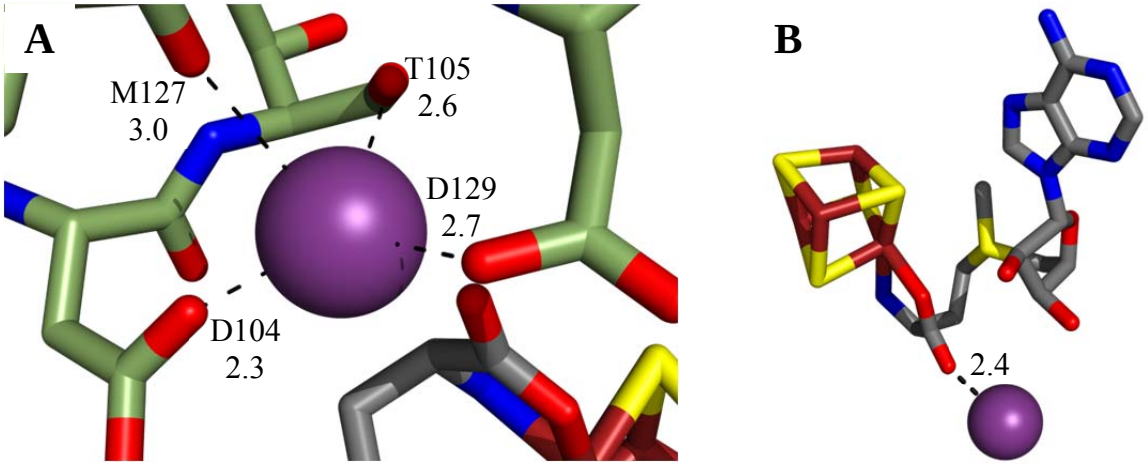

Figure 3.4. Interactions between the monovalent cation and PFL-AE (A) include two from peptide backbone oxygen atoms, Met127 (3.0 Å) and Thr105 (2.6 Å), and two from side chain residue oxygen atoms, Asp104 (2.3 Å) and Asp129 (2.7 Å). The interaction between the monovalent cation and SAM (B) includes one from the unbound carboxy moiety oxygen (2.4 Å).

the SAM carboxy oxygen atom that isn't bound by the unique Fe. However, the importance of this interaction remains to be determined.

Effect of Cations on PFL-AE Activity

To determine the effect of the monovalent cation on PFL-AE, coupled enzyme activity assays in the presence of five different cations (Na^+, K^+, NH_4^+, Rb^+, and Cs^+) were performed. The activity of PFL-AE reaches a maximum after approximately 5 minutes of photoreduction (unpublished data) at which point it is no longer in the linear range of activation. Activity assays at 5 minutes of photoreduction showed that K^+ (45.7

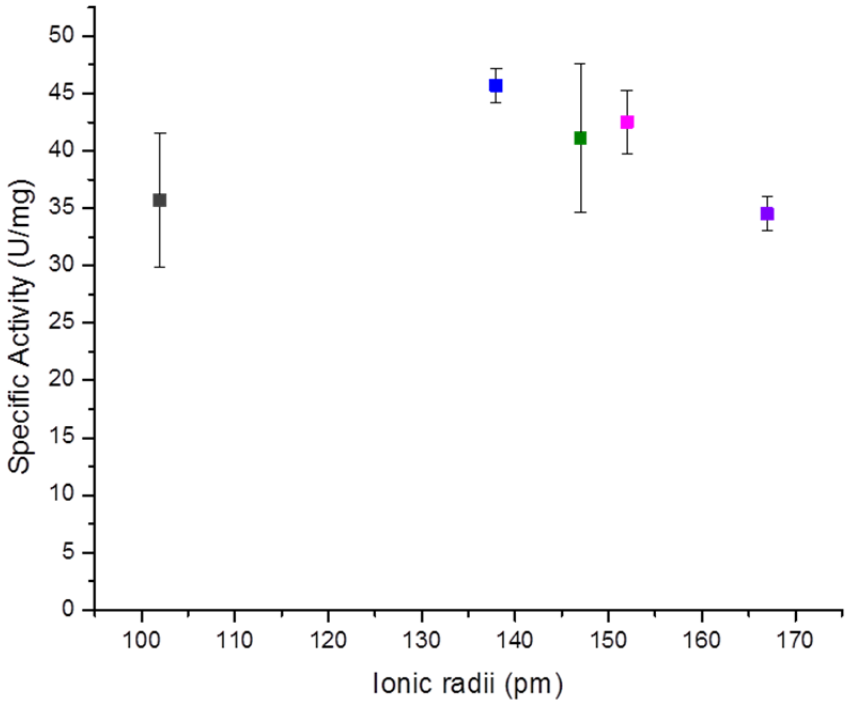

Figure 3.5. PFL-AE specific activity (U/mg) is directly correlated to the ionic radius of the cation present in the activity assay. PFL-AE shows a maximum activity with K^+ (blue) followed by NH_4^+ (green) and Rb^+ (pink). The lowest activity is seen with Na^+ (gray) and Cs^+ (purple). For these assays a concentration of 5 µM PFL, 0.05 µM PFL-AE containing approximately 4.0 Fe per protein, and 0.1 mM SAM in the presence of 100 mM of the specified cation was used.

± 1.5 U/mg) gave the highest specific activity of PFL-AE, which suggests it is the most likely candidate for the *in vivo* monovalent cation found in the active site of PFL-AE (Figure 3.5). However, NH_4^+ (41.1 ± 6.5 U/mg) and Rb^+ (42.5 ± 2.8 U/mg) also gave high specific activities within the same range as K^+. Na^+ (35.7 ± 5.8 U/mg) and Cs^+ (34.5 ± 1.5 U/mg) also showed activity to a lesser extent. There also appears to be a trend in the PFL-AE activity when analyzed with respect to the cations' ionic radii, and the use of different cations in the activity assays such as Li^+, Mg^{2+}, and Ca^{2+} will allow the relevance of this observation to be determined. The use of divalent cations may also give insight into the effect of the cation charge density on PFL-AE activity. Furthermore, the use of different concentrations of K^+ in the activity assays displayed the effect of cation concentration on PFL-AE activity. The assays exhibited an increase in specific activity with the increase in K^+ concentration (Figure 3.6). Interestingly the assay containing 0 mM K^+ also showed activity (previous unpublished data suggested that PFL-AE was not

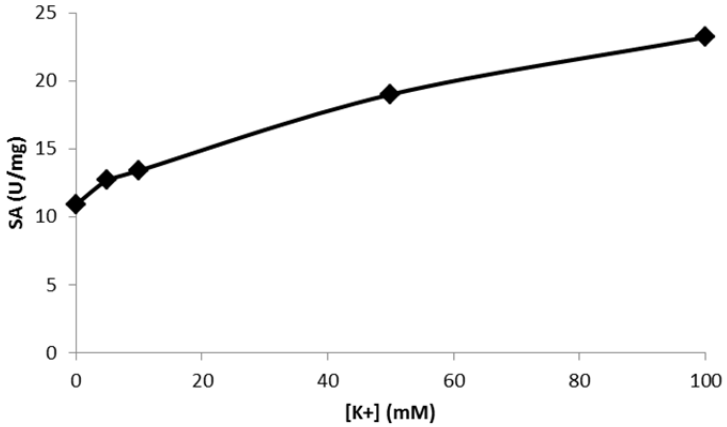

Figure 3.6. The effect of [K^+] on PFL-AE activity reported as specific activity (U/mg). The activity of PFL-AE increases with the increase in potassium concentration. Activity is also seen with 0 mM K^+. For these assays a concentration of 5 μM PFL, 0.05 μM PFL-AE containing approximately 2.5 Fe per protein, and 0.1 mM SAM was used. The ionic strength for each assay was maintained through the addition of choline chloride.

active without a monovalent cation) possibly indicating that the cation is not absolutely necessary for activity and instead acts to stimulate the activity.

Effect of Cations on the Electronic Structure of PFL-AE

The location of the monovalent cation within the active site suggests that it is likely to influence the electronic structure of the active site. This perturbation was investigated using EPR spectroscopy of PFL-AE in the presence of the monovalent cations used in the activity assays as well as with and without SAM. The different cations (also those with SAM) do indeed give rise to different signals (Figure 3.7). For

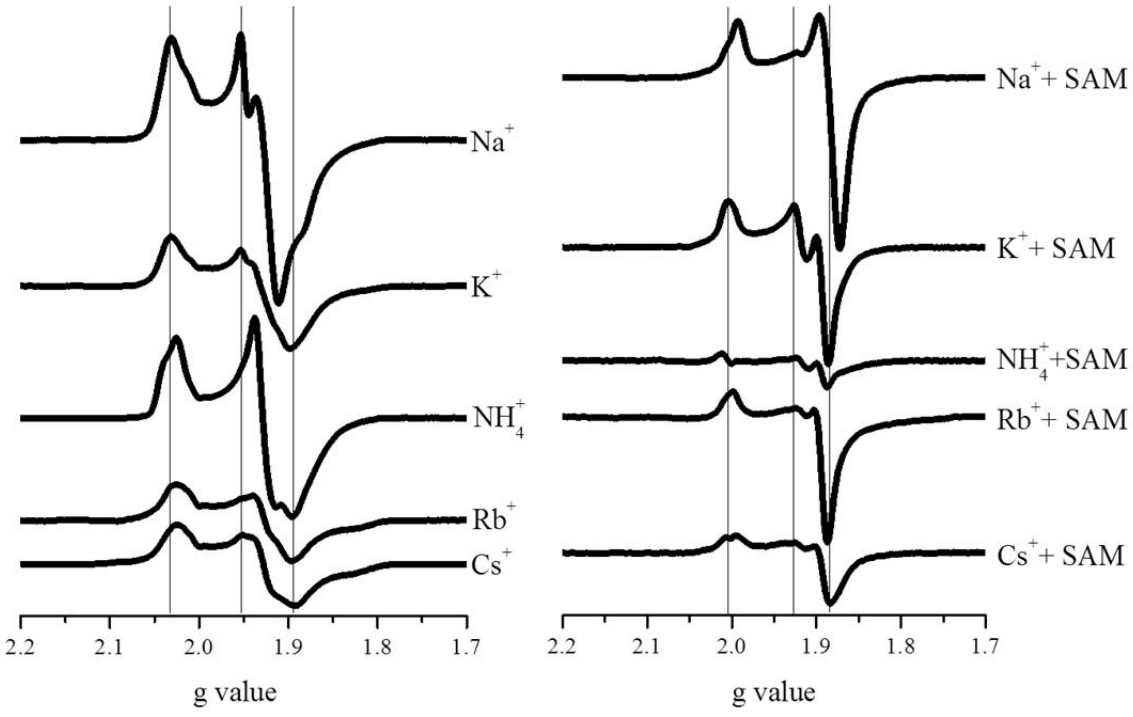

Figure 3.7. EPR spectra of PFL-AE in the presence of the different monovalent cations, Na^+, K^+, NH_4^+, Rb^+, and Cs^+ (left) and also in the presence of SAM (right). Each sample contained 200 μM PFL-AE containing approximately 3.2 Fe per protein in the presence of 200 mM of the cation indicated. For the samples containing SAM, SAM was added to a final concentration of 2 mM.

all of the cations examined, the addition of SAM changes the EPR signal observed. Upon the addition of SAM, the signal undergoes a change in lineshape, a shift in g values, and a decrease in the signal intensity (Figure S1 Appendix A). In the extreme case of PFL-AE in the presence of NH_4^+ and SAM, the signal is almost completely abolished. Comparing the changes in the EPR signals due to the presence of the different cations a change in lineshape is observed. For some of the signals there also appears to be a shift in certain g values. In addition, each signal appears to be a combination of two different spins as demonstrated by the shoulders on some of the EPR features (most easily observed in the samples containing PFL-AE in the presence of Na^+ or NH_4^+). Simulations of these two spins may help elucidate the composition of the signal to determine the source of the individual spins. The changes apparent in the EPR signals containing different monovalent cations demonstrate a change in electronic structure of the active site. Differences in the electronic structure may be related to an alteration in active site conformation due to the differences in cation radii, which may suggest that the variable PFL-AE activity in the presence of each cation is directly related to the active site electronic structure.

Binding Constant of K^+

The observation that the EPR signal of PFL-AE is altered in the presence of different cations led to the use of EPR to determine the K_D of K^+. EPR samples containing PFL-AE and SAM with different concentrations of K^+ showed a gradual change in intensity at g=1.86 (Figure 3.8). Increasing concentrations of the potassium ion caused a measurable decrease in this feature, which was used to determine the K_D of K^+

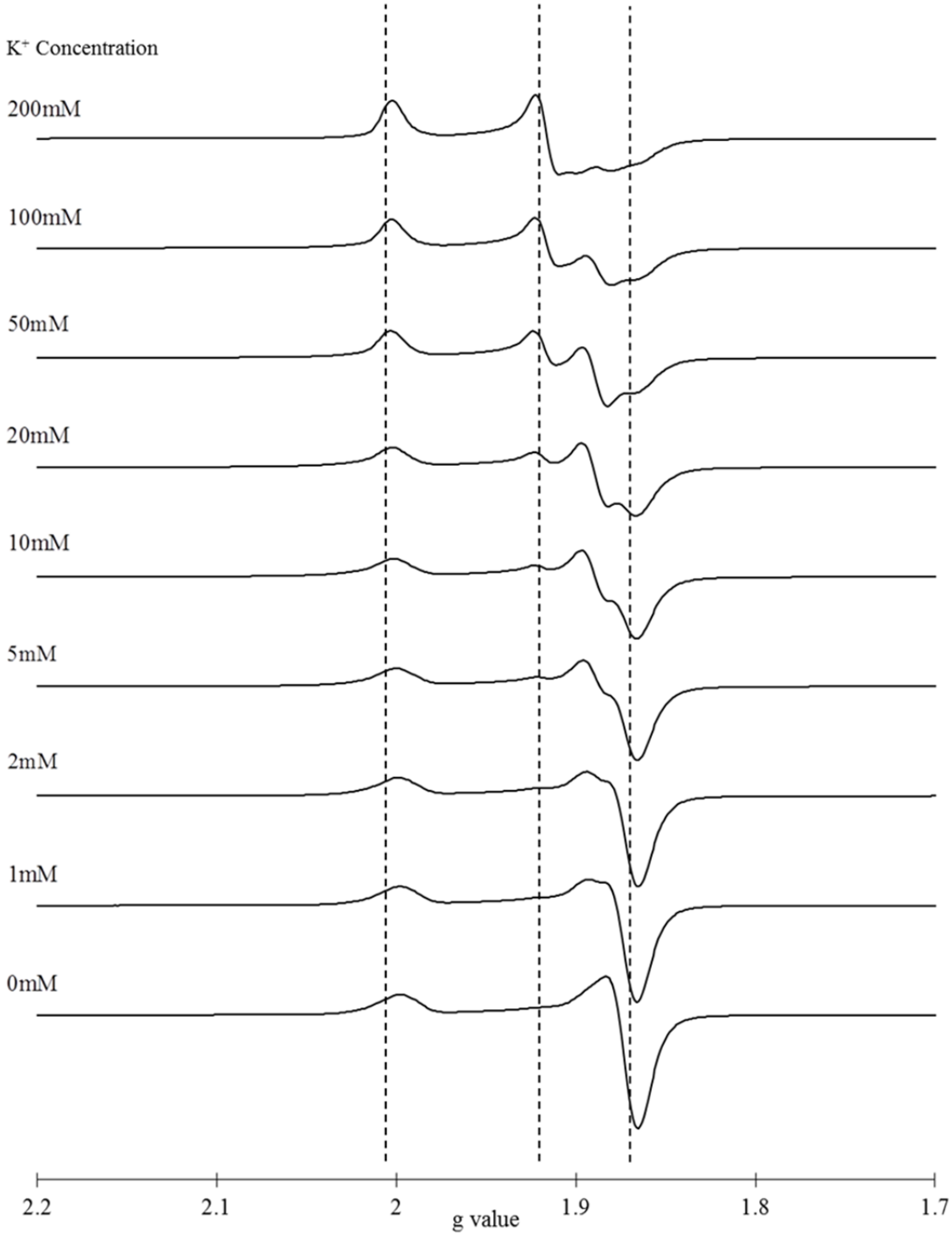

Figure 3.8. EPR spectra of 200 μM PFL-AE (containing approximately 3.5 Fe per protein) with 2 mM SAM in the presence of different K^+ concentrations. The intensity at g=1.86 was used to determine the K_D of K^+ in PFL-AE. Changes in intensity were also observed at g=1.92 however were not as drastic as g=1.86.

as approximately 6.5 mM (Figure 3.9). EPR samples excluding SAM were also explored as a means to determine the K_D, but the effect of increasing K^+ concentration on the EPR signal was not as strong (Figure S2 Appendix A).

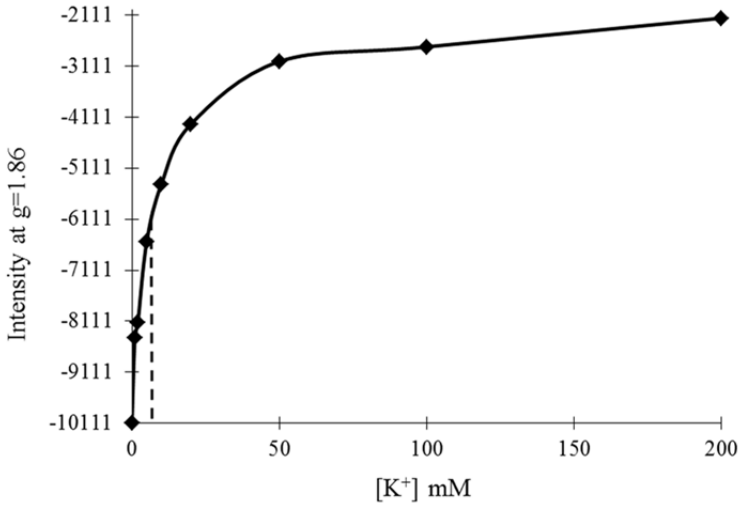

Figure 3.9. Plot of the change in the EPR intensity at g=1.86 of PFL-AE with SAM as a function of the change in K^+ concentration varying from 0 to 200 mM. The dashed line represents the estimated K_D value of 6.5 mM.

Discussion

During further analysis of the PFL-AE crystal structure, the presence of a monovalent cation in the active site was discovered. In the structure the monovalent cation is located at the back of the active site against the barrel. M^+ coordination to an enzyme is usually through carbonyl O atoms which is apparent in the interactions between the M^+ and four amino acids of PFL-AE: two are from the oxygen atoms of aspartate side chains, Asp104 and Asp129, and two from backbone oxygens, Thr105 and Met127, all of which are within 3 Å of the M^+. While M^+ sites usually occur where there is no secondary structure, all four of the residues mentioned above are part of the beta

sheets forming the inside of the TIM barrel. These interactions of the monovalent cation with amino acid residues may help the protein to achieve a conformation not available in aqueous solutions alone. This can be seen when PFL-AE is placed in choline chloride, a monovalent cation that is too large to be situated in the active site pocket; PFL-AE in choline chloride is less stable and prone to precipitation. Interestingly there is also an interaction between M^+ and SAM, a co-substrate of PFL-AE; the unbound oxygen from the carboxyl moiety is within 2.4 Å of M^+.

The location of the monovalent cation suggested that its presence or identity would have an effect on PFL-AE activity. When coupled enzyme activity assays were performed on PFL-AE in the presence of different cations, it was discovered that PFL-AE activity was highest in the presence of the potassium ion (although it was active in the presence of the other cations tested as well). The potassium ion is one of the most abundant physiologically available cations and can accumulate to intracellular concentrations averaging as high as 211 mM in *E. coli* cells [33]. This availability together with high PFL-AE activity may indicate that K^+ is the cation used *in vivo*. Not only does the potassium ion provide the highest activity of PFL-AE, but the activity is also dependent on the concentration of potassium with an increase in concentration showing and increase in activity. While the potassium ion concentration dependence of PFL-AE activity has been examined by Wong et al. [34] (although their PFL-AE only contained 1 Fe per protein) and found to have no effect on activity, the concentrations used were 0.1-1.6 M KCl. Many K^+ activated enzymes reach their maximum activity around 0.1 M or lower [35, 36]. In this study concentrations of 100 mM K^+ or under

were assayed to replicate more biologically relevant cellular concentrations, which average approximately 200 mM or less [33].

Given the location of the cation within the active site it is conceivable that the identity of the cation would influence the electronic structure of PFL-AE's active site; this is what is suggested by the EPR signals generated in the presence of the different monovalent cations. The difference in the EPR spectra is presumably a result of the slightly different conformation adopted by PFL-AE because of the change in ionic radii necessitating a shift in the amino acids that interact with the cation. The resulting EPR signals both in the presence and absence of SAM appear to consist of two spin signals. For the samples containing SAM the two spins could be attributed to clusters both bound and unbound by SAM as the SAM is added and only incubated for 5-10 minutes before the samples are frozen with liquid nitrogen to be stored for later analysis. Harder to explain are the samples without SAM, although the two spins may arise from how the samples are prepared. PFL-AE is purified in the presence of Na^+, and for the EPR samples the protein is diluted in the buffer containing the different cations meaning that a certain amount of Na^+ is still present. With two different cations in the sample the two different spins could be the cluster in the presence of each cation. However, this does not explain why the EPR spectrum of PFL-AE with Na^+ also appears to be composed of two spins. The presence of two spins in this spectrum may imply that PFL-AE does not constantly maintain a cation in the active site and the different spins arise from an active site with and without a monovalent cation bound. Future simulations of the EPR data may help provide evidence indicating that the two signals are a result of the presence of

different cations (or no cation) in the active site of PFL-AE or reveal that further explanations need to be explored. That PFL-AE may not always contain a cation in its active site is supported by the lack of tight binding as demonstrated by the K_D of approximately 6.5 mM calculated from the EPR spectroscopy where K^+ was titrated into PFL-AE. Other enzymes using potassium also show similar binding affinities for K^+ such as holotryptophanase (K_A=1.44 mM) [37], arsenate reductase (K_a=3.8 x 10^3 M^{-1}) [38], and ribokinase (K_d=5 mM) [39]. The crystal structures of PFL-AE also suggest that monovalent cation binding in the active site may be transient in nature. The structure without the PFL peptide did not show evidence of a monovalent cation, which would imply that both SAM and PFL may be necessary to hold the cation in the active site of PFL-AE.

From the evidence presented here it is difficult to categorize PFL-AE as a type I or II M^+-activated enzyme. The location of the monovalent cation in the active site (Figure 3.10) and its interaction with SAM would suggest that PFL-AE is a type I M^+ activated enzyme. However, the cation has no interactions with PFL, the other substrate, and PFL-AE still shows activity with 0 mM potassium ion indicating that the cation is not absolutely required for activity but instead only acts to stimulate activity. Both of these observations would place PFL-AE in the type II M^+ category. As prior assays in our lab suggested that PFL-AE was inactive in the absence of a cation, further activity assays in the presence of choline chloride or Tris alone will need to be completed in the future. These assays will aid in the determination of the requirement of a monovalent cation for PFL-AE activity and its placement in the category of a type I or II M^+ activated enzyme.

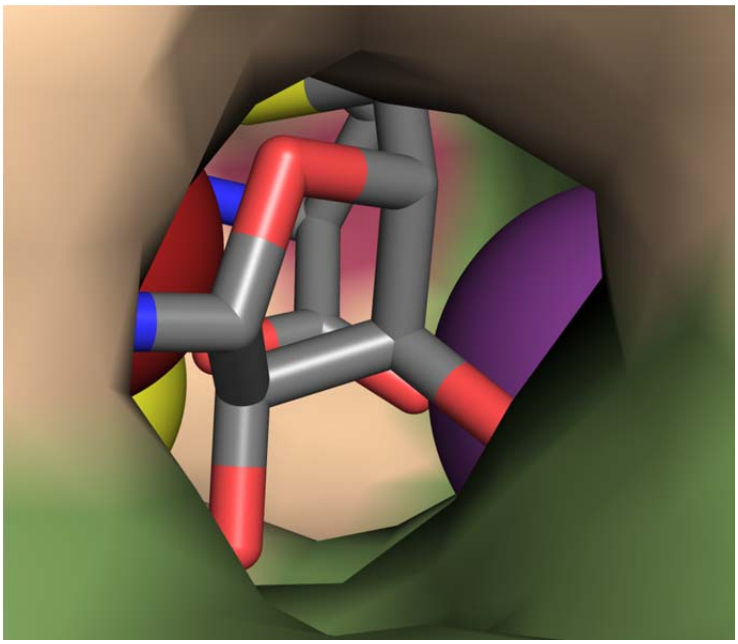

Figure 3.10. A surface representation of the PFL-AE active site as seen from the active site opening with the monovalent cation (shown as a purple sphere) projecting into the active site. Also shown is the interaction between the cation and the unbound carboxy oxygen (red) of SAM and the presence of the Fe-S cluster (red and yellow spheres).

Although PFL-AE cannot be classified at this point, the experimental data presented here show the large impact that it has on PFL-AE catalysis. With the cation positioned in the active site in such close proximity to the Fe-S cluster and with an interaction between itself and an oxygen of SAM, it is not surprising that the activity is affected by the identity and concentration of the cation, nor is it unexpected that the cation also affects the electronic structure of the active site. How the cation is able to accomplish this is still not completely understood. It does appear to bring some stability to PFL-AE as seen by the precipitation of the enzyme lacking an appropriate monovalent cation. The interaction of the cation with SAM may also be relevant to the activity of SAM perhaps by helping, along with other interaction between SAM and amino acids, with the correct

positioning of SAM in the active site or with the shuttling in and out of SAM and its cleavage products.

Of the radical SAM enzymes structurally characterized to date, PFL-AE is the only one that has been observed to contain a monovalent cation in its active site; it is also the only one for which the effect of the cation on activity has been explored. As new structures become available and the relevance of the cation is studied in other superfamily members, more enzymes utilizing a monovalent cation may be discovered.

Acknowledgements

The authors would like to thank Eric Shepard for help obtaining and valuable insight into the EPR data as well as Krista Shisler for assistance with the activity assays. Research on PFL-AE is supported by the National Institutes of Health grant GM54608 to J. B. B.

References

1. Sofia HJ, Chen G, Hetzler BG, Reyes-Spindola JF, and Miller NE (2001) Nucleic Acids Res. 29: 1097-1106.

2. Frey PA, Hegeman AD, and Ruzicka FJ (2008) Crit. Rev. Biochem. Mol. Biol. 43: 63-88.

3. Shepard EM, and Broderick JB. (2010) In Comprehensive Natural Products II: Chemistry and Biology (Mander L, and Liu H-W, Eds.), pp 625-661, Elsevier, Oxford.

4. Krebs C, Broderick WE, Henshaw TF, Broderick JB, and Huynh BH (2002) J. Am. Chem. Soc. 124: 912-913.

5. Walsby CJ, Ortillo D, Broderick WE, Broderick JB, and Hoffman BM (2002) J. Am. Chem. Soc. 124: 11270-11271.

6. Henshaw TF, Cheek J, and Broderick JB (2000) J. Am. Chem. Soc. 122: 8331-8332.

7. Knappe J, Neugebauer FA, Blaschkowski HP, and Gänzler M (1984) Proc. Natl. Acad. Sci. U.S.A. 81: 1332-1335.

8. Wagner AFV, Frey M, Neugebauer FA, Schafer W, and Knappe J (1992) Proc. Natl. Acad. Sci. U.S.A. 89: 996-1000.

9. Vey JL, Yang J, Li M, Broderick WE, Broderick JB, and Drennan CL (2008) Proc. Natl. Acad. Sci. U.S.A. 105: 16137-16141.

10. Becker A, Fritz-Wolf K, Kabsch W, Knappe J, Schultz S, and Volker Wagner AF (1999) Nat. Struct. Biol. 6: 969-975.

11. Becker A, and Kabsch W (2002) J. Biol. Chem. 277: 40036-40042.

12. Frey M, Rothe M, Wagner AF, and Knappe J (1994) J. Biol. Chem. 269: 12432-12437.

13. Peng Y, Veneziano SE, Gillispie GD, and Broderick JB (2010) J. Biol. Chem. 285: 27224-27231.

14. Page MJ, and Di Cera E (2006) Physiol. Rev. 86: 1049-1092.

15. Harding MM (2002) Acta. Crystallogr. D Biol. Crystallogr. 58: 872-874.

16. Ramirez-Silva L, and Oria-Hernandez J. (2008) In Advances in Protein Physcial Chemistry (Garcia-Hernandez E, and Fernandez-Velasco DA, Eds.), pp 249-277, Transworld Research Network.

17. Larsen TM, Benning MM, Rayment I, and Reed GH (1998) Biochemistry 37: 6247-6255.

18. Liao DI, Dotson G, Turner I, Jr., Reiss L, and Emptage M (2003) J. Inorg. Biochem. 93: 84-91.

19. Shibata N, Masuda J, Tobimatsu T, Toraya T, Suto K, Morimoto Y, and Yasuoka N (1999) Structure 7: 997-1008.

20. Wang J, and Boisvert DC (2003) J Mol Biol 327: 843-855.

21. Burdette SC, and Lippard SJ (2003) Proc. Natl. Acad. Sci. U.S.A. 100: 3605-3610.

22. Toraya T, Sugimoto Y, Tamao Y, Shimizu S, and Fukui S (1971) Biochemistry 10: 3475-3484.

23. Zhang Y, Dougherty M, Downs DM, and Ealick SE (2004) Structure 12: 1809-1821.

24. Rana S, Pozzi N, Pelc LA, and Di Cera E (2011) Proc. Natl. Acad. Sci. U.S.A. 108: 5221-5225.

25. Broderick JB, Henshaw TF, Cheek J, Wojtuszewski K, Smith SR, Trojan MR, McGhan RM, Kopf A, Kibbey M, and Broderick WE (2000) Biochem. Biophys. Res. Commun. 269: 451-456.

26. Nnyepi MR, Peng Y, and Broderick JB (2007) Arch. Biochem. Biophys. 459: 1-9.

27. Walsby CJ, Hong W, Broderick WE, Cheek J, Ortillo D, Broderick JB, and Hoffman BM (2002) J. Am. Chem. Soc. 124: 3143-3151.

28. Bradford MM (1976) Anal. Biochem. 72: 248-254.

29. Beinert H (1978) Methods Enzymol. 54: 435-445.

30. Conradt H, Hohmann-Berger M, Hohmann HP, Blaschkowski HP, and Knappe J (1984) Arch. Biochem. Biophys. 228: 133-142.

31. Brush EJ, Lipsett KA, and Kozarich JW (1988) Biochemistry 27: 2217-2222.

32. Külzer R, Pils T, Kappl R, Huttermann J, and Knappe J (1998) J. Biol. Chem. 273: 4897-4903.

33. Schultz SG, and Solomon AK (1961) J. Gen. Physiol. 45: 355-369.

34. Wong KK, Murray BW, Lewisch SA, Baxter MK, Ridky TW, Ulissi-DeMario L, and Kozarich JW (1993) Biochemistry 32: 14102-14110.

35. Evans HJ, and Wildes RA. (1971) In Potassium in Biochemistry and Physiology, pp 13-39, International Potash Institute, Berne, Switzerland.

36. Wilson RH, and Evans HJ. (1968) In The Role of Potassium in Agriculture (Kilmer VJ, Younts SE, and Brady NC, Eds.), pp 189-202, ASA, CSSA, SSSA, Madison, WI.

37. Suelter CH, and Snell EE (1977) J. Biol. Chem. 252: 1852-1857.

38. Lah N, Lah J, Zegers I, Wyns L, and Messens J (2003) J. Biol. Chem. 278: 24673-24679.

39. Andersson CE, and Mowbray SL (2002) J. Mol. Biol. 315: 409-419.

CHAPTER 4

NRVS REVEALS CHANGES IN THE PFL-AE CLUSTER UPON SAM AND SUBSTRATE ANALOG BINDING

Contribution of Authors and Co-Authors

Manuscripts in Chapters 3, 4, and 7

Author: Rachel U. Hutcheson

Contributions: Prepared PFL-AE NRVS samples in the presence of SAM and SAM + YfiD. Collected NRVS data at Argonne National Laboratories. Generated figures and wrote the manuscript in preparation for submission.

Co-author: Kaitlin S. Duschene

Contributions: Grew and purified ^{57}Fe PFL-AE and aided in the preparation of NRVS samples in the presence of SAM and SAM + YfiD.

Co-author: Adam V. Crain

Contributions: Grew ^{57}Fe PFL-AE for SAM and SAM + YfiD NRVS samples.

Co-author: Yi Peng

Contributions: Grew and purified ^{57}Fe PFL-AE and prepared NRVS samples for PFL-AE alone.

Co-author: J. Timothy Sage

Contributions: Collected NRVS data at Argonne National Laboratories, performed calculations and aided in the analysis of the data and the preparation of the manuscript and figures.

Co-author: Joan B. Broderick

Contributions: Provided important insight and overview of the preparation of the NRVS samples, interpretation of results, and aided in the preparation of the manuscript and figures.

Manuscript Information Page

Rachel U. Hutcheson, Kaitlin S. Duschene, Adam V. Crain, Yi Peng, J. Timothy Sage, Joan B. Broderick
Biochemistry
Status of the manuscript:
__X__Prepared for submission to a peer-reviewed journal
____ Officially submitted to a peer-reviewed journal
____ Accepted by a peer-reviewed journal
_____Published in a peer-reviewed journal

Published by the American Chemical Society

NRVS REVEALS CHANGES IN THE PFL-AE CLUSTER UPON SAM AND SUBSTRATE ANALOG BINDING

The following work is currently in progress to be submitted for publication

Rachel U. Hutcheson[1], Kaitlin S. Duschene[1], Adam V. Crain[1], Yi Peng[1], J. Timothy Sage[2], Joan B. Broderick[1]

1. *Department of Chemistry and Biochemistry and the Astrobiology Biogeocatalysis Research Center, Montana State University, Bozeman, MT 59717*
2. *Department of Physics, Northeastern University, Boston, MA 02115*

Abstract

Pyruvate formate-lyase activating enzyme (PFL-AE) is the radical SAM enzyme responsible for activating pyruvate formate-lyase (PFL). PFL-AE contains an Fe-S cluster that binds and reductively cleaves SAM to initiate the activation process. Herein we report the results of nuclear resonance vibrational spectroscopic (NRVS) studies designed to probe details of SAM and substrate binding to PFL-AE. Results showed that SAM binding had the largest impact on the cluster with more minor differences after substrate analog addition. Upon SAM and YfiD binding to PFL-AE, the NRVS data show an increase in the resilience and decrease in the stiffness force constants calculated. Stiffness is inversely correlated with bond length, so a decrease in this force constant would be consistent with the lengthening of the Fe-S bonds in the cluster. The increase in resilience is associated with the PFL-AE protein becoming more rigid around the Fe-S cluster suggesting the creation of a more defined active site through interactions of SAM with the cluster as well as surrounding amino acid residues.

Introduction

Pyruvate formate-lyase activating enzyme (PFL-AE) is a member of a superfamily called radical SAM (*S*-adenosylmethionine) [1]. Enzymes in this superfamily are characterized by the use of a [4Fe-4S] cluster, coordinated by the cysteines of a CX_3CX_2C motif, to reductively cleave SAM to form a transient 5'-deoxyadenosyl (dAdo) radical capable of hydrogen atom abstraction [2]. These enzymes catalyze many diverse chemical transformations including isomerization, complex cofactor biosynthesis, and large biomolecule modification [3, 4]. PFL-AE is responsible for activating the anaerobic metabolic enzyme PFL by utilizing the dAdo radical to abstract a hydrogen atom from glycine 734 of PFL creating the catalytically essential glycyl radical [5-7]. The formation of the glycyl radical is the first step in PFL conversion of pyruvate and coenzyme A (CoA) to formate and acetyl-CoA [8-10]. PFL, a central enzyme involved in anaerobic glucose metabolism, is active under anaerobic conditions, however when exposed to oxygen, the glycyl radical causes cleavage of the enzyme into a larger (82 kDa) N-terminal fragment and a smaller (3 kDa) C-terminal fragment [11]. PFL activity can be salvaged by YfiD, a small protein homologous to the C-terminal portion of PFL [12]. YfiD can be activated by PFL-AE to contain a glycyl radical and as such provides a suitable substrate analog that has been utilized in this study [12].

The [4Fe-4S] cluster of PFL-AE (Figure 4.1), which is necessary for substrate activation, is located within a partial $(\alpha/\beta)_6$ Triose-phosphate Isomerase Mutase (TIM) barrel [13]. In the crystal structures of PFL-AE with and without peptide (a mimic of the

PFL loop that contains G734), a large conformational change in the PFL-AE structure is apparent upon peptide binding. PFL-AE loop A harbors a conserved sequence motif (DGXGXR) important in interactions with PFL-AE and the peptide [13]. Upon substrate binding loop A swings up toward the active site allowing contacts with the peptide to be formed [13].

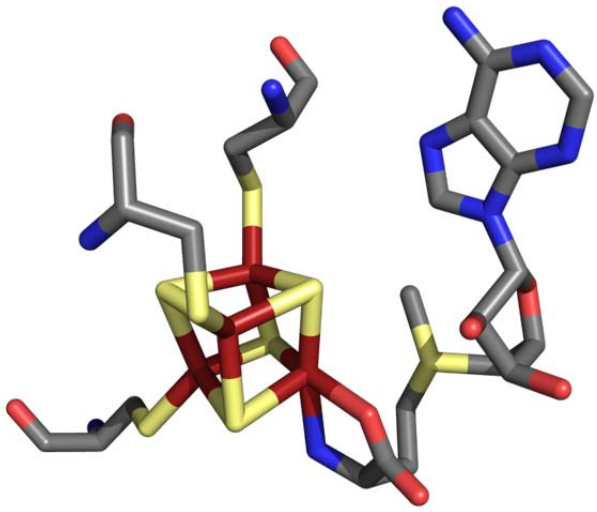

Figure 4.1. Representation of the [4Fe-4S] cluster (Fe shown as dark red and sulfur as yellow) found in the active site of PFL-AE. Three of the irons are coordinated by cysteine ligands and the fourth unique iron is bound by the carboxy and amino moieties of SAM.

While the crystal structures provide a global picture of the changes that occur within PFL-AE upon peptide binding, no major conformational changes are observed in the active site, and no crystal structure exists for PFL-AE without SAM to determine the effects of its binding to the cluster. Nuclear resonance vibrational spectroscopy (NRVS) provides a complimentary tool to the investigation of the effect of SAM and substrate binding specifically directed towards effects on the cluster, and PFL-AE represents the first radical SAM enzyme to be probed with this method.

The use of NRVS to analyze proteins containing metal based cofactors is a relatively new technique. NRVS is a synchrotron-based vibrational spectroscopy technique that utilizes a Mössbauer active isotope. In Mössbauer spectroscopy a nucleus absorbs a photon and is excited without a change in the vibrational state of the nucleus, resulting in a recoil-free absorption of a photon whose energy is exactly the difference in energy of the ground and excited nuclear states. Being performed on a solid, most of the recoil energy is converted into lattice vibration energy and should result in peaks that are displaced from the recoil-free resonance [14, 15]. These are not visible in traditional Mössbauer, which uses a moving source to emit Doppler-shifted photons whose transmission is recorded, as this would require Doppler velocities of hundreds of meters/second not attainable by typical instruments, also the sideband features are very weak due to broadening by vibrational lifetimes [16].

In NRVS, a combination of nuclear excitation and molecular vibrations, the sidebands corresponding to the complete set of vibrational modes of the isotope are revealed. NRVS utilizes an X-ray synchrotron source to obtain an intense, narrow energy width as compared to vibrational band widths producing spectra that are resolved [16]. A typical experiment consists of generating X-rays by undulating the charged particles in the synchrotron beam and tuning them to give an extremely small energy dispersion of 1 meV. The X-rays are then used to irradiate the sample with photons selected around the isotope resonance (14.413 keV for ^{57}Fe). Upon excitation a majority of the sample nuclei eject K shell electrons, which is followed by an electron falling from a higher level to fill the hole resulting in fluorescence with is measured with an avalanche photodiode detector

[17]. In the case of Fe-S cluster containing proteins NRVS allows all of the Fe-ligand modes involved in the iron atom motion to be quantitatively detected, as the observed signal intensity is directly proportional to the direction and magnitude of the motion [16]. The need for a specific isotope also allows for selectivity in that only the vibrational modes associated with that label will be observed allowing for the acquisition of very specific information.

From the NRVS data collected the vibrational density of states (VDOS) can be determined, and intensity at certain frequencies can be attributed to the different vibrational modes of the isotope. Two force constants, resilience and stiffness, can be calculated from the vibrational density of states. Resilience is a measure of the elasticity of the protein matrix through the force necessary to displace the probe isotope with the atoms around it free to respond [18, 19]. Stiffness, however, fixes the neighboring atoms and probes the average strength of their interactions with the isotope; it is also inversely related to the bond lengths of the isotope and atoms connected to it [20, 21]. These two force constants allow the changes to the PFL-AE cluster upon SAM or substrate analog to be analyzed.

Materials and Methods

PFL-AE Cloning, Growth, and Purification

PFL-AE was produced in the presence of ^{57}Fe for nuclear vibrational resonance spectroscopy experiments. The *pflA* gene encoding PFL-AE was inserted into the pCal-n-Ek vector and over expressed in *E. coli* BL21(DE3)pLysS competent cells as previously

described with the following modifications [22]. O-solution was comprised of 1mL of T-solution and 2.68 g of $MgCl_2 \cdot H_2O$ brought up to 50 mL using MQ water. A stock solution of ^{57}Fe was made by dissolving 120 mg of ^{57}Fe in 2mL of concentrated H_2SO_4 and brought up to 8 mL volume with MQ water. The pH of the stock solution was then neutralized by titrating KOH while monitoring the pH. Three additions of ^{57}Fe were made during cell growth, one at the start of the growth, the second at the time of induction, and the last after 30 minutes of purging with N_2 for a total concentration of 75 μM ^{57}Fe, and pH was monitored during the growth and maintained at pH 7.2.

PFL-AE was purified as previously described [22] with the following changes. The cells were initially lysed during incubation at ambient temperature for 1 h, and then centrifuged at 18,000 rpm for 30 min at 4˚C. The extract was decanted and a 20% ammonium sulfate cut was performed with gentle stirring on ice for 30 min after which it was centrifuged at 18,000 rpm for 30 min at 4˚C. The extract was decanted and a 60% ammonium sulfate cut was performed with gentle stirring on ice for 30 min followed by the last centrifugation at 18,000 rpm for 30 min at 4˚C. The supernatant was discarded and pellet was stored overnight at 4˚C. On day 2 of the purification, protein was resuspended in minimal amount of gel filtration buffer, 50 mM Tris, 200 mM NaCl, 1 mM DTT, pH 7.5 then loaded onto a Superdex 75 HR (GE Healthcare, Piscataway, NJ) AP-5 column (5 x 60 mm, Waters, Milford, MA) equilibrated with gel filtration buffer. The protein was eluted with buffer at 3 ml/min into 10 ml fractions. Fractions with the highest A_{426}/A_{280} were pooled and concentrated using Amicon Ultra-15 centrifugal filter

units (Millipore, Billerica, MA). The concentrated, purified protein was flash-frozen and stored in o-ring-sealed tubes at -80˚C.

YfiD Cloning, Growth, and Purification

The gene encoding YfiD (14.3 kDa) was inserted into the pCal-n-Ek vector and overexpressed in *E. coli* BL21(DE3)pLysS competent cells. Growth and purification of YfiD was performed following PFL purification procedures as described previously [2, 22, 23].

Protein and Iron Assays

Routine determinations of protein concentrations were carried out by the method of Bradford [24]. For PFL-AE a correction factor previously determined by amino acid hydrolysis [22] was applied to determine the actual protein concentration. Iron assays were carried out by using the method of Beinert [25].

SAM Synthesis and Purification

S-Adenosylmethionine was prepared according to published procedures [26, 27]. Briefly, SAM synthetase contained in a crude cell extract was combined with ATP and methionine. After an overnight incubation, the reaction was quenched with HCl, and insolubilites were removed by centrifugation. SAM was purified from the resulting mixture on an HR 10/10 column containing Source 15S resin.

NRVS Sample Preparation

Three different NRVS samples were prepared in an anaerobic chamber (Coy Laboratories). Sample 1contained 10 mM PFL-AE. Sample 2 was composed of 11 mM PFL-AE and 20 mM SAM. Sample 3 consisted of 7 mM PFL-AE, 11 mM SAM, and 7 mM YfiD . For each the sample cup was kept frozen in liquid nitrogen after samples were loaded and while the rest of the NRVS cell was assembled. The NRVS cell was then stored at -80° C.

NRVS Measurements and Analysis

NRVS measurements of the ^{57}Fe labeled PFL-AE samples were performed at sector 3-ID-D of the Advanced Photon Source, Argonne National Laboratories. The sample cells were maintained at low temperature in a helium flow cryostat and placed in a monochromatic X-ray beam, whose energy was scanned through the 14.4 keV ^{57}Fe resonance (from 40 meV below to 80 meV above) using a high-resolution monochromator [28]. An avalanche photodiode detected photons emitted by the excited ^{57}Fe atoms, which arrive with a delay on the order of 140 ns ^{57}Fe excited-state lifetime. Data accumulation was disabled during a time interval containing the arrival time of the X-ray pulse to repress the large background of electronically scattered 14.4 keV photons, which arrived in concurrence with the X-ray pulse. Results shown here are an average of 16-18 energy scans.

The PHOENIX [29] program was used to find the VDOS D($\bar{\nu}$) [18], and the resilience [18, 19] and stiffness [20, 21] force constants were calculated as previously described.

Results and Discussion

Data was collected at 55 K for the sample containing PFL-AE alone, 60 K for PFL-AE plus SAM, and 52 K for PFL-AE with SAM and YfiD. Upon analyzing the VDOS, all three samples exhibit vibrational features consistent with the presence of [4Fe-4S] clusters including Fe-S vibrations from cluster bonds and Fe-S cysteine bonds (Figure 4.2). Further, the data reveal only subtle changes on the iron-sulfur cluster upon SAM binding, or upon binding of SAM and YfiD. Based on changes at very low frequency, however, there is evidence that SAM binding causes the surrounding protein matrix to tighten up; these changes can be quantified as changes in the stiffness and resilience (Table 4.1).

As stiffness is inversely related to the bond lengths of the isotope, it would appear that the addition of SAM causes some of the Fe-S bonds to lengthen, although the specific bonds that undergo a change cannot be determined. This observation provides support for the Fe-S bond elongation upon SAM binding that was found in the XAS and DFT calculations performed on PFL-AE. Using S K-edge XAS an increase in the pre-edge intensity upon SAM binding to PFL-AE was observed [30]. DFT calculations were able to reproduce the pre-edge intensity increase, and in these models some of the Fe-S bond lengths are predicted to increase upon SAM binding as would be expected to correlate with a decrease in stiffness as observed in the NRVS results [30]. The importance or relevance of this lengthening awaits further investigation.

Upon binding SAM or SAM plus YfiD the resilience of the PFL-AE cluster increases from 15.9 to approximately 20 pN/pm, indicating that the protein matrix

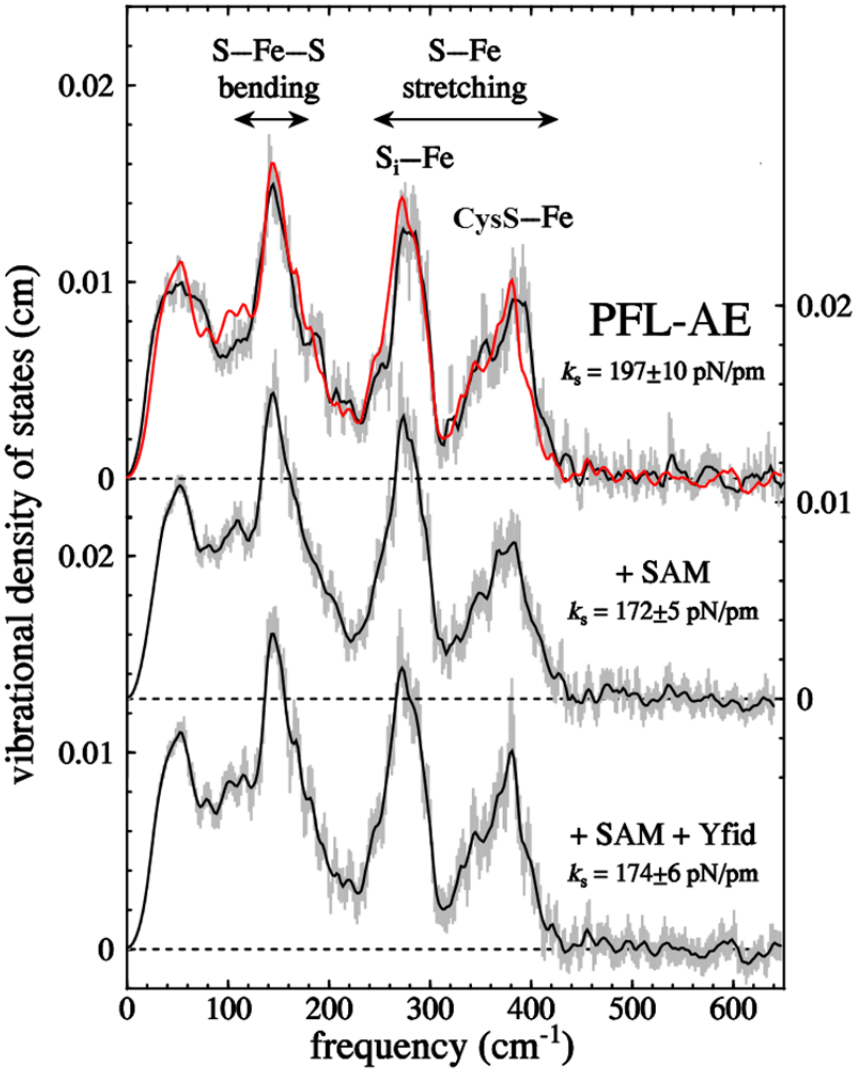

Figure 4.2. Experimentally determined VDOS for PFL-AE alone, PFL-AE with SAM (+SAM), and PFL-AE in the presence of both SAM and YfiD (+SAM +YfiD). In each spectrum the grey line is the experimental data and the black is the deconvoluted spectrum. The red line in the PFL-AE spectrum is the PFL-AE + SAM data overlaid with the data from PFL-AE alone demonstrating the slight differences observed between the two spectra. Frequencies associated with specific Fe-S vibrational modes such as bending and stretching are noted at the top, and the calculated stiffness (k_s) of each sample is also shown.

surrounding the [4Fe-4S] cluster tightens up. This suggests that the addition and binding of the co-substrate, SAM, induces a more defined structure whereby SAM perhaps helps to hold the active site opening in a more rigid and defined conformation through

Table 4.1. Results of the stiffness and resilience force constants calculated for PFL-AE alone, PFL-AE + SAM, and PFL-AE + SAM + YfiD samples. Upon binding of SAM as well as YfiD there is a decrease in stiffness and an increase in resilience as compared to the sample of PFL-AE without co-substrate (SAM) or substrate analog (YfiD).

	Force Constant (pN/pm)	
	Stiffness	Resilience
PFL-AE	197 ±10	15.9
PFL-AE + SAM	172 ± 5	20.0
PFL-AE + SAM + YfiD	174 ± 6	20.2

interactions with multiple adjacent residues. Furthermore, this supposition is supported by the published crystal structure of PFL-AE with SAM bound in which the SAM is bound by residues that are located in conserved motifs among the radical SAM superfamily such as the GGE and GxIxGxxE motifs. These two motifs serve to directly bind the methionine portion of SAM as well as stabilize the binding pocket of the adenine moiety respectively. In addition to these motifs, two histidines, H^{37} and H^{202}, pack against the adenine ring of SAM. Also in the crystal structure of PFL-AE with SAM, the SAM molecule is somewhat disordered and only becomes fully ordered when the peptide mimicking the PFL active site is also present. The peptide packs the SAM molecule between itself and the active site creating a more fully defined active site pocket presumably as another form of control for the reactive radical chemistry that occurs there. This stabilization could then be translated through the SAM molecule to the cluster via its coordination to the unique iron. There is also a larger conformational change upon substrate binding that takes place near the active site pocket; loop A swings into the active site making contact with the substrate, therefore also contributing to packing and rigidity of the active site [13]. This interaction would presumably be preserved in PFL-AE binding of YfiD; the twenty-two residues around the glycine where the radical is

generated are strictly conserved between PFL and YfiD. Additional interactions that would be expected to be similar between PFL and YfiD binding to PFL-AE include those between the PFL backbone and PFL-AE side chain residues. These interactions appear to orient the glycine in the active site, control the overall peptide conformation, and impart selectivity and would most likely be necessary for PFL-AE activation of YfiD as well.

Conclusions

The experimental NRVS data have helped to complete the emerging picture of the effects of SAM and substrate binding to PFL-AE. This data provides support to information gathered from other methods including S K-edge XAS and the x-ray crystal structure of PFL-AE and shows that SAM binding to the [4Fe-4S] cluster helps to stabilize the protein, and further stabilization is achieved upon substrate binding. The stabilization of the enzyme helps to create a more defined active site, which provides one way to contribute to the control of the highly reactive radical produced during catalysis.

Acknowledgements

For support of this research we thank the National Institutes of Health grant GM54608 to J. B. B. and the National Science Foundation under CHE-1026369 to J.T.S. Use of the Advanced Photon Source, an Office of Science User Facility operated for the U.S. Department of Energy Office (DOE) of Science by Argonne National Laboratory, was supported by the U.S. DOE under Contract No.

References

1. Sofia HJ, Chen G, Hetzler BG, Reyes-Spindola JF, and Miller NE (2001) Nucleic Acids Res. 29: 1097-1106.

2. Henshaw TF, Cheek J, and Broderick JB (2000) J. Am. Chem. Soc. 122: 8331-8332.

3. Frey PA, Hegeman AD, and Ruzicka FJ (2008) Crit. Rev. Biochem. Mol. Biol. 43: 63-88.

4. Shepard EM, and Broderick JB. (2010) In Comprehensive Natural Products II: Chemistry and Biology (Mander L, and Liu H-W, Eds.), pp 625-661, Elsevier, Oxford.

5. Knappe J, and Schmitt T (1976) Biochem. Biophys. Res. Commun. 71: 1110-1117.

6. Knappe J, Blaschkowski HP, Grobner P, and Schmitt T (1974) Eur. J. Biochem. 50: 253-263.

7. Knappe J, Schacht J, Mockel W, Hopner T, Vetter H, Jr., and Edenharder R (1969) Eur. J. Biochem. 11: 316-327.

8. Conradt H, Hohmann-Berger M, Hohmann HP, Blaschkowski HP, and Knappe J (1984) Arch. Biochem. Biophys. 228: 133-142.

9. Knappe J, Elbert S, Frey M, and Wagner AFV (1993) Biochem. Soc. Trans. 21: 731-734.

10. Knappe J, Neugebauer FA, Blaschkowski HP, and Gänzler M (1984) Proc. Natl. Acad. Sci. U.S.A. 81: 1332-1335.

11. Wagner AFV, Frey M, Neugebauer FA, Schafer W, and Knappe J (1992) Proc. Natl. Acad. Sci. U.S.A. 89: 996-1000.

12. Wagner AFV, Schultz S, Bomke J, Pils T, Lehmann WD, and Knappe J (2001) Biochem. Biophys. Res. Commun. 285: 456-462.

13. Vey JL, Yang J, Li M, Broderick WE, Broderick JB, and Drennan CL (2008) Proc. Natl. Acad. Sci. U.S.A. 105: 16137-16141.

14. Visscher WM (1960) Ann. Phys. 9: 194-210.

15. Singwi KS, and Sjolander A (1960) Phys. Rev. 120: 1093-1102.

16. Scheidt WR, Durbin SM, and Sage JT (2005) J. Inorg. Biochem. 99: 60-71.

17. Zeng W, Silvernail NJ, Scheidt WR, and Sage JT. (2008) In Encyclopedia of Inorganic Chemistry (Scott RA, and Lukehart CM, Eds.).

18. Leu BM, Zhang Y, Bu L, Straub JE, Zhao J, Sturhahn W, Alp EE, and Sage JT (2008) Biophys. J. 95: 5874-5889.

19. Zaccai G (2000) Science 288: 1604-1607.

20. Adams KL, Tsoi S, Yan J, Durbin SM, Ramdas AK, Cramer WA, Sturhahn W, Alp EE, and Schulz C (2006) J. Phys. Chem. B 110: 530-536.

21. Lipkin HJ (1995) Phys. Rev. B. 52: 10073-10079.

22. Broderick JB, Henshaw TF, Cheek J, Wojtuszewski K, Smith SR, Trojan MR, McGhan RM, Kopf A, Kibbey M, and Broderick WE (2000) Biochem. Biophys. Res. Commun. 269: 451-456.

23. Nnyepi MR, Peng Y, and Broderick JB (2007) Arch. Biochem. Biophys. 459: 1-9.

24. Bradford MM (1976) Anal. Biochem. 72: 248-254.

25. Beinert H (1978) Methods Enzymol. 54: 435-445.

26. Walsby CJ, Hong W, Broderick WE, Cheek J, Ortillo D, Broderick JB, and Hoffman BM (2002) J. Am. Chem. Soc. 124: 3143-3151.

27. Walsby CJ, Ortillo D, Broderick WE, Broderick JB, and Hoffman BM (2002) J. Am. Chem. Soc. 124: 11270-11271.

28. Toellner TS (2000) Hyperfine Interact. 125: 3-28.

29. Sturhahn W (2000) Hyperfine Interact. 125: 149-172.

30. Dey A, Peng Y, Broderick WE, Hedman B, Hodgson KO, Broderick JB, and Solomon EI (2011) J. Am. Chem. Soc. 133: 18656-18662.

CHAPTER 5

IDENTIFICATION OF A RADICAL INTERMEDIATE IN THE PFL-AE – CATALYZED REACTION

Introduction

Radical *S*-adenosylmethionine (SAM) enzymes are believed to utilize a very reactive 5'-dexoyadenosyl (dAdo) radical intermediate in catalysis, although to date this intermediate has not been directly observed. An allylically stabilized analog of the dAdo radical has been observed, however, in the reaction of the SAM analog *S*-3',4'-anhydroadenosylmethionine (anSAM) (Figure 5.1) with lysine 2,3-aminomutase (LAM)[1, 2]. Additional experimental support for the involvement of a SAM-derived dAdo radical intermediate includes the observation for several radical SAM enzymes of the stoichiometric production of deoxyadenosine and methionine from SAM cleavage and the transfer of a substrate based label to deoxyadenosine [3-14].

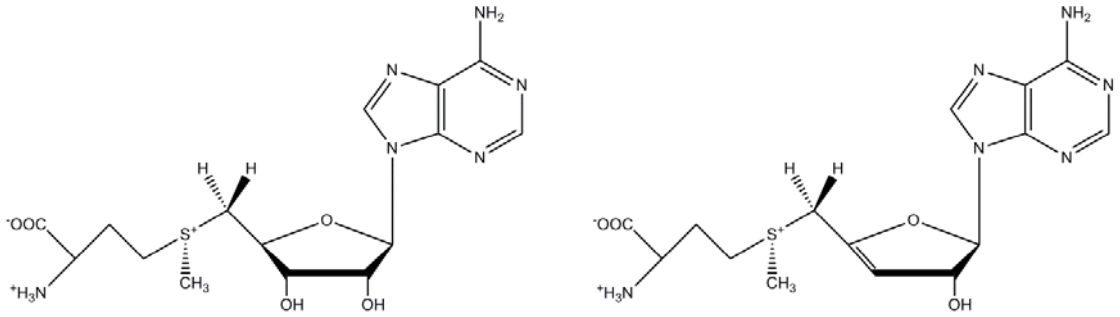

Figure 5.1. Structures of SAM on the left and anSAM on the right

While the data compiled to date present a compelling case for the involvement of the dAdo radical in radical SAM reactions, no direct observation of this radical has been made. One way to approach the detection and characterization of radical intermediates is through the use of rapid freeze quench (RFQ) in conjunction with electron paramagnetic resonance (EPR) and electron nuclear double resonance (ENDOR). RFQ is a technique that exploits the ability to rapidly mix a sample (on the millisecond timescale for this study) and immediately freeze it for further analysis [15]. In general, two samples are combined using a mixer and pushed through a tube of a certain length (which determines the mixing time) prior to freezing. The mixture is sprayed onto two spinning wheels that have been precooled and kept cold using either liquid nitrogen or a cold isopentane bath. The resulting frozen sample is then collected and packed into an EPR tube.

The use of EPR in conjunction with RFQ is especially valuable in the radical SAM superfamily as the catalytically active $[4Fe\text{-}4S]^{1+}$ cluster is EPR active, as are proposed radical intermediates. This allows the decrease of the cluster signal to be monitored as the reaction proceeds and a new signal is formed. Fortuitously, the final product of the PFL-AE reaction is a glycyl radical on PFL, which is also detectable by EPR; thus a progression from reduced cluster, to radical intermediate(s), and finally product radical is directly observable allowing the timescale of the reaction to be determined. In addition, SAM site-specifically labeled with NMR active nuclei can be utilized with ENDOR to identify and structurally characterize the novel radical intermediate.

ENDOR spectroscopy is a coupled technique utilizing the principles of EPR and NMR spectroscopy in which a sample containing a paramagnetic species and an atom(s) with a nuclear spin is analyzed. In ENDOR the EPR signal is saturated at which point a radio-frequency is applied to the sample, and coupling of the paramagnetic center with the nuclear spin causes a change in the EPR spectrum. The data obtained from ENDOR can also be used to calculate the distance between the unpaired electron and NMR active nuclei.

Materials and Methods

Protein Growth and Purification and SAM Synthesis and Purification

PFL and PFL-AE were grown and purified as previously described (Chapter 2) [16-19]. Briefly, the *Escherichia coli* genes *pflA* (PFL-AE) and *pflB* (PFL) were individually expressed in *Escherichia coli* BL21(DE3)pLysS. PFL-AE was anaerobically purified using a Waters AP-5 600 mm column containing preparatory grade Superdex 75 resin. PFL-AE used in these experiments contained approximately 3 Fe per protein as determined by the method of Beinert [20]. PFL was aerobically purified first on a Waters AP-5 300 mm column containing Accell Plus QMA resin followed by a HighLoad High Performance 16/10 phenyl sepharose column. PFL was degassed on a Schlenk line prior to use. Unlabeled and labeled SAM were synthesized and purified as previously described (Chapter 2) [19, 21]. For labeled SAM, L-methionine or ATP containing the label of interest were substituted for the unlabeled equivalent.

Sample Reduction and Rapid Freeze Quench

All handling of PFL-AE and PFL occurred in a Coy anaerobic chamber (Coy Laboratories, Grass Lake MI). A sample containing 550 μM PFL-AE, 200 mM KCl, 50 mM Tris, pH 7.5, 1 mM DTT, 100 μM sodium dithionite, and 200 μM 5-deazariboflavin (added last in the dark) as well as a sample containing 550 μM PFL, 10 mM oxamate, ~ 25 mM Tris, pH 7.5, 10 mM DTT, and 200 μM 5-deazariboflavin (added last in the dark) were photoreduced using a 300 W halogen lamp for 1 hour on an ice bath. After reduction, SAM (either labeled or unlabeled) was added to the PFL mixture to a final concentration of approximately 2 mM. For rapid freeze-quench 50 μL of the PFL-AE sample and 50 μL of the PFL sample were anaerobically loaded into separate RFQ tubing in the Coy Chamber. The samples were mixed by the rapid freeze-quench apparatus [22, 23] (kept anaerobic by constant purging with a buffer containing sodium dithionite) for varying amounts of time, frozen by spraying on two liquid nitrogen chilled copper wheels, and collected in EPR tubes for later analysis.

EPR and ENDOR

Continuous wave (CW) X-band EPR spectra were recorded on a Bruker model E-500 spectrometer equipped with an Oxford ESR-910 flow cryostat for liquid helium. Typical experiment parameters were 12 K and 9.38 GHz, with 9.9 mW microwave power, 100 kHz modulation frequency, and 10.5 G modulation amplitude.

CW Q-band EPR and ENDOR measurements were recorded on modified Varian E- 110 spectrometer. EPR spectra were obtained at 2 K using a 100 kHz field modulation in dispersion mode under rapid-passage condition which gives an absorption

shape. CW ENDOR spectra were collected at 2 K and broadened radio frequency bandwidth to 100 kHz to improve the signal-noise ratio [24]. Pulse Q-band EPR and ENDOR spectra were collected on a spectrometer described earlier [25], equipped with a helium immersion dewar for measurements at ~ 2 K.

Results

For the rapid freeze-quench experiments PFL-AE was anaerobically photoreduced with 5-deazariboflavin to obtain PFL-AE containing a $[4Fe\text{-}4S]^{1+}$ cluster. Reduction of the cluster was confirmed by EPR, which showed a nearly axial signal with g values consistent with a $[4Fe\text{-}4S]^{1+}$ cluster. The ability of the reduced PFL-AE to activate PFL was also tested by EPR; PFL-AE was mixed with PFL and SAM, and this sample was allowed to react for approximately one minute before it was frozen with liquid nitrogen.

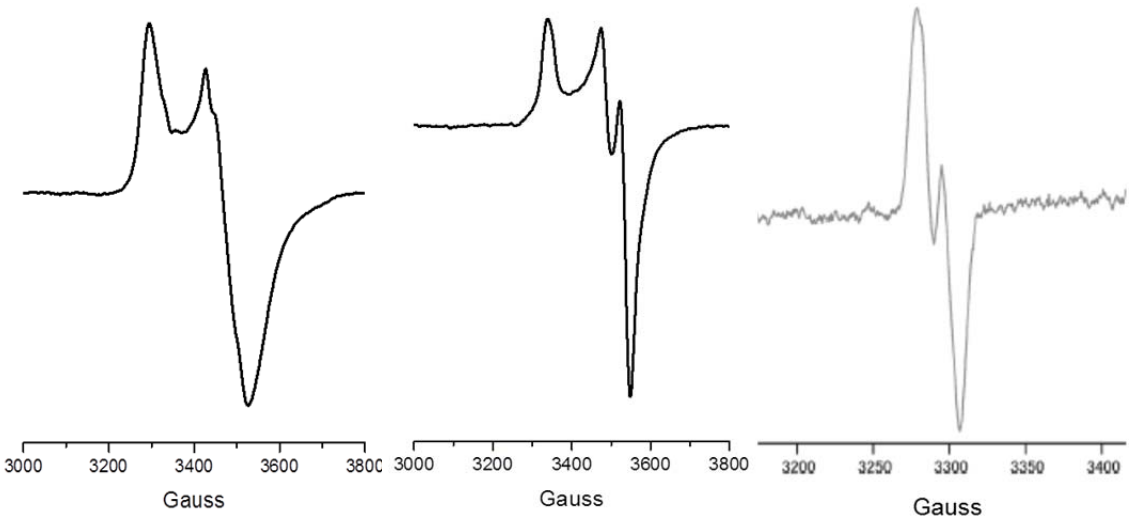

Figure 5.2. The $[4Fe\text{-}4S]^{1+}$ cluster of PFL-AE (left) generally gives rise to a nearly axial EPR signal, and addition of SAM (center) alters the spectrum to a more rhombic signal with g values around 2.01, 1.89, and 1.88. The glycyl radical (right) appears as a split isotropic signal centered around g=2.00.

The EPR spectrum of this sample showed a split, due to the nuclear spin on the Cα hydrogen, isotropic signal centered around g=2.00 typical of a glycyl radical. This demonstrated that our reduction techniques were able to produce PFL-AE containing the active cluster capable of catalysis (Figure 5.2).

Reduced PFL-AE was mixed with PFL and SAM using the rapid freeze-quench apparatus for 25, 300, and 500 milliseconds, and these samples were analyzed by EPR

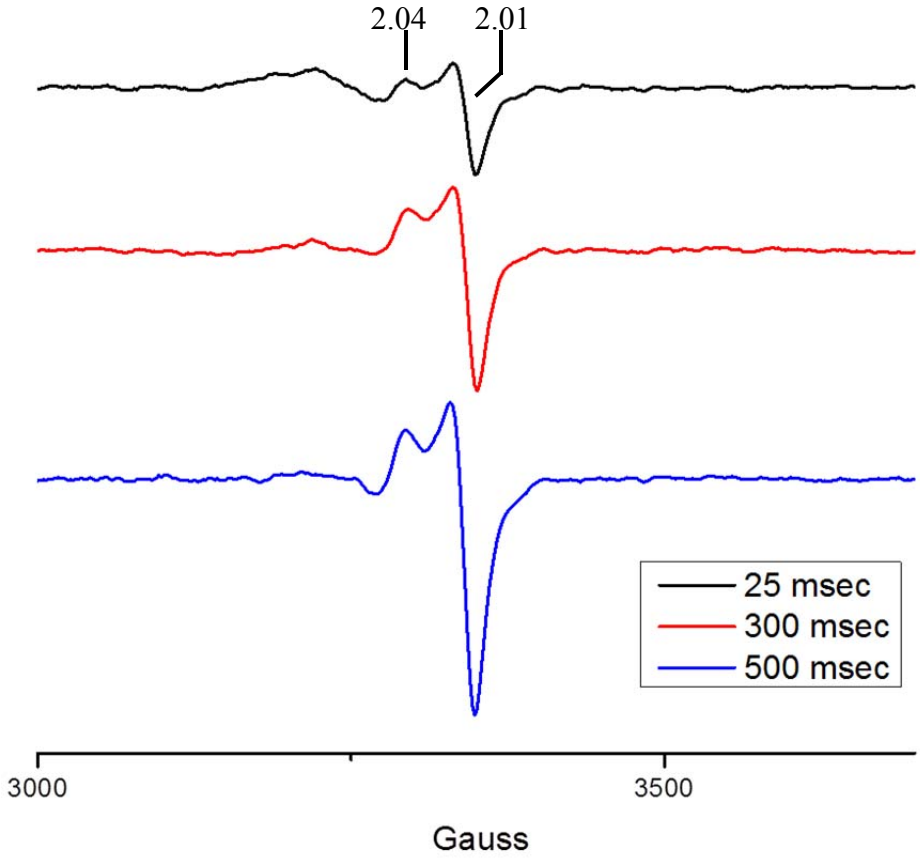

Figure 5.3. EPR signals observed in samples prepared by RFQ, in which reduced PFL-AE was mixed with PFL and unlabeled SAM for 25, 300, and 500 milliseconds prior to freeze-quench. Initial concentrations were 550 µM PFL-AE and 550 µM PFL with 2 mM SAM, and after mixing in a 1:1 ratio, final concentrations were 225 µM PFL-AE, 225 µM PFL, and 1 mM SAM. EPR signals resulting from rapid freeze quench were axial with g values of 2.04 and 2.01. An increase in intensity of the signal with longer mixing times was also observed.

spectroscopy. The EPR spectra obtained from these experiments are axial with g values of 2.04 and 2.01 (Figure 5.3). The signals also showed an increase in intensity with longer mixing times before quenching. Upon analysis of the EPR signals detected in this study as well as earlier ones, it was apparent that these signals were neither the reduced $[4Fe\text{-}4S]^{1+}$ cluster of PFL-AE nor the glycyl radical on PFL. The signal is also inconsistent with cluster degradation to a [3Fe-4S] or [2Fe-2S] cluster; a $[3Fe\text{-}4S]^{1+}$ cluster in PFL-AE gives rise to a nearly isotropic EPR signal around g=2.02 [16]. Rather the observed signals are from a new uncharacterized paramagnetic species. The lack of a signal corresponding to the $[4Fe\text{-}4S]^{1+}$ cluster of PFL-AE indicated that it was oxidized

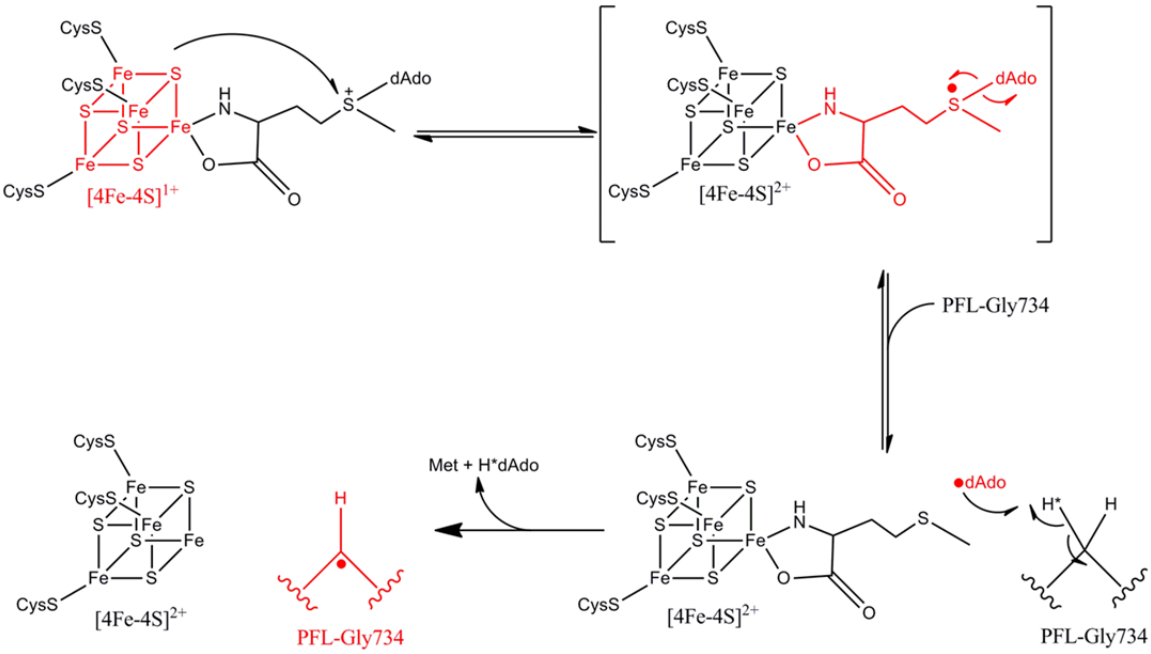

Scheme 5.1. Proposed formation of paramagnetic species (shown in red) during PFL-AE catalyzed activation of PFL. The paramagnetic species include the $[4Fe\text{-}4S]^{1+}$ cluster of PFL-AE formed upon reduction, the sulfuranyl radical resulting from inner-sphere electron transfer from the cluster to the sulfonium of SAM, the 5'-deoxyadenosyl radical generated by reductive cleavage of the S-5'C of SAM, and the glycyl radical product of the overall reaction.

during initiation of catalysis. A glycyl radical signal was also absent from these spectra implying that the reaction had not progressed to completion. These results suggest that the observed paramagnetic species is most likely a reaction intermediate of the PFL-AE catalyzed reaction.

The PFL-AE catalyzed reaction contains four possible paramagnetic species (Scheme 5.1). The paramagnetic species include the $[4Fe\text{-}4S]^{1+}$ cluster of PFL-AE formed upon reduction, the sulfuranyl radical resulting from inner-sphere electron transfer from the cluster to the sulfonium of SAM, the 5'-deoxyadenosyl radical generated by reductive cleavage of the S-5'C of SAM, and the glycyl radical product of the overall reaction. As stated previously the EPR spectra obtained are not consistent with the $[4Fe\text{-}4S]^{1+}$ cluster nor the glycyl radical. The oxidation of the cluster concomitant with the production of the new signal as well as its disappearance with the generation of the glycyl radical indicate that the new signal observed is one of the intermediate radicals produced during PFL-AE catalysis. To allow characterization of the paramagnetic species using ENDOR, the RFQ experiment was also done with uniformly labeled *S*-[adenosyl-^{13}C, ^{15}N]-methionine (Figure 5.5 A). If the radical intermediate is indeed a SAM based radical, the use of labeled SAM (in these experiments uniformly labeled on the adenosyl moiety) should allow for coupling between one or more of the nuclear spins with the unpaired electron producing an ENDOR signal. However, while an EPR signal identical to the one produced without labeled SAM was observed (Figure 5.4), only weak ENDOR signals were detected. Other labeled SAM molecules are being synthesized (Figure 5.5 B and C), which may

provide stronger ENDOR signals and allow for characterization of the new paramagnetic species.

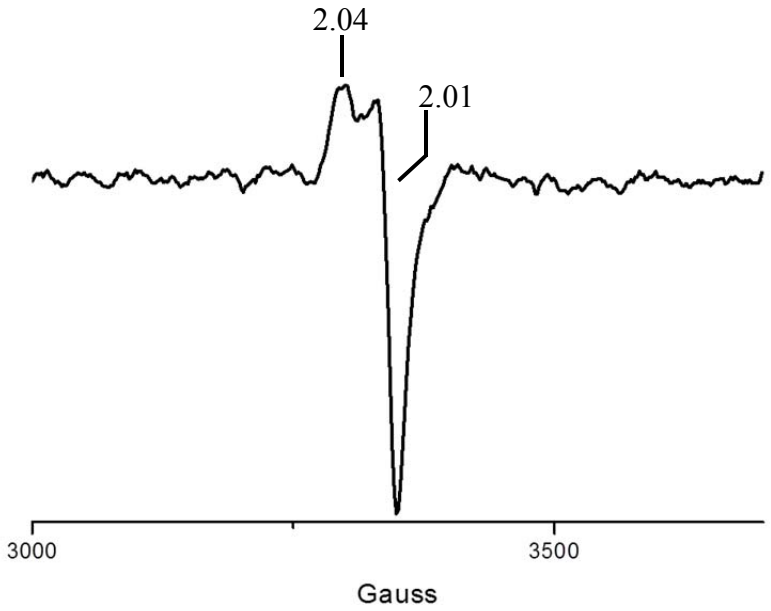

Figure 5.4. EPR signal obtained after mixing 550 μM PFL-AE with 550 μM PFL and 2 mM *S*-[adenosyl-^{13}C, ^{15}N]-methionine for 500 milliseconds using RFQ. Final concentrations were 225 μM PFL-AE, 225 μM PFL, and 1 mM labeled SAM.

Conclusions

RFQ-EPR has been used to provide evidence for a paramagnetic intermediate in the reaction of PFL-AE with SAM and PFL. The newly observed species is neither the reduced $[4Fe\text{-}4S]^{1+}$ cluster nor the PFL glycyl radical is indicative of an intermediate species created during the catalysis of SAM cleavage and hydrogen atom abstraction. Other evidence that suggests that this is a relevant intermediate includes the oxidation of the $[4Fe\text{-}4S]^{1+}$ cluster resulting in loss of the $[4Fe\text{-}4S]^{1+}$ signal, an increase in the signal

intensity of the intermediate with longer mixing times , and the decrease of this new signal with the emergence of the glycyl radical signal (data not shown).

The identity of the intermediate is unknown at this stage, and although it is possible that it is the 5'-deoxyadenosyl radical, the 5'-deoxyadenosyl radical is highly reactive rendering it difficult to trap. Also the signal is broader than would be expected for the dAdo radical The paramagnetic intermediate could also conceivably be a sulfuranyl radical created before the homolytic cleavage of the S-5'C bond (Scheme 5.1). Sulfuranyl radicals, while readily decomposing through S-C bond cleavage, have been detected by EPR at low temperatures [26].

To aid in the identification of the source of the intermediate signal, RFQ-ENDOR was employed; while ENDOR spectroscopy of the radio labeled samples using *S*-[adenosyl-^{13}C, ^{15}N]-methionine (Figure 5.5 (A)) gave rise to a signal too weak to be analyzed, the EPR spectrum revealed that the new signal was still being produced. This suggests that the method of generating the intermediate is sound, and a different labeled SAM may be more amenable to obtaining an ENDOR signal. To this end, other labeled SAM molecules that may provide suitable ENDOR signals include *S*-adenosyl-[methyl-^{13}C]methionine (Figure 5.5 (B)) as well as *S*-[adenosyl-^{2}H]-methionine (Figure 5.5 (C)). Once an ENDOR signal is obtained, further characterization and identification of this newly observed intermediate can proceed, offering further insight into the radical SAM mechanism of SAM cleavage and subsequent hydrogen atom abstraction.

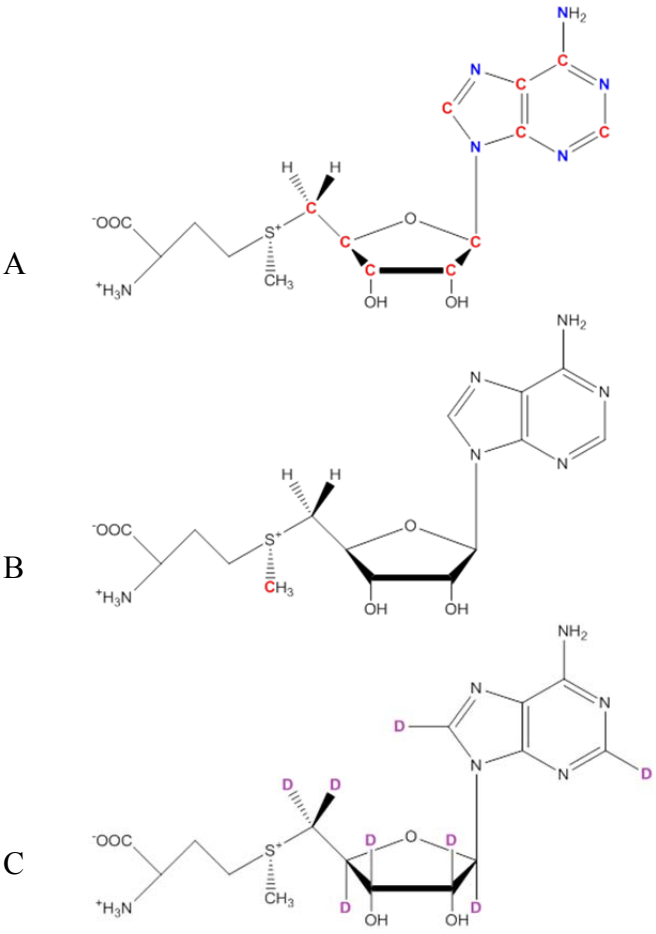

Figure 5.5. Labeled SAM for RFQ-ENDOR experiments (Red C indicates ^{13}C, Blue N indicates ^{15}N, and Purple D indicates ^{2}H). (A) was used in the current study and (B) and (C) will be synthesized and used in future studies.

References

1. Magnusson OT, Reed GH, and Frey PA (1999) J. Am. Chem. Soc. 121: 9764-9765.

2. Magnusson OT, Reed GH, and Frey PA (2001) Biochemistry 40: 7773-7782.

3. Benjdia A, Leprince J, Sandström C, Vaudry H, and Berteau O (2009) J. Am. Chem. Soc. 131: 8348-8349.

4. Cheek J, and Broderick JB (2002) J. Am. Chem. Soc. 124: 2860-2861.

5. Escalettes F, Florentin D, Bui BTS, Lesage D, and Marquet A (1999) J. Am. Chem. Soc. 121: 3571-3578.

6. Frey PA, Rothe M, Wagner AFV, and Knappe J (1994) J. Biol. Chem. 269: 12432-12437.

7. Gambarelli S, Luttringer F, Padovani D, Mulliez E, and Fontecave M (2005) Chembiochem : a European journal of chemical biology 6: 1960-1962.

8. Grove TL, Benner JS, Radle MI, Ahlum JH, Landgraf BJ, Krebs C, and Booker SJ (2011) Science 332: 604-607.

9. Guianvarc'h D, Florentin D, Bui BTS, Nunzi F, and Marquet A (1997) Biochem. Biophys. Res. Commun. 236: 402-406.

10. Kilgore JL, and Aberhart DJ (1991) J. Chem. Soc., Perkin Trans. 1: 79-84.

11. Knappe J, Neugebauer FA, Blaschkowski HP, and Gänzler M (1984) Proc. Natl. Acad. Sci. U.S.A. 81: 1332-1335.

12. Ruszczycky MW, Choi S-h, and Liu H-w (2010) J. Am. Chem. Soc. 132: 2359-2369.

13. Yan F, and Fujimori DG (2011) Proc. Natl. Acad. Sci. U.S.A. 108: 3930-3934.

14. Yokoyama K, Numakura M, Kudo F, Ohmori D, and Eguchi T (2007) J. Am. Chem. Soc. 129: 15147-15155.

15. Bray RC (1961) Biochem. J. 81: 189-193.

16. Broderick JB, Henshaw TF, Cheek J, Wojtuszewski K, Smith SR, Trojan MR, McGhan RM, Kopf A, Kibbey M, and Broderick WE (2000) Biochem. Biophys. Res. Commun. 269: 451-456.

17. Henshaw TF, Cheek J, and Broderick JB (2000) J. Am. Chem. Soc. 122: 8331-8332.

18. Nnyepi MR, Peng Y, and Broderick JB (2007) Arch. Biochem. Biophys. 459: 1-9.

19. Walsby CJ, Hong W, Broderick WE, Cheek J, Ortillo D, Broderick JB, and Hoffman BM (2002) J. Am. Chem. Soc. 124: 3143-3151.

20. Beinert H (1978) Methods Enzymol. 54: 435-445.

21. Walsby CJ, Ortillo D, Broderick WE, Broderick JB, and Hoffman BM (2002) J. Am. Chem. Soc. 124: 11270-11271.

22. Schmidt B, Mahmud G, Soh S, Kim SH, Page T, O'Halloran TV, Grzybowski BA, and Hoffman BM (2011) Appl. Magn. Reson. 40: 415-425.

23. Lin Y, Gerfen GJ, Rousseau DL, and Yeh SR (2003) Anal. Chem. 75: 5381-5386.

24. Hoffman BM, Derose VJ, Ong JL, and Davoust CE (1994) J. Magn. Reson., Ser. A 110: 52-57.

25. Davoust CE, Doan PE, and Hoffman BM (1996) J. Magn. Reson., Ser. A 119: 38-44.

26. Chatgilialoglu C, Castelhano AL, and Griller D (1985) J. Org. Chem. 50: 2516-2518.

CHAPTER 6

CONLUDING REMARKS ON PFL-AE

Pyruvate formate-lyase activating enzyme (PFL-AE) is one of the best characterized radical SAM enzymes to date. Studies of PFL-AE have provided the basis for much of the current understanding of radical SAM enzymes, including the requirement for a reduced $[4Fe\text{-}4S]^{+}$ cluster in catalysis, and the coordination of SAM to a unique iron of this cluster via the amino and carboxylate moieties of SAM [1, 2]. Such studies have led to a proposed mechanism where the $[4Fe\text{-}4S]^{1+}$ cluster reductively cleaves the S-5'C of the bound SAM through inner sphere electron transfer [1]. This cleavage generates methionine and a highly reactive 5'-deoxyadenosyl radical, which directly abstracts a hydrogen atom from the substrate; at this point the reaction diverges depending on the specific chemistry the radical SAM enzyme catalyzes. Evidence of the involvement of the 5'-deoxyadenosyl radical includes the stoichiometric production of 5'-deoxyadenosine and methionine as products of turnover [3-7], label transfer from substrate into 5'-dAdo [6-14], and the characterization by EPR of a stabilized allylic 5'-dAdo radical intermediate formed when the SAM analog 3',4'-anhydro-SAM (anSAM) was used in place of SAM in the reaction of lysine 2,3-aminomutase [15, 16]. No direct evidence such as a radical intermediate, however, has yet been detected for any of the radical SAM enzymes.

With the use of rapid freeze quench techniques in conjunction with EPR and ENDOR, PFL-AE is continuing to provide illumination on the common mechanism of

this widely diverse collection of enzymes. RFQ-EPR of PFL-AE mixed with PFL and SAM has revealed the production of an as yet unidentified intermediate during reductive SAM cleavage, and the possibility that this intermediate is a SAM sulfur-based radical is intriguing. The ability to observe and probe this short-lived intermediate provides a unique and exciting opportunity to advance our understanding of the radical chemistry catalyzed by these enzymes. It will also give insight into the generation of the 5'deoxyadenosyl radical used by these enzymes and how its production is tightly controlled to keep deleterious side reactions from occurring *in vivo*. In order to move forward in the characterization of the reaction intermediate additional experiments with labeled SAM molecules employing RFQ-ENDOR will need to be performed. Our hypothesis is that one or more of these labeled SAM molecules will supply a sufficient signal that can be analyzed and used to determine the identity of the intermediate.

Further exploration of the effects of SAM and substrate binding on the structure and properties of PFL-AE has been accomplished through the use of nuclear resonance vibrational spectroscopy (NRVS). The application of NRVS to proteins is a relatively new area, and PFL-AE represents the first radical SAM enzyme to be studied in this manner. The necessity of utilizing a Mössbauer active isotope (^{57}Fe in the case of the Fe-S cluster containing radical SAM enzymes) for NRVS allows for selectivity in its application because only the vibrational modes of the designated isotope will be observed; this permits effects on the Fe-S cluster to be directly observed without interfering signals. For PFL-AE the effects on the cluster of SAM and substrate analog

(YfiD) binding were determined through the calculation of two force constants, stiffness and resilience [17-20], from the NRVS data collected.

The stiffness force constant is inversely proportional to bond length, so the decrease seen upon SAM and YfiD binding implies that some of the Fe-S bonds lengthen, although which specific Fe-S bonds undergo a change cannot be determined by NRVS. Recent S K-edge XAS along with DFT calculations on PFL-AE supports this observation [21]. The XAS data showed an increase in the pre-edge intensity upon SAM binding to PFL-AE, which was reproduced using DFT calculations. In certain resulting models an increase in some of the Fe-S bonds upon SAM binding was predicted as would be expected from the NRVS data. Whether this bond lengthening upon substrate binding is a recurring theme in radical SAM enzymes awaits further investigation. However, unpublished EXAFS data from our lab on SPL showed elongated Fe…Fe distances in the presence of SAM, which may indicate longer Fe-S bonds. The occurrence of Fe-S bond lengthening with the binding of SAM in multiple radical SAM enzymes suggests that this may play an important role in the chemistry performed by radical SAM enzymes, although whether this is valid for all members of the superfamily remains to be seen and awaits further spectroscopic evidence.

Resilience is related to the rigidity of the protein around the cluster, and when SAM and YfiD were added to PFL-AE, an increase in resilience was observed indicating that the protein matrix tightened up around the active site creating a more defined environment in which the reaction can proceed. Such tightening could be accomplished through SAM interacting with amino acid residues in the vicinity of the active site as well

as the packing of SAM in the active site when YfiD binds as it closes off the opening to the active site. In the crystal structure of PFL-AE SAM was found to interact with two motifs which are highly conserved among the radical SAM superfamily. These motifs are involved in directly binding the methionine portion of SAM as well as stabilizing the binding pocket of the adenine moiety. While the interactions between YfiD and PFL-AE have not been established, twenty-two of the PFL residues around the glycine where the radical is formed are completely conserved in YfiD. As PFL-AE is capable of generating a glycyl radical on YfiD, it is probable that the interactions between the peptide backbone of the PFL peptide and the side chains of PFL-AE including the DGXGXR motif are preserved in the binding of YfiD. The combination of these interactions is the most likely source of the increased resilience seen upon binding of SAM and YfiD to PFL-AE.

Although PFL-AE shares all of the major attributes of the radical SAM superfamily, it also has a unique active site containing a monovalent cation. This cation is in close proximity, within 3 Å, to four amino acid oxygens, two from the protein back-bone (Thr105 and Met127) and two from aspartate residues (Asp104 and Asp129). Yet, even more fascinating is its position in relation to SAM; the monovalent cation is 2.4 Å from the unbound carboxyl oxygen of SAM. The location of the cation in the active site and its close proximity to the co-substrate SAM would suggest a role in the catalysis of the reaction performed by PFL-AE which is born out in activity assays of PFL-AE in the presence of different monovalent cations and the dependence of the enzymes activity on the concentration of the cation. When five different monovalent cations, Na^+, K^+, NH_4^+, Rb^+, and Cs^+, were individually used in the PFL-AE activity assay, different specific

activities of PFL-AE were calculated for each condition. The highest activity obtained was 45.7 ± 1.5 U/mg in the presence of K^+ suggesting it as the most likely candidate for the monovalent cation found *in vivo*, although the presence of the other cations gave high activities of PFL-AE as well: Na^+ (35.7 ± 5.8 U/mg), NH_4^+ (41.1 ± 6.5 U/mg), Rb^+ (42.5 ± 2.8 U/mg), and Cs^+ (34.5 ± 1.5 U/mg). There also appears to be a trend in the specific activity calculated for PFL-AE with respect to the ionic radius of the cation present. Additionally, the dependence of PFL-AE activity on the cation concentration was examined using different concentrations of K^+ in the activity assays and balancing the ionic strength with choline chloride, a very large monovalent cation whose size precludes its entry into the active site of PFL-AE. The assays demonstrated an increase in the specific activity of PFL-AE with the increase in K^+ concentration. Interestingly the assay with 0 mM K^+ also showed activity as there should be no activity if PFL-AE is dependent upon the cation for the initiation of catalysis. This suggests that the cation may not be absolutely required for activity but instead may stimulate activity. However more activity assays will need to be performed and different activation conditions will need to be investigated to confirm this hypothesis as previous assays indicated that PFL-AE was not active in the absence of a cation.

The close proximity of the cation to SAM and its location within the active site implied that it may affect the electronic properties of the active site, and such effects can be seen in EPR samples prepared in the presence of the individual cations. PFL-AE in the presence of each cation both with and without SAM displays different EPR signals probably due to slightly different conformations of the enzyme and thus the active site

caused by the different monovalent cation radii. The signals seem to be composed of two spins, which for the samples with SAM could be construed as clusters both bound and unbound by SAM. For the samples without SAM the two spins could arise from the sample preparation where PFL-AE was diluted into the buffer containing the different monovalent cations. PFL-AE is purified in the presence of Na^+, and it is probable that not all of the Na^+ in the active site is exchanged for the other cations. However, even the EPR sample containing Na^+ appears to contain two spins. This may suggest that the PFL-AE active site may not consistently contain a monovalent cation and that the two spins correspond to an active site with or without a monovalent cation present. Future simulations of the EPR data may help provide evidence for and insight into the source of the two spins.

The studies on PFL-AE presented herein demonstrate that while the necessity of the monovalent cation is still unclear, it is evident that the cation has direct effects on the activity of PFL-AE as well as the electronic structure of the active site lending initial insight into the role of the cation and its location in the active sight. Although the presence of a monovalent cation in the active site of a radical SAM enzyme seems unique to PFL-AE, PFL-AE has provided understanding into the superfamily as a whole through the NRVS studies showing the effects of SAM and substrate analog binding on the [4Fe-4S] cluster that are also supported by crystal structures and EXAFS data of other radical SAM enzymes. PFL-AE has also revealed a radical reaction intermediate through RFQ-EPR that when identified and characterized will bring new insight into the mechanism of SAM cleavage, which will be fascinating to explore with other superfamily members.

References

1. Henshaw TF, Cheek J, and Broderick JB (2000) J. Am. Chem. Soc. 122: 8331-8332.

2. Walsby CJ, Ortillo D, Broderick WE, Broderick JB, and Hoffman BM (2002) J. Am. Chem. Soc. 124: 11270-11271.

3. Guianvarc'h D, Florentin D, Bui BTS, Nunzi F, and Marquet A (1997) Biochem. Biophys. Res. Commun. 236: 402-406.

4. Knappe J, Neugebauer FA, Blaschkowski HP, and Gänzler M (1984) Proc. Natl. Acad. Sci. U.S.A. 81: 1332-1335.

5. Ruszczycky MW, Choi S-h, and Liu H-w (2010) J. Am. Chem. Soc. 132: 2359-2369.

6. Benjdia A, Leprince J, Sandström C, Vaudry H, and Berteau O (2009) J. Am. Chem. Soc. 131: 8348-8349.

7. Yokoyama K, Numakura M, Kudo F, Ohmori D, and Eguchi T (2007) J. Am. Chem. Soc. 129: 15147-15155.

8. Cheek J, and Broderick JB (2002) J. Am. Chem. Soc. 124: 2860-2861.

9. Frey PA, Rothe M, Wagner AFV, and Knappe J (1994) J. Biol. Chem. 269: 12432-12437.

10. Escalettes F, Florentin D, Bui BTS, Lesage D, and Marquet A (1999) J. Am. Chem. Soc. 121: 3571-3578.

11. Kilgore JL, and Aberhart DJ (1991) J. Chem. Soc., Perkin Trans. 1: 79-84.

12. Gambarelli S, Luttringer F, Padovani D, Mulliez E, and Fontecave M (2005) Chembiochem : a European journal of chemical biology 6: 1960-1962.

13. Grove TL, Benner JS, Radle MI, Ahlum JH, Landgraf BJ, Krebs C, and Booker SJ (2011) Science 332: 604-607.

14. Yan F, and Fujimori DG (2011) Proc. Natl. Acad. Sci. U.S.A. 108: 3930-3934.

15. Magnusson OT, Reed GH, and Frey PA (1999) J. Am. Chem. Soc. 121: 9764-9765.

16. Magnusson OT, Reed GH, and Frey PA (2001) Biochemistry 40: 7773-7782.

17. Adams KL, Tsoi S, Yan J, Durbin SM, Ramdas AK, Cramer WA, Sturhahn W, Alp EE, and Schulz C (2006) J. Phys. Chem. B 110: 530-536.

18. Leu BM, Zhang Y, Bu L, Straub JE, Zhao J, Sturhahn W, Alp EE, and Sage JT (2008) Biophys. J. 95: 5874-5889.

19. Lipkin HJ (1995) Phys. Rev. B. 52: 10073-10079.

20. Zaccai G (2000) Science 288: 1604-1607.

21. Dey A, Peng Y, Broderick WE, Hedman B, Hodgson KO, Broderick JB, and Solomon EI (2011) J. Am. Chem. Soc. 133: 18656-18662.

CHAPTER 7

RADICAL SAM ENZYMES IN METHYLATION AND MEHTYLTHIOLATION

Contribution of Authors and Co-Authors

Manuscripts in Chapters 3, 4, and 7

Author: Rachel U. Hutcheson

Contributions: Researched the literature and prepared the manuscript and figures.

Co-author: Joan B. Broderick

Contributions: Researched the literature and aided in the preparation of the manuscript and figures.

Manuscript Information Page

Rachel U. Hutcheson and Joan B. Broderick
Metallomics
Status of the manuscript:
____ Prepared for submission to a peer-reviewed journal
____ Officially submitted to a peer-reviewed journal
____ Accepted by a peer-reviewed journal
__X__ Published in a peer-reviewed journal

Published by the Royal Society of Chemistry
In Volume 4, 1149-1154 (2012)

Metallomics

Integrated biometal science

www.rsc.org/metallomics

Volume 4 | Number 11 | November 2012 | Pages 1127–1227

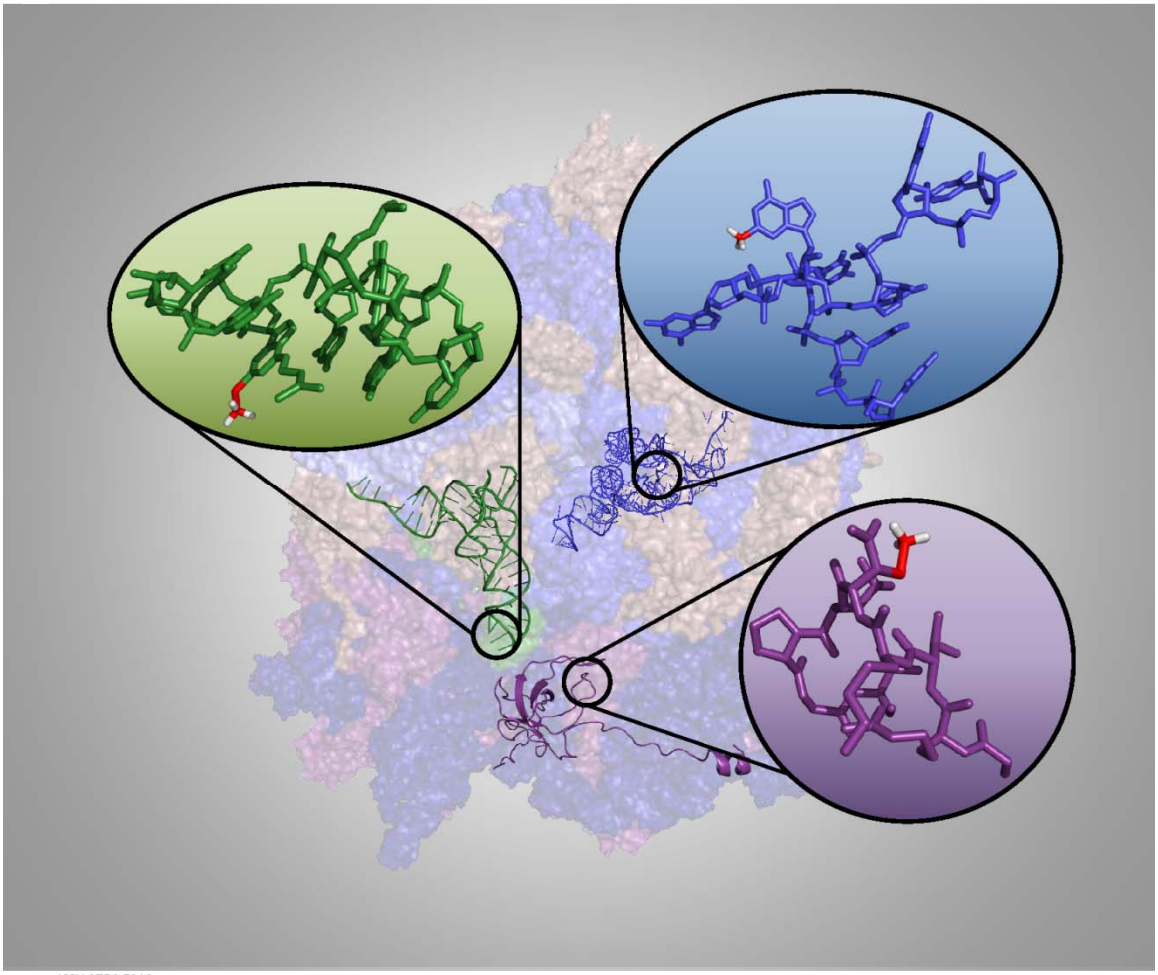

ISSN 1756-5901

RSC Publishing

MINIREVIEW

Rachel U. Hutcheson and Joan B. Broderick

Radical SAM enzymes in methylation and methylthiolation

Indexed in MEDLINE!

1756-5901(2012)4:11;1-R

Metallomics

Cite this: *Metallomics*, 2012, **4**, 1149–1154

www.rsc.org/metallomics

MINIREVIEW

Radical SAM enzymes in methylation and methylthiolation

Rachel U. Hutcheson and Joan B. Broderick*

Received 10th July 2012, Accepted 30th August 2012
DOI: 10.1039/c2mt20136d

Radical *S*-adenosyl-L-methionine (SAM) enzymes are a large and diverse superfamily with functions ranging from enzyme activation through a single H atom abstraction to complex organic and metal cofactor synthesis involving a series of steps. Though these enzymes carry out a variety of functions, they share common structural and mechanistic characteristics. All of them contain a site-differentiated [4Fe–4S] cluster, ligated by a CX_3CX_2C or similar motif, which binds SAM at the unique iron. The $[4Fe–4S]^{1+}$ state of the cluster reductively cleaves SAM to produce a 5′-deoxyadenosyl radical, which serves to initiate the diverse reactions catalyzed by these enzymes. Recent highlights in the understanding of radical SAM enzymes will be presented, with a particular emphasis on enzymes catalyzing methylation and methythiolation reactions.

Structure and function of radical SAM enzymes

Radical *S*-adenosylmethionine (SAM or AdoMet) enzymes are part of a rapidly growing and very large superfamily first identified in 2001.[1] This superfamily contains thousands of enzymes, whose functionality is extremely diverse; known functions include assembly of complex cofactors, enzyme activation, methylation and methylthiolation, DNA repair, sulfur insertion, and tRNA modification as well as numerous others.[2,3] Radical SAM enzymes are characterized by a CX_3CX_2C motif or variations thereof, in which the Cys thiolates coordinate three irons of a $[4Fe–4S]^{2+/1+}$ cluster. The fourth iron of the [4Fe–4S] cluster is coordinated by the amino and carboxy groups of SAM, and is generally referred to as the unique iron due to its distinct ligand environment.[4,5] The $[4Fe–4S]^{1+}$ state of the cluster reductively cleaves SAM to create a 5′-deoxyadenosyl (dAdo) radical and methionine (Met).[6] The dAdo radical abstracts a hydrogen atom from the substrate to form a substrate-based radical that functions to carry out specific reactions dependent on each individual enzyme.

Structurally characterized members of the superfamily reveal a conserved core domain consisting of a full $(\alpha/\beta)_8$ or partial $(\alpha/\beta)_6$ TIM barrel fold (Fig. 1).[7,8] The variance of the TIM barrel completeness and openness correlates with the substrate

Department of Chemistry and Biochemistry and the Astrobiology Biogeocatalysis Research Center, Montana State University, Bozeman, MT 59717, USA.
E-mail: jbroderick@chemistry.montana.edu; Tel: +1 406 994 6160

Rachel U. Hutcheson

Rachel Hutcheson was born and raised in Montana and attended Seattle University where she received a Bachelor of Science in Biochemistry in 2005. She is currently pursuing her PhD in Biochemistry at Montana State University, with a focus on elucidating central mechanistic and structural questions for the radical SAM enzyme PFL-AE. Her research interests are in bioinorganic chemistry with a focus on Fe–S cluster containing enzymes.

Joan B. Broderick

Joan Broderick was born in 1965. She received a Bachelor of Science in Chemistry from Washington State University and a PhD from Northwestern University, where she was a National Science Foundation Graduate Fellow. She was an American Cancer Society postdoctoral fellow at MIT before joining the faculty at Amherst College as Assistant Professor in 1993. She moved to Michigan State University in 1998 and to Montana State University in 2005, where she is currently Professor of Chemistry and Biochemistry. Her research interests are in mechanistic bioinorganic chemistry, with a particular focus on enzymes utilizing iron–sulfur clusters to catalyze radical reactions.

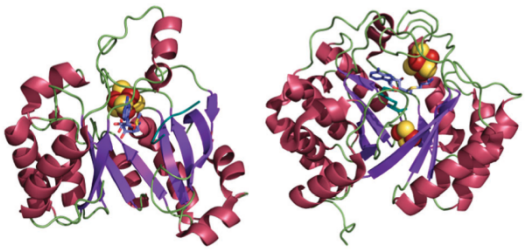

Fig. 1 Representative structures of Radical SAM enzymes. Left: Structure of the pyruvate formate-lyase activating enzyme (PFL-AE), which acts on a 170 kDa protein substrate and has a partial $(\alpha/\beta)_6$ TIM barrel fold (PDB ID 3CB8). Right: Structure of biotin synthase (BioB), which acts on a small molecule substrate (dethiobiotin) and has a complete $(\alpha/\beta)_8$ TIM barrel fold (PDB ID 1R30).

size, with the less complete, more open barrels present in enzymes acting upon larger substrates. Within this barrel the [4Fe–4S] cluster is located on a loop containing the CX_3CX_2C motif at the N-terminal end of the core domain. The opening of the barrel that provides access to the active site can be closed off by other protein components or the substrate, allowing for a more controlled reaction of the radical(s) produced during turnover.

Apart from this core domain, radical SAM enzymes can also contain additional elements that aid in their function. In some instances the enzyme contains a second binding motif for an additional Fe–S cluster. A second cluster is usually found in radical SAM enzymes involved in sulfur insertion (Fig. 1, right).[9–13] Evidence suggests that this second cluster is in fact the source of the sulfur atom incorporated into the substrate. Secondary clusters could also be used to transfer electrons. Radical SAM enzymes that modify RNA also have a supplementary domain at either the N- or C-terminus.[14,15] This domain is thought to be necessary for substrate recognition and interaction.[14,15]

Regioselectivity of S–C bond cleavage

Although there are three S–C bonds in SAM, one each to the methyl, the methionine γ-carbon, and the 5′-carbon, until recently it appeared that radical SAM enzymes catalyzed the reductive cleavage of only the S–C(5′) bond of SAM, and subsequently exploited the 5′-deoxyadenosyl radical for direct H atom abstraction (Table 1). Evidence for the involvement of the 5′-dAdo radical includes, in a number of enzymes, the stoichiometric production of 5′-deoxyadenosine and methionine as products of turnover,[16–20] label transfer from substrate into 5′-dAdo,[19–27] and the characterization by EPR of a stabilized allylic 5′-dAdo radical intermediate formed when the SAM analog 3′,4′-anhydro-SAM (anSAM) was used in place of SAM in the reaction of lysine 2,3-aminomutase.[28,29] Evidence has been mounting, however, for the involvement of alternate S–C cleavage events upon the enzymatic reductive cleavage of SAM in certain enzymes.

In Dph2 from *Pyrococcus horikoshii*, which performs the first step in diphthamide biosynthesis by addition of an 3-amino-3-carboxypropyl (ACP) group to a specific histidine residue on the translational elongation factor 2 (EF2), reductive cleavage of SAM by an iron–sulfur cluster leads to cleavage of the bond between the sulfur and the methionine γ-carbon (Table 1). This cleavage results in formation of an ACP radical and methylthioadenosine (MTA). Dph2 does not contain the canonical radical SAM cysteine motif; rather, the protein is a homodimer with each monomer containing three conserved cysteines (C59, C163, and C287), each from a different domain, capable of binding a [4Fe–4S] cluster.[30] The reduced $[4Fe–4S]^{1+}$ state of the cluster cleaves SAM homolytically between the sulfur and methionine γ-carbon to form the ACP radical.[31] The ACP radical does not mediate an H-atom abstraction, however, and instead attacks C-2 on the imidazole ring of the modified histidine residue resulting in addition to the ring.[30]

Evidence suggests that the B_{12}-independent glycerol dehydratase activating enzyme (GD-AE) also catalyzes cleavage of the S–C(γ) bond rather than the S–C(5′) bond.[32] GD-AE is part of a subset of radical SAM enzymes that activate glycyl radical enzymes (GREs) by H atom abstraction from a specific glycine residue of their respective substrates.[33,34] When investigating the activation of glycerol dehydratase (GD), it was discovered that instead of production of dAdo and Met, the products of SAM cleavage were MTA and 2-aminobutyrate, implicating the involvement of the ACP radical.[32]

The selective cleavage of SAM between either the sulfur and 5′-carbon bond or the sulfur and methionine γ-carbon bond may be related to the alignment of the Fe–S cluster and bond to be broken.[35,36] One proposal by Kampmeier suggests that

Table 1 *S*-Adenosylmethionine (SAM), left, has three S–C bonds. The radical produced upon homolytic cleavage of each of these bonds is indicated (with A representing adenosine), as are representative enzymes where known

S-Adenosylmethionine	Bond cleaved	Radical produced	Enzyme examples
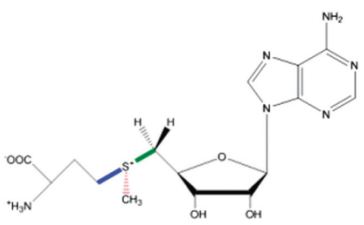	S—5′C	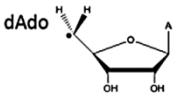	Radical SAM enzymes: MTases, MTTases
	S—γC		Dph2, GD-AE
	$S—CH_3$	Methyl $\bullet CH_3$	None known

the cleavage can be thought of as a displacement reaction at the sulfonium with the unique Fe of the [4Fe–4S] cluster taking the place of the S–C bond. This would require the unique Fe as well as the S–C bond on SAM to be broken to be collinear.[36] The crystal structures of several radical SAM enzymes which cleave SAM to produce dAdo and Met support this theory with the observed geometry of SAM bound in the active site.[37 41] However, it remains to be seen whether the enzymes that utilize the ACP radical bind SAM in an alternate fashion as would be necessary for the Fe and S–C(γ) bond broken to be collinear. The idea that the type of radical produced is related to the alignment of SAM with the [4Fe–4S] cluster is intriguing, and further structural studies of enzymes that use SAM in different fashions will help to either confirm this hypothesis or give new understanding into how an alternate radical could be produced.

Radical SAM methylation

It has long been suspected that the radical SAM superfamily contains methylases (MTases), but it is only recently that two have begun to be characterized. The bacterial enzymes RlmN, which is endogenous and thought to be important in ribosome function, and Cfr, which is acquired and confers antibiotic resistance, are methyltransferases that act upon A2503 in 23S rRNA. RlmN methylates the C2 position,[42] while Cfr methylates C8 preferentially but can also act upon C2.[43,44] Both of these enzymes contain the typical CX_3CX_2C motif that binds a [4Fe–4S] cluster. Both enzymes also utilize two SAM molecules; one is reductively cleaved to form the dAdo radical intermediate, and the second is used as the source of the methyl group.[44]

The mechanism by which A2503 is methylated by RlmN has recently been explored using isotopic labels. Using *S*-adenosyl-L-[methyl-^3H]methionine it was observed that the tritium label was incorporated into 23S rRNA, indicating that the methyl group is provided by SAM; production of dAdo, Met, and *S*-adenosylhomocysteine (SAH or AdoHcy) during the reaction was also detected.[44] From these results a mechanism was put forth in which SAM is cleaved to form the dAdo radical.[44] This radical then abstracts the C2 H from A2503 to generate a substrate radical that is then methylated by a second molecule of SAM.[44] This proposal was further revised when the use of A2503 labeled with deuterium at C2 showed no incorporation of deuterium into dAdo.[27] When SAM deuterated at the methyl position (d_3-SAM) was used in the reaction, however, the C2 of A2503 was doubly deuterated while dAdo was mono-deuterated.[27] These results led to a proposal in which the dAdo radical abstracts a hydrogen atom from the methyl group of the second molecule of SAM, resulting in a mono deuterated dAdo molecule and a SAM-methyl radical.[27] This SAM-methyl radical was then proposed to attach to C2 of A2503 with a hydride shift from C2 to the added methyl group giving a doubly deuterated product.[27]

However, another report published at the same time indicated that the hydrogen abstracted was neither from the substrate A2503 nor SAM but rather from a modified cysteine residue.[26] Use of d_3-SAM in single-turnover conditions showed no deuterium incorporation into A2503, and when RlmN was expressed and purified from methionine auxotrophic *E. coli* supplemented with d_3-Met, which also contains deuterium at the methyl position, deuterium was detected in the methylated adenosine substrate as well as dAdo.[26] This indicated that the hydrogen abstracted probably came from a protein bound methyl group, and mass spectrometry on wild-type RlmN revealed that Cys^{355} contains the methyl modification.[26] The proposed mechanism based on these results begins with the methylation of Cys^{355} by the first SAM molecule through a nucleophilic substitution typical of other SAM methylations. The second molecule of SAM is reductively cleaved by the reduced Fe–S cluster to produce the dAdo radical which abstracts one of the hydrogens from the methyl group just added to Cys^{355}. This new methyl radical is what then attacks C2 on A2503; the product is finally released when Cys^{118}, as a thiolate, attacks Cys^{355} forming a disulfide bond (Fig. 2, left).[26]

This mechanism is further supported by additional results from Grove *et al.*;[45] they demonstrated that all five cysteines, the three cluster ligands as well as two additional cysteines, are necessary for enzyme functionality. Interestingly, RlmN lacking a [4Fe–4S] cluster does not contain the methylated cysteine modification, which is only restored with the addition of SAM as well as the reconstitution of the cluster. This indicates that the cluster participates in both reductive SAM cleavage as well as the methylation of Cys^{355}.[45]

The proposed mechanism of Cfr is similar to RlmN,[26] which is not surprising as Cfr appears to have evolved from RlmN.[46] However, the ability of Cfr to methylate not only C8, the preferential site, but also C2 of A2503 suggests that there is a difference if not in mechanism then at least in substrate recognition and binding.

The structure of RlmN was just recently solved using X-ray crystallography and showed that, similar to other radical SAM enzymes, RlmN contains a partial $(\alpha/\beta)_6$ TIM barrel with the [4Fe–4S] cluster ligated at the carboxy end of the barrel (Fig. 2, right). In addition to this core radical SAM domain, RlmN contains an N-terminal domain of sixty residues in four short α-helices arranged in a variation of the HhH_2 fold, which is usually involved in substrate recognition of nucleic acids;[47,48] it is attached to the core by three β strands (β′1–3), which expand the barrel laterally. On the C-terminal end another extension consists of a β strand (β7), which reaches across the barrel opening and terminates in an α helix. These two additional β strand extensions are mechanistically important; the β7 strand contains the catalytically active Cys^{355} residue, which is methylated in the crystal structure, and positions it within 3.3 Å of the SAM methyl group, and the β′1–3 strand contains the other cysteine, Cys^{118}, which is thought to be necessary for completion of the catalytic cycle by releasing the newly methylated substrate.[14] The structure of RlmN thus provides further support for the mechanism proposed by Grove *et al.* as illustrated in Fig. 2.[14,26,45]

Radical SAM methylthiolation

There are only five known naturally occurring methylthio modifications, which occur on different components of the translation machinery. Four of these occur on tRNA, all on adenosine, while the fifth occurs on a small ribosomal protein (S12) at an aspartate residue. The function of the methylthio groups is not completely known, however some insight can be

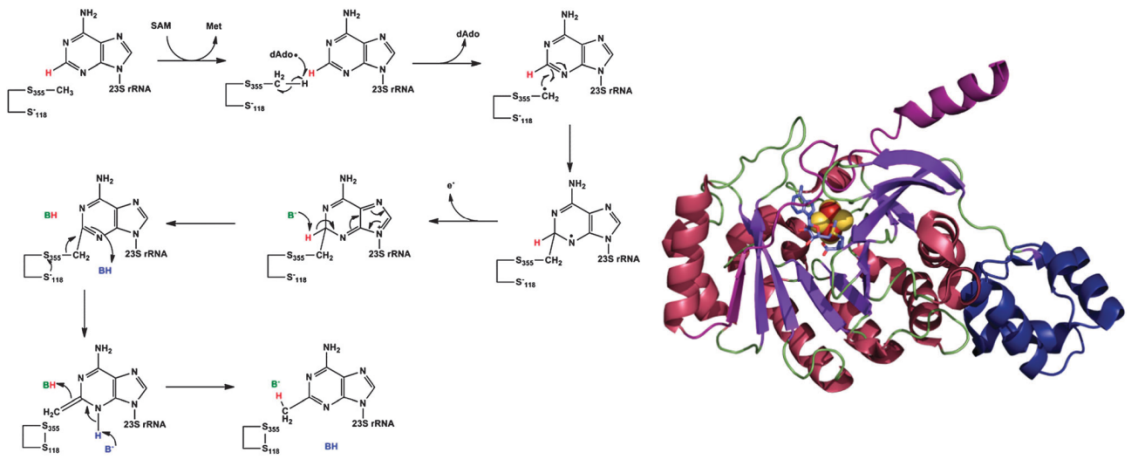

Fig. 2 Left: Mechanism for the second step in methylation as proposed by Grove *et al.*[45] The methylated cysteine (S355) was generated by SAM dependent methylation in the first step. Right: Structure of RlmN as determined by X-ray crystallography with the N-terminal domain in dark purple and the C-terminal extension in blue (PDB ID 3RFA).

gained from the positioning of the modifications within the translation machinery. The tRNA contains the methylthio group at the 3′ nucleotide (A-37) immediately following the anticodon and the modification on aspartate 89 of S12 projects into the acceptor site of the ribosome; these locations for the modifications implicate a role in codon–anticodon stability and translational efficiency and fidelity.[49–53]

The first methylthiotransferase (MTTase) to be characterized was MiaB,[54] which converts i^6A to ms^2i^6A; the time between the characterization of MiaB and the next MTTase was rather long, however study of this subclass of radical SAM enzymes has gained momentum in the past few years. Since the initial report on MiaB, two other MTTases have been identified. RimO is responsible for modifying the ribosomal protein,[55] and MtaB converts t^6A to ms^2t^6A.[56] What is interesting about this subclass of radical SAM enzymes is the bifunctional nature of MTTases, combining sulfur insertion with methylation.[57] Also, in addition to the radical SAM Fe–S cluster coordinated by the CX_3CX_2C motif, MTTases contain a second [4Fe–4S] cluster coordinated by three other conserved cysteines that is essential for function.[11]

Because of the two different functions a single MTTase carries out, it has been difficult to ascertain a complete mechanism. However, what has been gleaned from biochemical studies has provided answers to some aspects of the methylthiolation process. Like radical SAM methyltransferases, MTTases require two molecules of SAM per turnover, one for dAdo radical production and one to provide the methyl group. The observed products from these two uses of SAM are methionine and dAdo from SAM cleavage and SAH from methylation. It is thought, although not biochemically shown for certain, that the second Fe–S cluster is the source of the inserted sulfur, as is also thought to be the case in other radical SAM enzymes that catalyze sulfur insertion.[9–13]

These observations coupled with an understanding of radical SAM reactions in general have led to mechanistic proposals for MTTases (Fig. 3, left). Two of these mechanisms, using RimO as a model, involve a first step of reductive cleavage of SAM to form the dAdo radical, which then abstracts a hydrogen atom from the β-carbon of Asp89 on S12.[12] The substrate radical then attacks a μ-sulfido bridging ligand of the non-radical SAM Fe–S cluster. At this point the two mechanisms diverge; in one pathway, which is believed to be the more likely, the second molecule of SAM methylates the sulfur to which the Asp residue is attached causing a release of the methylthiolated Asp from the cluster.[12] In the alternate pathway the Asp bound cluster degrades forming a thiolated Asp intermediate.[12] It is this intermediate that is then methylated by the second molecule of SAM. A third possibility exists in which a sulfur on the secondary Fe–S cluster is methylated by one SAM molecule. The methylated sulfur would then be attacked by the Asp radical generated by the other molecule of SAM, releasing the final product.[12]

In order to carry out their reactions MTTases contain three domains, an N-terminal UPF0004 domain, a central radical SAM domain, and a C-terminal TRAM domain.[55] The UPF domain contains three of the conserved cysteines that in MiaB ligate one of the Fe–S clusters.[11] This domain is also most commonly found with the other two present in MTTases. The radical SAM domain contains the typical CX_3CX_2C motif ligating the other Fe–S cluster. The TRAM domain, which is only found in radical SAM enzymes of the MTTase subclass, is thought to be involved in substrate recognition.[55]

The structures of two of these domains, radical SAM and TRAM, were recently revealed in a crystal structure of RimO from *Thermatoga maritima* (Fig. 3, right).[15] The structure was obtained for the apo-enzyme crystals prepared with the use of subtilisin, which presumably cleaved the UPF domain from the rest of the protein; however, from the position of the N-terminus of the radical SAM domain, it can be postulated that the UPF domain can interact with the radical SAM Fe–S cluster as modeled from other radical SAM structures.[15] The radical SAM domain includes a partial $(\alpha/\beta)_6$ TIM barrel, and a superposition of RimO with the radical SAM enzyme MoaA (molybdenum cofactor biosynthesis) allowed the likely positions

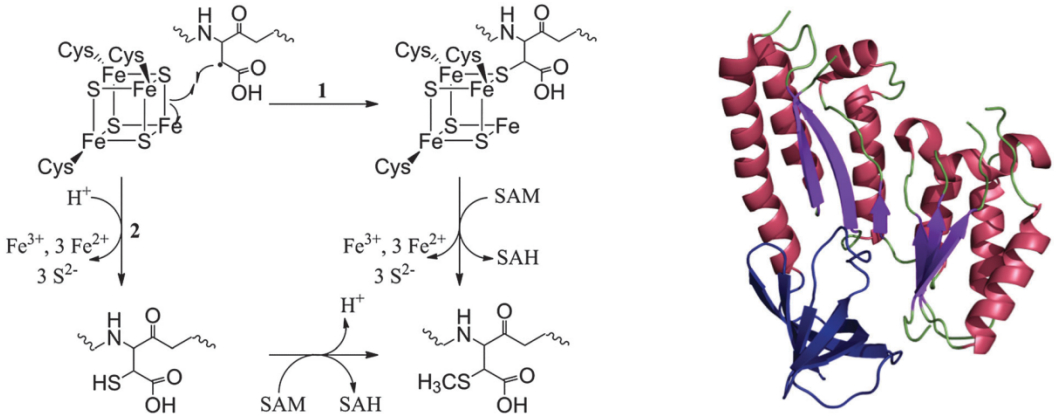

Fig. 3 Left: Two proposed mechanisms for radical SAM methylthiolation.[12] Right: Structure of apo-RimO as determined by X-ray crystallography, with only the radical SAM (purple and maroon) and TRAM (blue) domains visible (PDB ID 2QGQ).

of the radical SAM Fe–S cluster as well as SAM to be determined.[15] The location of the TRAM domain is at the distal edge of the concave surface of the radical SAM domain allowing access of the macromolecular substrates to the active site while still closely interacting with them. In RimO the putative surface of substrate binding is negatively charged, complementing the positively charged substrate, the ribosomal S12 protein.[15] While these results give an insight into MTTases, a better understanding of the mechanism and the role of the second Fe–S cluster will be possible once the structure of the holo-enzyme has been determined.

Conclusions

Methyltransferases and methylthiotransferases are two subclasses of an extensive superfamily of radical SAM enzymes. These two, however, are unique and puzzling in their ability to use two molecules of SAM in two distinct capacities: as a methyl group donor and as the source of the dAdo radical. Because of the dual roles of SAM, two adenosyl products, SAH and dAdo, are formed. Deoxyadenosine is known to inhibit radical SAM enzymes,[58] and SAH, while not directly studied in the radical SAM MTases, would likely result in a similar inhibition as this is the case with MTase enzymes that utilize a direct SN2 methyl substitution.[59] Further, evidence suggests that *in vivo* ratios of SAM to SAH, sometimes referred to as the methylation index, affects the activities of MTases.[60,61] An interesting and as-yet unexplored question is how the methylation index affects the activities of radical SAM enzymes, particularly those involved in methylation and methylthiolation.

For the MTases it is interesting that the dAdo radical abstracts a hydrogen atom from the methyl group of the second SAM molecule after the methyl has been added to a conserved cysteine. Another fascinating implication that deserves further investigation is the role of the radical SAM [4Fe–4S] cluster in methylation of the cysteine residue. To date no other radical SAM enzymes show a secondary role for their dAdo radical producing clusters. The dual role for the radical SAM cluster adds yet another complexity to the ability of radical SAM enzymes to control difficult and sensitive radical chemistry.

The presence of two Fe–S clusters in the MTTases is not surprising, as radical SAM enzymes involved in sulfur insertion all have additional clusters that are thought to be the source of the sulfur. A mechanistic anomaly within this subgroup concerns tRNA modification: direct hydrogen atom abstraction from the substrate would be from an sp^2 hybridized carbon for which there is no precedence in the radical SAM family. Further mechanistic studies using labeled substrates as well as a crystal structure of a holo-MTTase could help to illuminate how MTTases use the second Fe–S cluster as well as whether the sp^2 hydrogen is in fact the one abstracted. Further insights into the biological significance of the methylthio modifications that these enzymes impart are being revealed. Just recently the eukaryotic MTTase Cdkal1 was linked to the development of type 2 diabetes. Cdkal1 synthesizes ms^2t^6A in $tRNA^{Lys}$ (UUU); mice pancreatic cells that were deficient in this enzyme misread the Lys codon in proinsulin, which resulted in a reduction of glucose-stimulated proinsulin synthesis.[62]

Radical SAM enzymes catalyze a remarkably diverse range of chemical reactions, all of which are initiated by the reductive homolytic cleavage of an S–C bond of SAM, in order to generate a carbon-centered radical intermediate. Most radical SAM enzymes characterized to date appear to cleave only the S–C(5′) bond to generate the 5′-dAdo radical intermediate, although two enzymes have been recently shown to catalyze reductive cleavage of the S–C(γ) bond to generate the alternate 3-amino-3-carboxypropyl (ACP) radical.[31,32] Although reductive homolytic cleavage of the third S–C bond of SAM to generate a methyl radical has not been demonstrated, the MTases and MTTases discussed in this review do cleave (presumably in a nucleophilic, heterolytic manner) the S–C(methyl) bond of SAM to provide the methyl group required for the reaction.[44,57] These enzymes thus represent fascinating examples of the dual use of SAM (as a methyl donor and a radical precursor) in a single enzyme.

Acknowledgements

Research on radical SAM enzymes in the Broderick lab is supported by the National Institutes of Health grant GM54608 and the Department of Energy Grant DE-FG02-10ER16194.

The Astrobiology Biogeocatalysis Research Center is supported by NASA (NNA08C-N85A).

Notes and references

1 H. J. Sofia, G. Chen, B. G. Hetzler, J. F. Reyes-Spindola and N. E. Miller, *Nucleic Acids Res.*, 2001, **29**, 1097–1106.
2 E. M. Shepard and J. B. Broderick, in *Comprehensive Natural Products II: Chemistry and Biology*, ed. L. Mander and H.-W. Liu, Elsevier, Oxford, 2010, vol. 8, pp. 625–661.
3 P. A. Frey, A. D. Hegeman and F. J. Ruzicka, *Crit. Rev. Biochem. Mol. Biol.*, 2008, **43**, 63–88.
4 C. Krebs, W. E. Broderick, T. F. Henshaw, J. B. Broderick and B. H. Huynh, *J. Am. Chem. Soc.*, 2002, **124**, 912–913.
5 C. J. Walsby, D. Ortillo, W. E. Broderick, J. B. Broderick and B. M. Hoffman, *J. Am. Chem. Soc.*, 2002, **124**, 11270–11271.
6 T. F. Henshaw, J. Cheek and J. B. Broderick, *J. Am. Chem. Soc.*, 2000, **122**, 8331–8332.
7 J. L. Vey and C. L. Drennan, *Chem. Rev.*, 2011, **111**, 2487–2506.
8 D. P. Dowling, J. L. Vey, A. K. Croft and C. L. Drennan, *Biochim. Biophys. Acta.*, 2012, 1178–1195.
9 N. B. Ugulava, B. R. Gibney and J. T. Jarrett, *Biochemistry*, 2001, **40**, 8343–8351.
10 R. M. Cicchillo, K.-H. Lee, C. Baleanu-Gogonea, N. M. Nesbitt, C. Krebs and S. J. Booker, *Biochemistry*, 2004, **43**, 11770–11781.
11 H. L. Hernández, F. Pierrel, E. Elleingand, R. Garcia-Serres, B. H. Huynh, M. K. Johnson, M. Fontecave and M. Atta, *Biochemistry*, 2007, **46**, 5140–5147.
12 K.-H. Lee, L. Saleh, B. P. Anton, C. L. Madinger, J. S. Benner, D. F. Iwig, R. J. Roberts, C. Krebs and S. J. Booker, *Biochemistry*, 2009, **48**, 10162–10174.
13 S. Arragain, S. K. Handelman, F. Forouhar, F.-Y. Wei, K. Tomizawa, J. F. Hunt, T. Douki, M. Fontecave, E. Mulliez and M. Atta, *J. Biol. Chem.*, 2010, **285**, 28425–28433.
14 A. K. Boal, T. L. Grove, M. I. McLaughlin, N. H. Yennawar, S. J. Booker and A. C. Rosenzweig, *Science*, 2011, 1089–1092.
15 S. Arragain, R. Garcia-Serres, G. Blondin, T. Douki, M. Clemancey, J.-M. Latour, F. Forouhar, H. Neely, G. T. Montelione, J. F. Hunt, E. Mulliez, M. Fontecave and M. Atta, *J. Biol. Chem.*, 2010, **285**, 5792–5801.
16 D. Guianvarc'h, D. Florentin, B. T. S. Bui, F. Nunzi and A. Marquet, *Biochem. Biophys. Res. Commun.*, 1997, **236**, 402–406.
17 J. Knappe, F. A. Neugebauer, H. P. Blaschkowski and M. Gänzler, *Proc. Natl. Acad. Sci. U. S. A.*, 1984, **81**, 1332–1335.
18 M. W. Ruszczycky, S.-h. Choi and H.-w. Liu, *J. Am. Chem. Soc.*, 2010, **132**, 2359–2369.
19 A. Benjdia, J. Leprince, C. Sandström, H. Vaudry and O. Berteau, *J. Am. Chem. Soc.*, 2009, **131**, 8348–8349.
20 K. Yokoyama, M. Numakura, F. Kudo, D. Ohmori and T. Eguchi, *J. Am. Chem. Soc.*, 2007, **129**, 15147–15155.
21 J. Cheek and J. B. Broderick, *J. Am. Chem. Soc.*, 2002, **124**, 2860–2861.
22 P. A. Frey, M. Rothe, A. F. V. Wagner and J. Knappe, *J. Biol. Chem.*, 1994, **269**, 12432–12437.
23 F. Escalettes, D. Florentin, B. T. S. Bui, D. Lesage and A. Marquet, *J. Am. Chem. Soc.*, 1999, **121**, 3571–3578.
24 J. L. Kilgore and D. J. Aberhart, *J. Chem. Soc., Perkin Trans. 1*, 1991, 79–84.
25 S. Gambarelli, F. Luttringer, D. Padovani, E. Mulliez and M. Fontecave, *ChemBioChem*, 2005, **6**, 1960–1962.
26 T. L. Grove, J. S. Benner, M. I. Radle, J. H. Ahlum, B. J. Landgraf, C. Krebs and S. J. Booker, *Science*, 2011, **332**, 604–607.
27 F. Yan and D. G. Fujimori, *Proc. Natl. Acad. Sci. U. S. A.*, 2011, **108**, 3930–3934.
28 O. T. Magnusson, G. H. Reed and P. A. Frey, *J. Am. Chem. Soc.*, 1999, **121**, 9764–9765.
29 O. T. Magnusson, G. H. Reed and P. A. Frey, *Biochemistry*, 2001, **40**, 7773–7782.
30 X. Zhu, B. Dzikovski, X. Su, A. T. Torelli, Y. Zhang, S. E. Ealick, J. H. Freed and H. Lin, *Mol. BioSyst.*, 2011, **7**, 74–81.
31 Y. Zhang, X. Zhu, A. T. Torelli, M. Lee, B. Dzikovski, R. M. Koralewski, E. Wang, J. Freed, C. Krebs, S. E. Ealick and H. Lin, *Nature*, 2010, **465**, 891–896.
32 J. M. Demick and W. N. Lanzilotta, *Biochemistry*, 2011, **50**, 440–442.
33 C. Raynaud, P. Sarçabal, I. Meynial-Salles, C. Croux and P. Soucaille, *Proc. Natl. Acad. Sci. U. S. A.*, 2003, **100**, 5010–5015.
34 J. R. O'Brien, C. Raynaud, C. Croux, L. Girbal, P. Soucaille and W. N. Lanzilotta, *Biochemistry*, 2004, **43**, 4635–4645.
35 J. B. Broderick, *Nature*, 2010, **465**, 877–878.
36 J. A. Kampmeier, *Biochemistry*, 2010, **49**, 10770–10772.
37 G. Layer, J. Moser, D. W. Heinz, D. Jahn and W.-D. Schubert, *EMBO J.*, 2003, **22**, 6214–6224.
38 F. Berkovitch, Y. Nicolet, J. T. Wan, J. T. Jarrett and C. L. Drennan, *Science*, 2004, **303**, 76–79.
39 P. Hänzelmann and H. Schindelin, *Proc. Natl. Acad. Sci. U. S. A.*, 2004, **101**, 12870–12875.
40 B. W. Lepore, F. J. Ruzicka, P. A. Frey and D. Ringe, *Proc. Natl. Acad. Sci. U. S. A.*, 2005, **102**, 13819–13824.
41 J. L. Vey, J. Yang, M. Li, W. E. Broderick, J. B. Broderick and C. L. Drennan, *Proc. Natl. Acad. Sci. U. S. A.*, 2008, **105**, 16137–16141.
42 S.-M. Toh, L. Xiong, T. Bae and A. S. Mankin, *RNA*, 2008, **14**, 98–106.
43 A. M. B. Giessing, S. S. Jensen, A. Rasmussen, L. H. Hansen, A. Gondela, K. Long, B. Vester and F. Kirpekar, *RNA*, 2009, **15**, 327–336.
44 F. Yan, J. M. LaMarre, R. Rohrich, J. Wiesner, H. Jomaa, A. S. Mankin and D. G. Fujimori, *J. Am. Chem. Soc.*, 2010, **132**, 3953–3964.
45 T. L. Grove, M. I. Radle, C. Krebs and S. J. Booker, *J. Am. Chem. Soc.*, 2011, **133**, 19586–19589.
46 K. H. Kaminska, E. Purta, L. H. Hansen, J. M. Bujnicki, B. Vester and K. S. Long, *Nucleic Acids Res.*, 2010, **38**, 1652–1663.
47 X. Shao and N. V. Grishin, *Nucleic Acids Res.*, 2000, **28**, 2643–2650.
48 D. J. Miller, N. Ouellette, E. Evdokimova, A. Savchenko, A. Edwards and W. F. Anderson, *Protein Sci.*, 2003, **12**, 1432–1442.
49 I. Díaz and M. Ehrenberg, *J. Mol. Biol.*, 1991, **222**, 1161–1171.
50 E. M. Gustilo, F. A. Vendeix and P. F. Agris, *Curr. Opin. Microbiol.*, 2008, **11**, 134–140.
51 M. Kaczanowska and M. Rydén-Aulin, *Microbiol. Mol. Biol. Rev.*, 2007, **71**, 477–494.
52 A. L. Konevega, N. G. Soboleva, V. I. Makhno, Y. P. Semenkov, W. Wintermeyer, M. V. Rodnina and V. I. Katunin, *RNA*, 2004, **10**, 90–101.
53 J. Urbonavičius, Q. Qian, J. M. B. Durand, T. G. Hagervall and G. R. Björk, *EMBO J.*, 2001, **20**, 4863–4873.
54 F. Pierrel, G. R. Björk, M. Fontecave and M. Atta, *J. Biol. Chem.*, 2002, **277**, 13367–13370.
55 B. P. Anton, L. Saleh, J. S. Benner, E. A. Raleigh, S. Kasif and R. J. Roberts, *Proc. Natl. Acad. Sci. U. S. A.*, 2008, **105**, 1826–1831.
56 B. P. Anton, S. P. Russell, J. Vertrees, S. Kasif, E. A. Raleigh, P. A. Limbach and R. J. Roberts, *Nucleic Acids Res.*, 2010, **38**, 6195–6205.
57 F. Pierrel, T. Douki, M. Fontecave and M. Atta, *J. Biol. Chem.*, 2004, **279**, 47555–47563.
58 M. R. Challand, T. Ziegert, P. Douglas, R. J. Wood, M. Kriek, N. M. Shaw and P. L. Roach, *FEBS Lett.*, 2009, **583**, 1358–1362.
59 S. Clarke and K. Banfield, in *Homocysteine in Health and Disease*, ed. R. Carmel and D. W. Jacobsen, Cambridge University Press, Cambridge, UK, 2001, pp. 63–78.
60 V. Zappia, C. R. Zydek-Cwick and F. Schlenk, *J. Biol. Chem.*, 1969, **244**, 4499–4509.
61 A. F. Perna, D. Ingrosso, V. Zappia, P. Galletti, G. Capasso and N. G. De Santo, *J. Clin. Invest.*, 1993, **91**, 2497–2503.
62 F.-Y. Wei, T. Suzuki, S. Watanabe, S. Kimura, T. Kaitsuka, A. Fujimura, H. Matsui, M. Atta, H. Michiue, M. Fontecave, K. Yamagata, T. Suzuki and K. Tomizawa, *J. Clin. Invest.*, 2011, **121**, 3598–3608.

CHAPTER 8

INITIAL CHARACTERIZATION OF A PUTATIVE RADICAL SAM METHYLTHIOTRANSFERASE

Introduction

The Northeast Structural Genomics Consortium (NESG) is a large scale structural genomics center that utilizes X-ray crystallography and nuclear magnetic resonance (NMR) to determine the tertiary structure of proteins. They utilize a high-throughput protein production platform that allows them to screen thousands of proteins and produce hundreds of protein structures [1]. These structures are then placed in the Protein Data Bank (PDB). One of these proteins, TM1862 from *Thermatoga maritima*, was of interest as a radical SAM enzyme because of its sequence homology to MiaB, a radical SAM methylthiotransferase (MTTase), as well as its radical SAM core domain of a partial

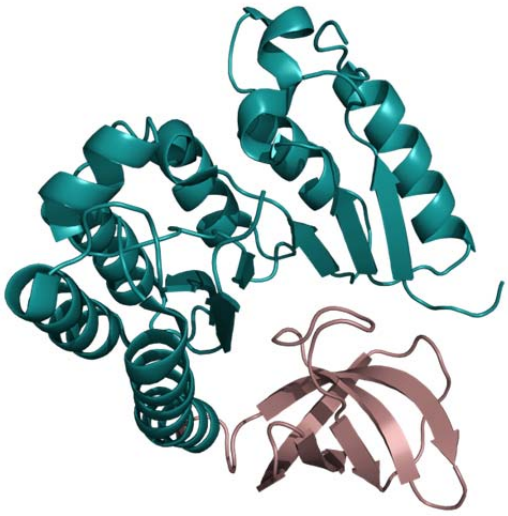

Figure 8.1. Crystal structure of TM1862 (PDB ID 2QGQ) [2] with the radical SAM domain shown in teal and the TRAM domain in violet.

$(\alpha/\beta)_6$ TIM barrel (Figure 8.1). Because of these similarities we decided to express and characterize this protein in an attempt to functionally characterize it.

Materials and Methods

Transformation and Growth of TM1862

The plasmid VR77 containing TM1862 in a pET21-d vector with a C terminal 6X His tag was a generous gift from the NESG. VR77 (approximately 1 ng/μL) was transformed into *Escherichia coli* Rosetta(DE3)pLysS for protein expression. A glycerol stock was made by growing one colony in 5 mL of LB media with 50 μg/mL ampicillin overnight at 37°C, 250 rpm shaking and adding 3.5 mL of the growth to 1.5 mL sterile glycerol. The stock was immediately aliquoted into 1 mL portions, frozen with liquid nitrogen, and stored at -80°C. For overexpression 50 mL of LB media with 50 μg/mL ampicillin was inoculated with one colony of TM1862 expressing *E. coli* and grown overnight at 37°C and 250 rpm shaking.

Growth with Minimal Media The overnight culture was added to 10 L of minimal media with 50 μg/mL of ampicillin, glucose solution, and vitamins. Minimal media consists of 100g Casamino acids, 84.2g MOPS, 8.0g Tricine, 14.7g NaCl, 16.0g KOH, and 5.1g NH_4Cl in 9.8 L of H_2O; the glucose solution contains 50g glucose in 200mL H_2O, 25mL "O" solution (0.1 g $FeCl_2 \cdot 4H_2O$ dissolved in 10 mL of 12 M HCl with 1 mL "T" solution [18.4 mg $CaCl_2 \cdot 2H_2O$, 64 mg H_3BO_3, 40 mg $MnCl_2 \cdot 4H_2O$, 18 mg $CoCl_2 \cdot 6H_2O$, 4 mg $CuCl_2 \cdot 2H_2O$, 340 mg $ZnCl_2$, and 605 mg $Na_2MoO_4 \cdot 2H_2O$ diluted to 100 mL with H_2O] and 2.68 g $MgCl_2 \cdot 6H_2O$ brought up to a final volume of 50 mL with

H_2O), 25mL 1M KH_2PO_4, 12.5mL 276mM K_2SO_4, and 62.5mL 0.1M $CaCl_2$; vitamins are 10mg each of biotin, pantothenic acid, vitamin B12, thiamine, folic acid, riboflavin, niacinamide, thioctic acid, and pyridoxine. The growth was incubated at 37°C in a 10 L New Brunswick benchtop fermentor with 200 rpm stirring, and compressed air was purged through the fermentor at a flow rate of 5 L/min. When the cells reached an OD_{600} of approximately 0.5, isopropyl-β-D-thiogalactopyranoside (IPTG) was added to a final concentration of 1 mM to induce protein expression, and the media was supplemented with 750 mg of $Fe(NH_4)_2(SO_4)•6H_2O$. The growth was allowed to continue for an additional 2 hours at which point it was cooled. When the temperature reached 30°C, the fermentor was purged with nitrogen, and at 20°C it was moved to a 4°C deli fridge where nitrogen sparging continued overnight and 750 mg of $Fe(NH_4)_2(SO_4)•6H_2O$ was again added. Cells were harvested by centrifugation at 6,000 rpm for 10 minutes at 4°C, frozen with liquid nitrogen and stored at -80°C. Average cell yields are approximately 2.5 g/L.

Growth with LB Media The overnight culture was added to 10 L of LB media with 50 μg/mL of ampicillin and incubated at 37°C in a 10 L New Brunswick benchtop fermentor with 250 rpm stirring. Compressed air was purged through the fermentor at a flow rate of 5 L/min. When the cells reached an OD_{600} of approximately 0.5, isopropyl-β-D-thiogalactopyranoside (IPTG) was added to a final concentration of 1 mM to induce protein expression. The growth was allowed to continue for an additional 3 hours at which point the cells were harvested by centrifugation at 6,000 rpm for 10 minutes at 4°C, frozen with liquid nitrogen and stored at -80°C. Average cell yields are approximately 1.6 g/L.

Purification of TM1862

Purification was carried out under anaerobic conditions in a Coy anaerobic chamber (Coy Laboratories, Grass Lake, MI) for all following steps. Cells were thawed and suspended, at an approximate ratio of 2 mL lysis buffer per 1 g of cell paste, in 20 mM sodium phosphates, pH 7.4, 200 mM NaCl, 10 mM imidazole, 1% Triton X-100, 5% (w/v) glycerol, 10 mM $MgCl_2$, 8 mg lysozyme (per 50 mL buffer), 1 mM phenylmethylsulfonyl fluoride (PMSF), and trace amounts of RNase A and DNase I (approximately 0.1 mg each per 50 mL buffer). The suspension was put on ice and homogenized by agitation with a 30 mL syringe and 18 gauge needle for 1 hour. The lysed cells were centrifuged at 18,000 rpm for 30 min at 4°C, and the supernatant heated at 75°C for approximately 20 minutes before it was loaded onto a 5 mL HisTrap HP nickel affinity column that was pre-equilibrated with 20 mM sodium phosphates, pH 7.4, 200 mM NaCl, 10 mM imidazole, and 5% (w/v) glycerol (Buffer A). Buffer B was identical to Buffer A except it contained 500 mM imidazole instead of 10 mM. Buffer A was used to wash the column for 10 column volumes (CVs) after which a stepwise gradient of Buffer B was used to elute the protein (5 CVs of 10% Buffer B, 5 CVs of 20% Buffer B, and 5 CVs of 50% Buffer B). Finally the column was washed with 10 CVs of 100% Buffer B. TM1862 began to eluted off the column in three peaks at 20%, 50% , and 100% Buffer B, and fractions containing color and an absorbance at 426 nm were pooled, concentrated, and buffer exchanged into 50 mM Tris, pH 7.4, 200 mM NaCl, and 1 mM DTT using an Amicon stirred cell with a YM 30 membrane. The

protein was then aliquoted into screw cap vials with o-rings, flash-frozen, and stored at -80°C.

If further purification was required, TM1862 purified on a Ni affinity column was subjected to gel filtration on a Waters AP-5 600 mm column containing preparatory grade superdex 75 resin which was first washed with 1 mM dithionite to help eliminate residual oxygen and then equilibrated with Gel Filtration Buffer (50 mM Tris, pH 7.4, 200 mM NaCl, 1 mM DTT). The Gel Filtration Buffer was washed over the column for a total of 900 mL, and TM1862 begins to elute around 500 mL of filtrate. Fractions containing a dark brown color and a high ratio of 426/280 nm absorbance were pooled and concentrated using an Amicon stirred cell with a YM 30 membrane, flash-frozen, and stored at -80°C.

Protein Reconstitution

In Coy anaerobic chamber (Coy Laboratories, Grass Lake, MI) purified TM1862 was centrifuged to remove any precipitate, diluted to approximately 50 μM (final concentration after iron and sulfide additions) with 50 mM Tris, pH 7.4, 200 mM NaCl, and 5 mM DTT, and stirred for 15 minutes. An eight fold excess of iron ($FeCl_3$) was added very slowly and incubated with stirring for 20 minutes after which an eight fold excess of sulfide (Na_2S) was slowly added. The complete mixture was stirred for an additional two hours, centrifuged to remove the precipitate, and concentrated before loading onto a G-25 Sephadex (P-10 desalting) column equilibrated with 50 mM Tris, pH 7.4, 200 mM NaCl, and 5 mM DTT. The protein was eluted with the same buffer and

fractions containing a brown color were collected, flash frozen with liquid N_2, and stored at -80°C.

Protein and Iron Quantitation

Protein concentration was determined by the method of Bradford [3] using a dye kit from Bio-Rad and bovine serum albumin as a standard. Briefly, 0.1 mg/mL BSA was added to a total of 800 µL H_2O in differing amounts (usually to a final amount of 1, 2, 3, 4, 5, and 6 µg BSA in each standard) to which 200 µL of Bradford dye was added. The samples were incubated at room temperature for approximately 30 minutes, and then the absorbance at 595 nm was recorded using a Thermo Scientrific Evolution 60 spectrophotometer to create a standard curve. Protein samples were made (by substituting protein for BSA) such that the absorbance fell within the standard curve range. Iron assays were performed according to the method of Beinert [4]. An iron standard of 10 µg/mL was used to create a standard curve by adding differing amounts (usually to a final amount of 0.4, 0.8, 1.2, 1.6, and 2.0 µg Fe in each standard) to a final volume of 1 mL. Protein samples were made (by substituting protein for Fe standard) such that the absorbance fell within the standard curve range. To each of the samples 500 µL of 1:1 1.2 M HCL: 4.5% $KMnO_4$ was added, and they were then incubated for 2 hours in a 65°C water bath. After the incubation, 100 µL of Reagent B (4.90 g ammonium acetate and 4.4 g ascorbic acid were dissolved in 5 mL H_2O; 40 mg each of neocuproine and ferrozine were added, and the volume was brought up to 12.5 mL with H_2O) was added to each. The samples were vortexed for approximately 5 seconds every

10 minutes for a total of 30 minutes at room temperature. The absorbance at 562 nm was recorded using a Thermo Scientrific Evolution 60 spectrophotometer.

EPR and UV-Vis Spectroscopy

In a Unilab MBraun anaerobic chamber with ≤1 ppm O_2, 200 μM TM1862 (non-reconstituted), 5 mM DTT, 50 mM Tris, pH 7.5, and 75 μM 5-deazariboflavin (added last in the dark) or 1 mM sodium dithionite were combined. Samples containing 5-deazariboflavin were placed in an EPR tube, and photoreduction was accomplished by illumination with a 300 W halogen lamp in an ice bath for one hour, and samples without SAM were frozen with liquid nitrogen. For samples with SAM the solution was removed from the EPR tube; SAM was added to a final concentration of 0.6 mM and allowed to incubate for 5-10 minutes before being placed back in the EPR tube and frozen in liquid nitrogen. Samples containing sodium dithionite were placed on ice for 10 minutes then placed in an EPR tube and frozen with liquid nitrogen. For those containing SAM, SAM was added to a final concentration of 0.6 mM and incubated on ice for 5-10 minutes, placed in an EPR tube, and frozen with liquid nitrogen.

EPR spectra were recorded on a Bruker ESP300E X-band spectrometer equipped with a liquid helium cryostat and temperature controller from Oxford Instruments. Typical experiment parameters were 12 K and 9.24 GHz, with 2 mW microwave power and 10 G modulation amplitude. Each spectrum shown is the average of two scans.

For UV-Vis spectroscopy, the 250 μL EPR samples were diluted to 800 μL with 50 mM Tris, pH 7.4, and 200 mM NaCl. Scans from 300 to 800 nm were performed on a Cary 6000i UV-Vis spectrophotometer.

Alignment of TM1862 with MiaB and RimO

TM1862 was aligned with MiaB from *E. coli* and *T. maritima* as well as RimO from *E. coli* using ClustalX [5], and the NCBI protein BLAST using the "Align two or more sequences" option was used to determine percent identity.

TM1862 Crystal Setup

In an MBraun Unilab anaerobic glovebox TM1862 protein that had been purified by Ni affinity chromatography as well as gel filtration was used for the crystal setup and was approximately 0.51 mM. SAM was added to the protein to a final concentration of 2 mM. Conditions screened were the Hampton Cryo conditions 1 through 50. Briefly, 30 µL of a Hampton Cryo condition followed by 20 µL of the protein and SAM with a small air space between were placed in a 1.5-1.8 x 90 mm capillary tube. The tube was sealed with wax and briefly spun just until the two layers were touching. This was repeated for each of the 50 conditions. The capillary tubes were stored in the glovebox and removed only to check for crystals.

Transformation of TM1862 into a *miaB*$^-$ Cell Line

The VR77 vector containing TM1862 was transformed into TX3346 (*miaB*$^-$) *Escherichia coli*, which was a generous gift from the Winkler lab at the University of Texas. Briefly, *miaB*$^-$ cells were grown in 5 mL of LB media overnight at 37°C and 225 rpm shaking. The following day 500 µL of growth was added to 50 mL of LB media and incubated at 37°C and 225 rpm shaking until the OD_{600} was approximately 0.5 at which point the culture was spun down at 2,000 rpm for 10 minutes. The media was removed;

the cell pellet was washed with 5 mL of ice cold sterile 0.1 M $CaCl_2$, and spun again at 2,000 rpm for 10 minutes. The wash was removed and the cell pellet was resuspended in 500 µL of the 0.1 M $CaCl_2$. The cells were aliquoted into 200 µL samples into prechilled sterile eppendorf tubes, frozen in liquid nitrogen, and stored at -80°C until use. For transformation, 5 µL of VR77 (approximately 1 ng/µL) was added to one tube of *miaB*$^-$ cells and incubated on ice for 30 minutes. The cells were heat shocked at 42°C for 90 seconds and placed back on ice for 2 minutes. The transformed cells were plated on LB media with 50 µg/mL ampicillin and grown overnight at 37°C. A glycerol stock was made by growing one colony in 5 mL of LB media with 50 µg/mL ampicillin overnight at 37°C, 250 rpm shaking and adding 3.5 mL of the growth to 1.5 mL sterile glycerol. The stock was immediately aliquoted into 1 mL portions, frozen with liquid nitrogen, and stored at -80°C.

Analysis of tRNA Modification

TM1862 in *miaB*$^-$ cells, as well as *miaB*$^-$ cells as a control, were grown by plating cells from a glycerol stock on LB media (50 µg/mL ampicillin were added to the one with the TM1862 gene) and incubating overnight at 37°C. One colony from each plate was used to inoculate individual portions of 5 mL of LB media (50 µg/mL ampicillin were added to the one with the TM1862 gene) and grown overnight at 37°C with 250 rpm shaking. The following morning 500 µL of overnight growth was added to 50 mL of LB media (50 µg/mL ampicillin were added to the one with the TM1862 gene) and grown at 37°C with 250 rpm shaking until the OD_{600} was approximately 0.4 at which point the temperature was shifted to 45°C. The growth was allowed to continue for an

additional 3 hours. Cells were harvested by centrifugation at 4°C and 2,500 rpm, flash frozen with liquid nitrogen, and stored at -80°C.

The isolation of RNA from the cells was performed using TRIzol® Reagent from Invitrogen. For each cell pellet 1 mL of TRIzol® Reagent was added and pipetted to lyse the cells. The sample was incubated at room temperature for 5 minutes, and 200 µL of chloroform was added. It was then shaken vigorously for 15 seconds and allowed to sit at room temperature for 3 minutes. The phases were separated by centrifugation at 4°C and 12,500 rpm for 15 minutes. The top aqueous phase was removed and saved (~600 µL recovered) being careful to not nick the interface, and 120 µL of 12 M LiCl was added to precipitate high molecular weight RNA. The sample was centrifuged at 4°C and 12,500 rpm for 20 minutes. The supernatant was removed, and 500 µL of isopropanol was added to it and incubated at room temperature for 10 minutes. The precipitate was retained by centrifugation at 4°C and 12,500 rpm for 20 minutes. The pellet was washed with 1 mL of ice cold ethanol, vortexed to mix, and centrifuged at 4°C and 9.900 rpm for 5 minutes. The ethanol was removed, and the pellet was air-dried for 1 hour before dissolving in 50 µL of sterile water and storing at -20°C.

For RNA hydrolysis, a sample containing 150 µg of RNA in a volume of 50 µL was heated for 2 minutes in a boiling water bath. The sample was cooled in an ice bath, and 5 µL of 10 mM $ZnSO_4$ and 10µL containing 2 units of nuclease P1 in 30 mM sodium acetate, pH 5.4 were added. An overnight incubation was performed in a 37°C water bath. The following day 10 µL of 0.5 M Tris, pH 8.3 and 10 µL containing 1 unit of

bacterial alkaline phosphatase in 2.5 M ammonium sulfate were added. The sample was incubated in a 37°C water bath for 2 hours and stored at -20°C.

To prepare a sample for HPLC analysis hydrolyzed RNA samples were boiled for 1 minute and spun down in a microcentrifuge at 13,000 rpm for 10 minutes to pellet the precipitate. The supernatant was applied to a Microcon microcentrifuge filter with a YM-3 membrane and spun. The flow-through was retained and stored at -20°C.

HPLC analysis was performed by injecting 10 µL of prepared, hydrolyzed RNA on a Waters 4.6 x 150 mm Spherisorb ODS2 column. The buffers utilized were Buffer A (10 mM $NH_4H_2PO_4$, pH 5.1, and 20% methanol) and Buffer B (10 mM $NH_4H_2PO_4$, pH 4.9, 20% methanol, and 15% isopropanol). A program was developed to separate i^6A and ms^2i^6A from the rest of the nucleosides based off of the method of Gehrke and Kuo [6] in which 98% Buffer A was run for 10 minutes followed by a gradient to 98% Buffer B over 21 minutes. Once at 98% Buffer B, it was run for 10 minutes and a subsequent gradient back down to 98% Buffer A was run over 10 minutes (all steps were run at 1 mL/min). The peaks eluting at approximately 3.25 minutes and 5.75 minutes were collected for UV-Vis analysis. UV-Vis scans from 200 nm to 350 nm were completed on a Cary 6000i UV-Vis spectrophotometer.

Transformation of TM1862 into a *rimO*$^-$ Cell Line

The VR77 vector containing TM1862 was transformed into ER3051 (*rimO*$^-$) *Escherichia coli* (with kanamycin resistance), which was a generous gift from New England Biolabs. One colony of *rimO*$^-$ was inoculated into 5 mL of LB media with 50 µg/mL kanamycin and grown overnight at 37°C and 250 rpm shaking. One milliliter of

overnight growth was used to inoculate 50 mL of LB media with 50 μg/mL kanamycin and grown at 37°C with 250 rpm shaking until the OD_{600} was approximately 0.5. The cells were chilled on ice for 20 minutes and then centrifuged at 4°C and 4,000 x g for 20 minutes. The supernatant was decanted and the cells resuspended in 50 mL of ice cold 10% glycerol. The cells were centrifuged as before, and the ice cold 10% glycerol wash was repeated a second time with 25 mL and third with 5 mL. After the final centrifugation, the cells were resuspended in 150 μL of ice cold 10% glycerol, aliquoted into 40 μL portions in sterile eppendorf tubes, flash frozen with liquid nitrogen, and stored at -80°C until use. To one tube of RimO- 2 μL of VR77 (approximately 1 ng/μL) were added, and the cells were incubated on ice for 1 minute. The cells were then placed in a 1 mm electroporation cuvette and pulsed using a BioRad MicroPulser Electroporater on the Ec1 setting. Immediately following 1 mL of warm S.O.C. media (2% (w/v) tryptone (pancreatic digest of casein), 0.5% (w/v) yeast extract, 8.6 mM NaCl, 2.5 mM KCl, 20 mM $MgSO_4$, and 20 mM glucose) was added, and the cells were transferred to another sterile eppendorf tube. The cells were grown at 37°C and 225 rpm for 1 hour; 150 μL of the transformation was plated on LB media with 50 μg/mL or both ampicillin and kanamycin. The plate was incubated at 37°C overnight. A glycerol stock was made by growing one colony in 5 mL of LB media with 50 μg/mL ampicillin and kanamycin overnight at 37°C, 250 rpm shaking and adding 3.5 mL of the growth to 1.5 mL sterile glycerol. The stock was immediately aliquoted into 1 mL portions, frozen with liquid nitrogen, and stored at -80°C.

Analysis of Ribosomal S12 Protein Modification

TM1862 in *rimO*$^-$ cells, as well as *rimO*$^-$ cells as a control, were grown by plating cells from a glycerol stock on LB media with 50 µg/mL kanamycin (50 µg/mL ampicillin were added to the one with the TM1862 gene) and incubating overnight at 37°C. One colony from each plate was used to inoculate individual portions of 5 mL of LB media with 50 µg/mL kanamycin (50 µg/mL ampicillin were added to the one with the TM1862 gene) and grown overnight at 37°C with 250 rpm shaking. The following morning 500 µL of overnight growth was added to 50 mL of LB media with 50 µg/mL kanamycin (50 µg/mL ampicillin were added to the one with the TM1862 gene) and grown at 37°C with 250 rpm shaking until the OD_{600} was approximately 0.5 at which point the temperature was shifted to 45°C. The growth was allowed to continue for an additional 3 hours. Cells were harvested by centrifugation at 4°C and 2,500 rpm, flash frozen with liquid nitrogen, and stored at -80°C.

Ribosome isolation was accomplished by adding 8 mL of Ribosome Lysis Buffer (RLB: 100 mM NH_4Cl, 50 mM $MgCl_2$, 20 mM Tris, pH 7.5, 1 mM DTT, 0.5 mM EDTA) to an individual cell pellet. The sample was placed on ice and a Branson Sonifier 450 was used to sonicate the cells at 30% and output setting 3. Sonication was performed for 30 seconds followed by 30 seconds rest on ice and repeated until the cells were disrupted. The lysed cells were centrifuged at 30,000 x g for 90 minutes at 4 °C, and the supernatant (S30 extract) was removed and centrifuged again at 100,000 x g for 16 hours minimum at 4°C using a sucrose cushion (1.1 M sucrose in RLB was used to fill half of the centrifuge tube and the S30 extract was placed on top. The resulting pellet was

resuspended in approximately 1 mL of RLB. To further separate the ribosomal proteins 100 µL of 1 M $MgCl_2$ and 2 mL of glacial acetic acid were added. The sample was incubate on ice for 90 minutes, inverting occasionally to mix. The sample was spun down in a microcentrifuge at 13,000 rpm and 4°C for 15 minutes to remove the precipitate. The supernatant was flash frozen with liquid nitrogen and stored at -80°C. Samples were submitted to the Montana State University Mass Spectrometry Facility in the Chemistry and Biochemistry Department for further analysis.

Results

TM1862 Growth, Purification, and Reconstitution

Overexpression of TM1862 from a pET21-d vector was accomplished via IPTG induction, and the protein produced was easily observed on an SDS-PAGE gel (Figure 8.2). Average cell yields were 2.25 g per liter of media. During purification on a HisTrap HP nickel affinity column, TM1862 eluted in three peaks, each during a different step (Figure 8.3 and 8.4). All of the fractions containing TM1862 protein were retained. Any methods requiring cleaner protein we further purified using gel filtration, and the TM1862 protein eluted in one peak (Figure 8.5 and 8.6). The ratio of the absorbance at 426 to 280 nm was determined, and fractions containing the highest ratio were pooled. Protein yields were obtained in good amount. After purification on the affinity column, approximately 20 mg of TM1862 per gram of cells was obtained, and the following gel purification reduced that to 5 mg protein per gram of cells.

Purified TM1862 protein contained 1 to 1.5 Fe per protein, though based on the sequence homology to MiaB it should contain 8 Fe per protein in two [4Fe-4S] clusters. To increase the iron content of TM1862 purified protein was reconstituted with iron and sulfide. Reconstituted TM1862 generally contained anywhere from 8 to 16 Fe per protein, and the extra iron was thought to bind the His tag used for purification. In an attempt to remove the excess iron EDTA was added in differing concentrations from 250 to 750 μM to the reconstituted TM1862, however even the lowest EDTA concentration stripped all but four irons (one cluster) per protein.

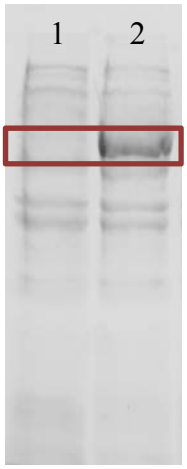

Figure 8.2. SDS-PAGE gel of overexpression of the TM1862 protein. The lanes show the protein content of the growth 1: pre-induction and 2: post-induction with IPTG. The location of the TM1862 protein is boxed in red.

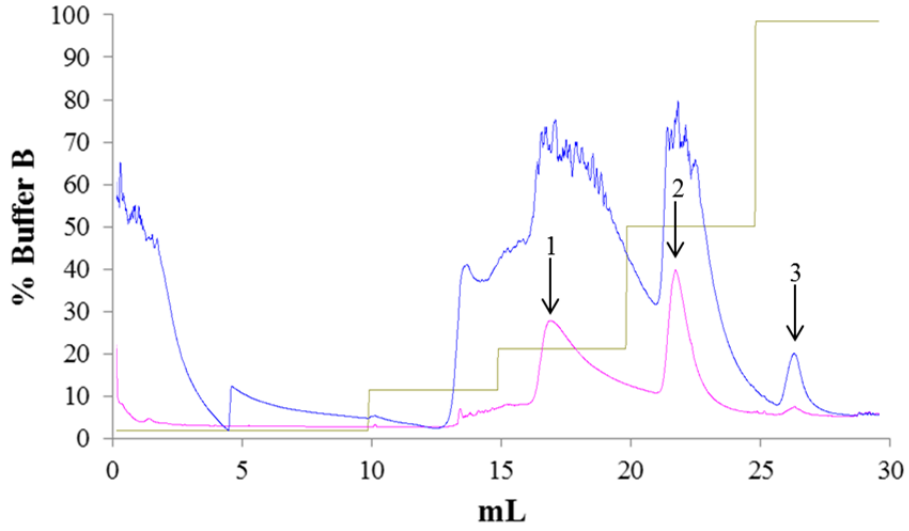

Figure 8.3. Chromatogram of TM186 protein purification on a HisTrap nickel affinity column using Buffer A (20 mM sodium phosphates, pH 7.4, 200 mM NaCl, 10 mM imidazole, and 5% (w/v) glycerol) and Buffer B (20 mM sodium phosphates, pH 7.4, 200 mM NaCl, 500 mM imidazole, and 5% (w/v) glycerol). The blue trace represents the absorbance at 280 nm and the red at 426 nm. Peaks that contained TM1862 protein are labeled 1 (20% Buffer B), 2 (50% Buffer B), and 3 (100% Buffer B).

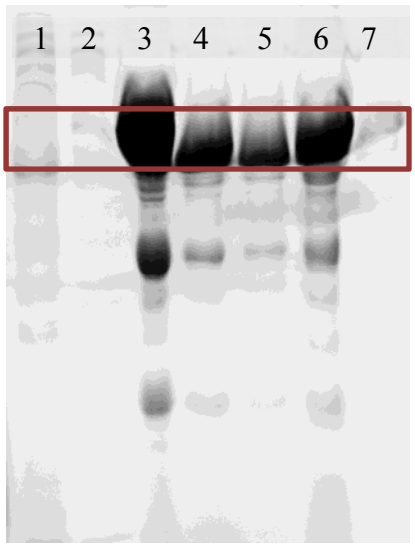

Figure 8.4. SDS-PAGE gel of the wash step (lane 1), 10% Buffer B step (lane 2), fractions 4-6 (lane 3), fractions 7-10 (lane 4), fractions 11-13 (lane 5), fractions 14-16 (lane 6), and fractions 23-24 (lane 7) from the chromatogram in figure 8.3. The location of the TM1862 protein is boxed in red.

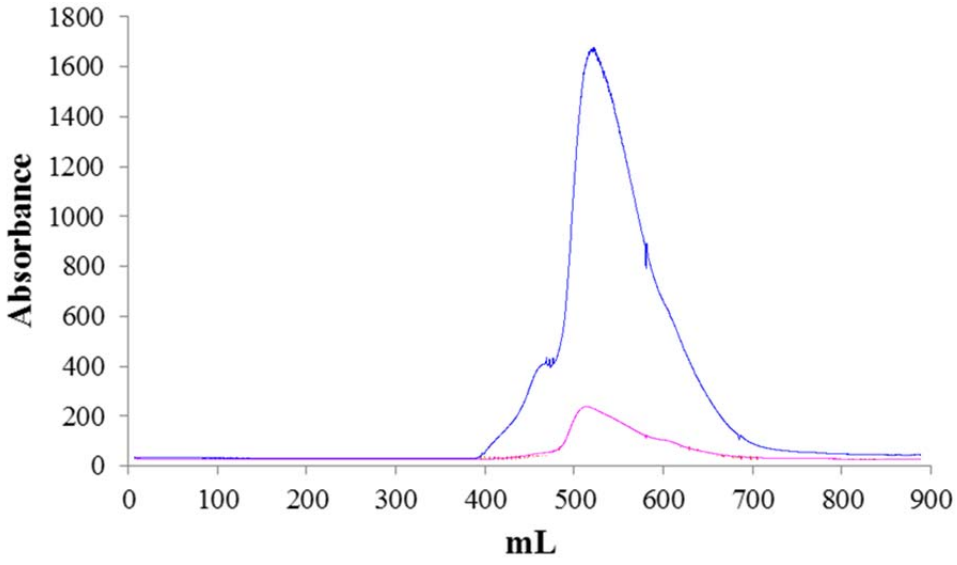

Figure 8.5. Chromatogram of TM1862 purification on a Superdex 75 gel filtration column using Gel Filtration Buffer (50 mM Tris, pH 7.4, 200 mM NaCl, 1 mM DTT). The blue trace represents the absorbance at 280 nm and the red at 426 nm.

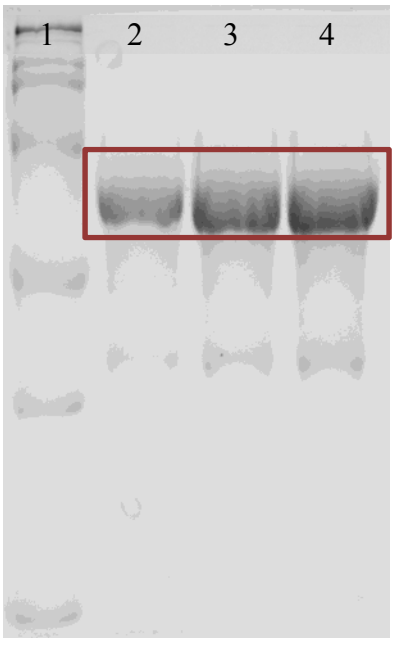

Figure 8.6. SDS-PAGE gel of the pooled fractions from Figure 8.5. Lanes are a molecular weight marker (lane 1), fractions 10-12 (lane 2), fractions 13-15 and 21-23 (lane 3), and fractions 16-20 (lane 4). The location of the TM1862 protein is boxed in red.

EPR and UV-Vis Spectroscopy

As-isolated TM1862 protein gave a very weak nearly isotropic EPR signal typical of a $[3Fe\text{-}4S]^{1+}$ cluster (Figure 8.7). TM1862 anaerobically reduced with either sodium

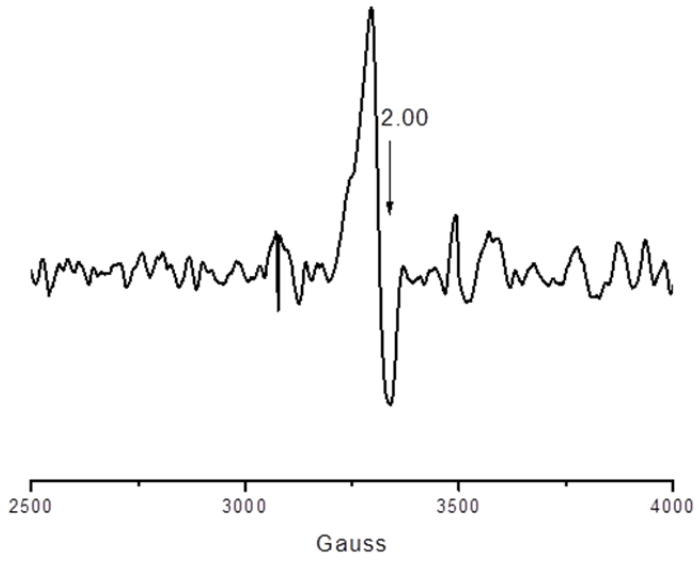

Figure 8.7. EPR spectrum of TM1862 as-isolated. The signal is nearly isotropic centered around g=2.00 and is indicative of a $[3Fe\text{-}4S]^{1+}$ cluster.

dithionite or 5-deazariboflavin produced axial signals typical of a $[4Fe\text{-}4S]^{1+}$ cluster (Figure 8.8). The signal to noise is low due to low signal intensity resulting from low iron content of the protein used to make the EPR samples. The EPR results show that TM1862 does contain a [4Fe-4S] cluster that can be reduced to the $[4Fe\text{-}4S]^{1+}$ state. The addition of SAM to the reduced protein samples did not appear to have an effect on the EPR signal. Often the addition of SAM to a reduced radical SAM protein containing a $[4Fe\text{-}4S]^{1+}$ cluster causes a change in the g values and lineshape due to SAM binding to the cluster. However, in the case of TM1862 the lack of change does not necessarily mean that SAM is not binding. Not all radical SAM EPR signals are drastically changed

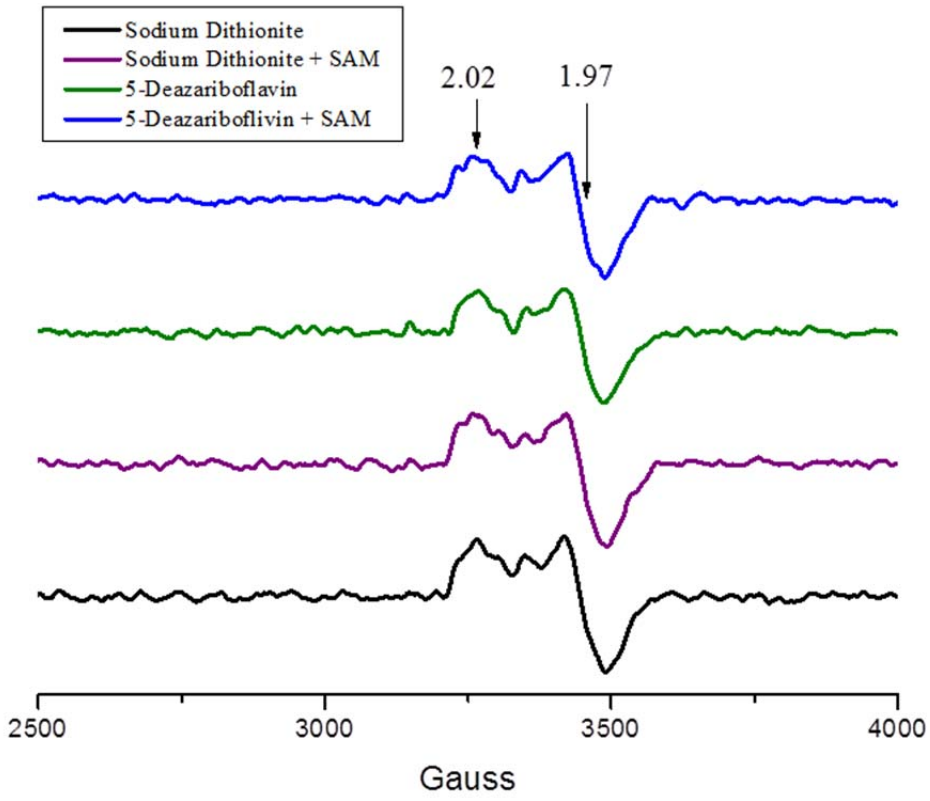

Figure 8.8. EPR spectra of TM1862 reduced with sodium dithionite or 5-deazariboflavin both in the presence and absence of SAM. All EPR signals are nearly axial, and the g values obtained for all spectra were 2.02 and 1.97 as indicated by the arrows. The properties of these signals is consistent with the Fe-S clusters in TM1862 being reduced to $[4Fe\text{-}4S]^{1+}$ clusters.

in the presence of SAM as is the case with the *E. coli* RimO methylthiotransferase [7]. Additionaly, because of the low iron content in TM1862, there may not be enough SAM bound cluster to cause a visible shift. The presence of a reducible [4Fe-4S] cluster was also supported by UV-Vis spectroscopy. The as-isolated protein showed a feature at approximately 420 nm that was decreased in the samples containing sodium dithionite or 5-deazariboflavin as reductants (Figure 8.9). This decrease is due to the diminished

ligand to metal charge transfer of the reduced cluster as compared to the non-reduced cluster.

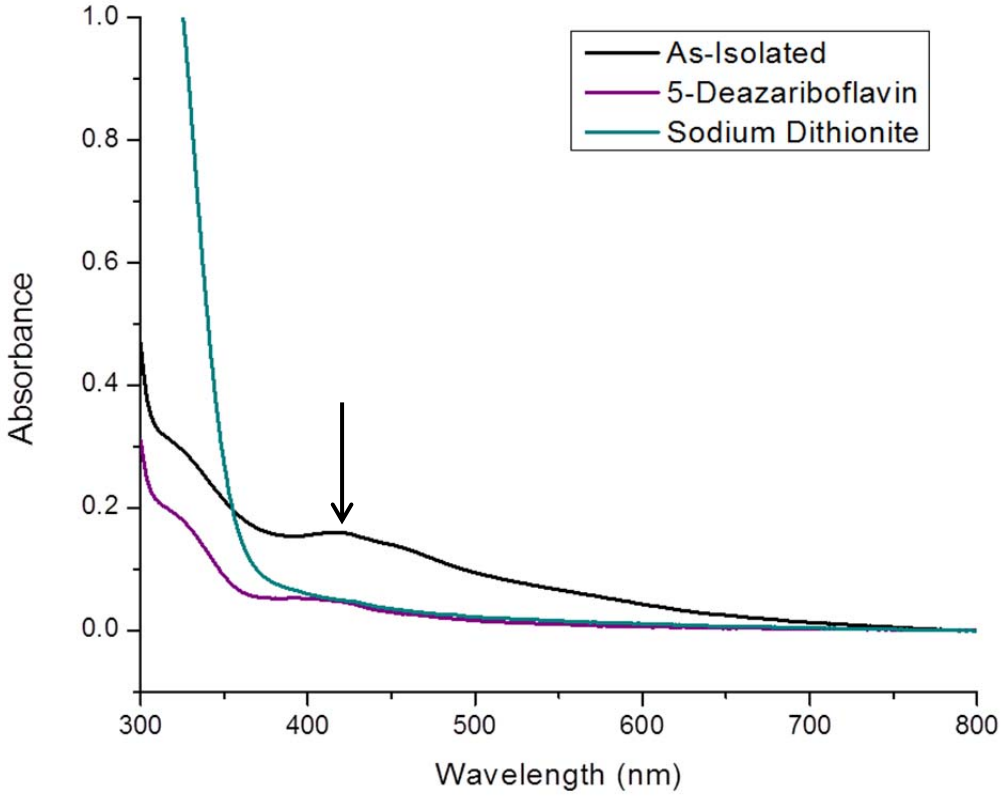

Figure 8.9. UV-Vis spectra of TM1862 as-isolated and reduced with 5-deazariboflavin or sodium dithionite. The arrow indicates the feature at approximately 420 nm that decreases upon reduction of the protein.

TM1862 Alignment and Crystal Setup

To catalyze their reactions methylthiotransferases (MTTases) contain three distinct domains. The first domain is located at the N-terminal end of the protein and is designated UPF004. The UPF004 domain contains three conserved cysteines that bind one of the [4Fe-4S] clusters in MiaB from *E. coli* [8]. It is also most commonly found with the other two MTTase domains. The second domain between the N- an C-terminl

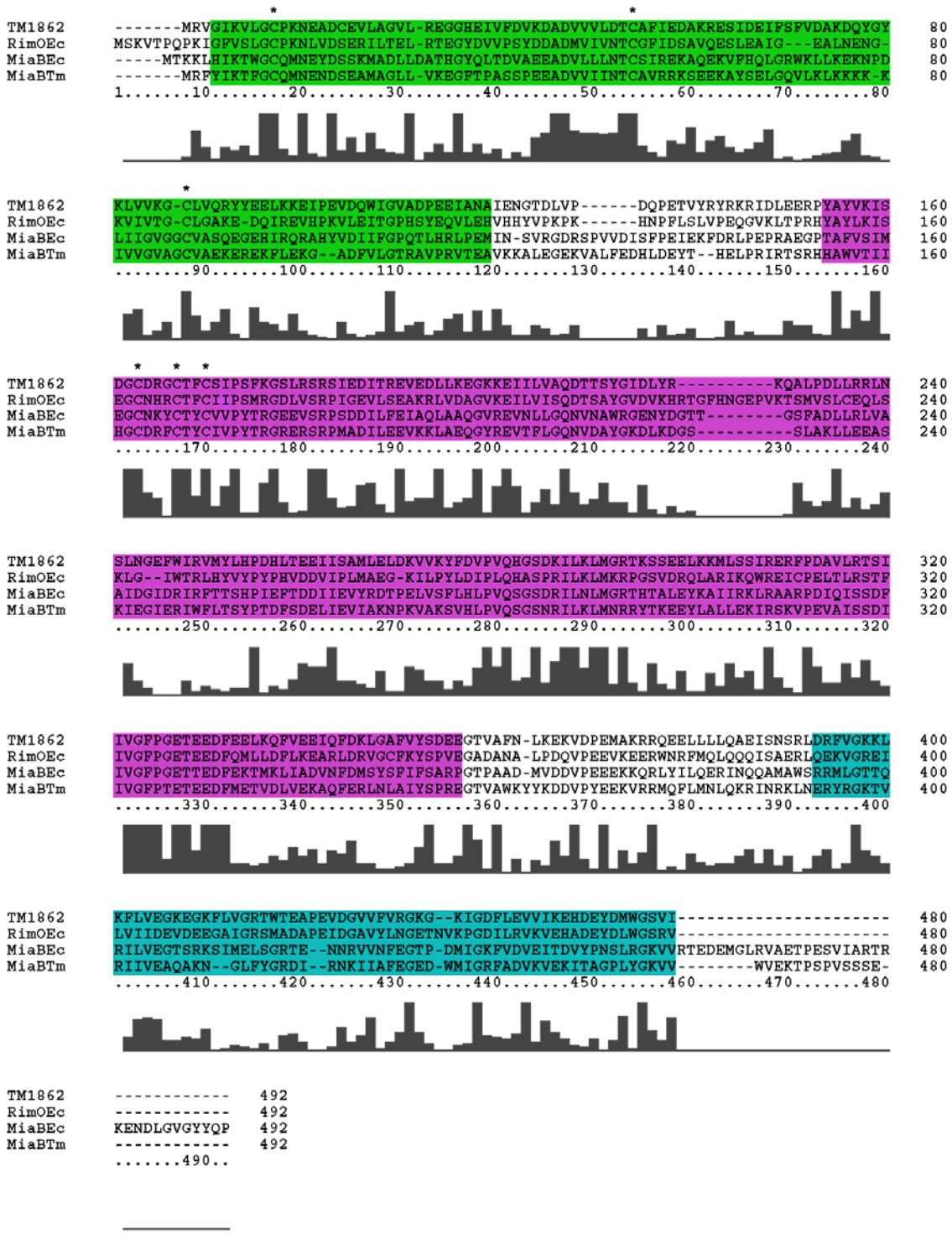

Figure 8.10. Clustal X alignment of TM1862 with RimO from *E. coli* (RimOEc) and MiaB from *E. coli* (MiaBEc) and *T. maritima* (MiaBTm). The conserved domains are UPF0004 (green), radical SAM (purple), and TRAM (blue). The six conserved cysteines involved in cluster binding are indicated with an asterisk above each.

domains is a radical SAM core domain containing the CX_3CX_2C motif necessary to bind the second 5'-deoxyadensyl radical producing [4Fe-4S] cluster. The final domain is the C-terminal TRAM domain, which in RNA modifying enzymes is involved in substrate recognition [9]. When TM1862 was aligned with MiaB from *E. coli and T. maritima* and RimO from *E. coli* (Figure 8.10) there was 30-33% identity with the MiaB proteins and 36% identity with the RimO. The TM1862 protein contains all three domains with the six conserved cysteines for Fe-S cluster binding.

The crystal structure of TM1862 is of the apo-enzyme and only contains the radical SAM and TRAM domains due to the presence of subtilisin in the crystallization buffer (Figure 8.1). In an attempt to crystalize the holo-enzyme with all three domains intact, a crystal screen of TM1862 was prepared anaerobically, however no crystals were obtained.

TM1862 Function

In order to determine the function of TM1862, the vector containing the gene expressing TM1862 was transformed into a *miaB*$^-$ cell line (Figure 8.11) to determine if it could modify i^6A to ms^2i^6A (which is lacking in the *miaB*$^-$ cells). The RNA produced was isolated and separated using HPLC (Figure 8.12). The two peaks eluting at approximately 3.25 minutes and 5.75 minutes were collected, and UV-Vis scans from 200 nm to 350 nm were completed. The spectra of the two peaks were compared to published spectra of i^6A and ms^2i^6A. The peak at 3.5 minutes was neither modified nucleoside, and the peak at 6.0 minutes corresponds to i^6A (Figure 8.13). As there was no apparent modification of i^6A by TM1862, its function as a RimO enzyme (which

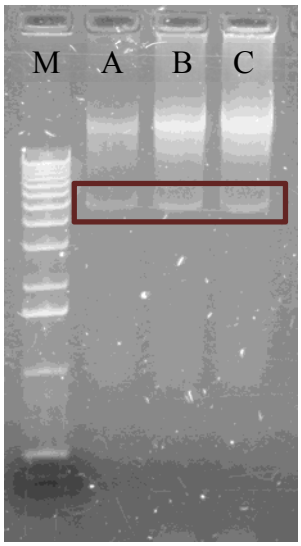

Figure 8.11. Confirmation of transformation of the TM1862 containing plasmid into *miaB*$^-$ cells was accomplished by extracting the DNA from the cells and running the extract on a 1% agarose gel to confirm the presence of the plasmid. Lane M is the DNA ladder, and lanes A, B, and C are DNA from three separate colonies. The boxed area indicates the location of the 6.6 kb vector, which runs at approximately 5 kb because it is circular and uncut.

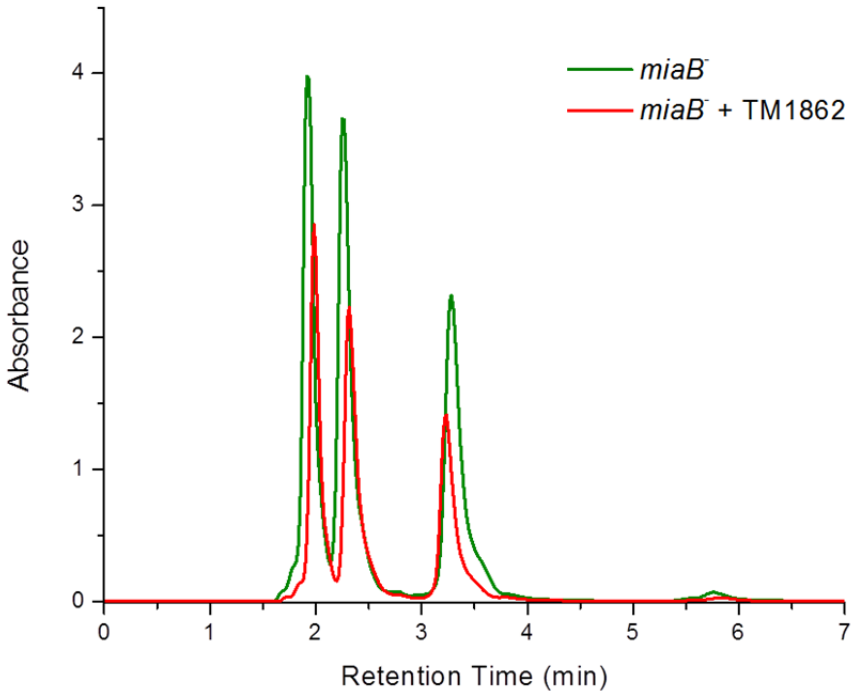

Figure 8.12. HPLC chromatogram of the separated nucleosides isolated from *miaB*$^-$ cells (green trace) or *miaB*$^-$ cells transformed with TM1862 (red trace).

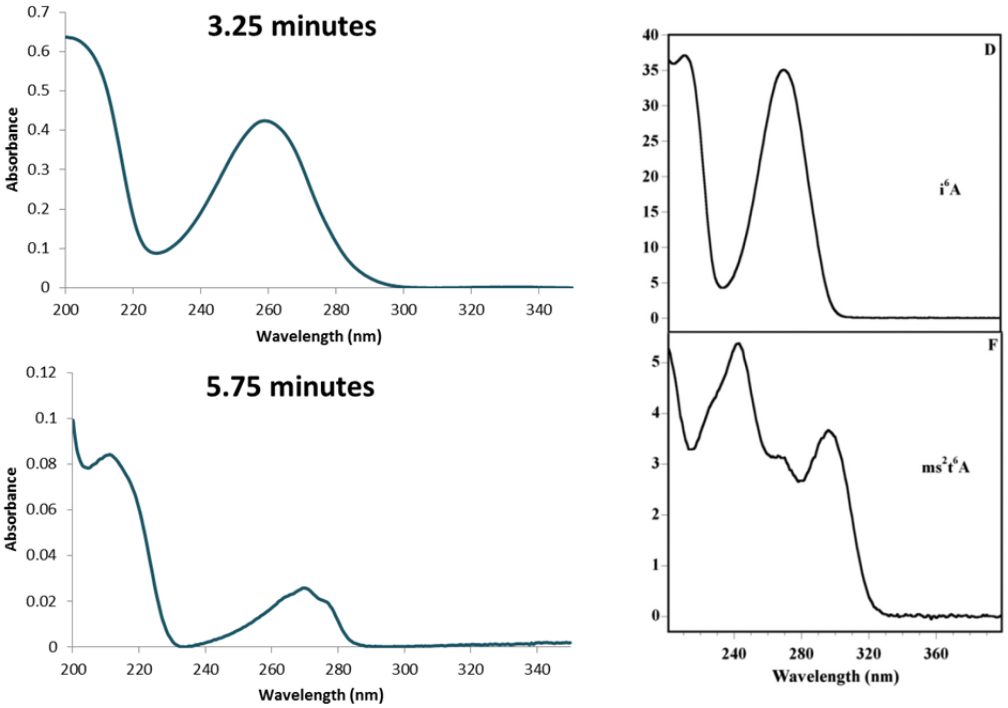

Figure 8.13. Left: UV-Vis analysis of the components of the peaks collected around 3.25 (top) and 5.75 (bottom) minutes during the HPLC separation of nucleosides from *miaB*$^-$ transformed with TM1862 as shown in Figure 8.11. Right: UV-Vis spectrum of i^6A (top) and ms^2i^6A (bottom) used as a reference from [10].

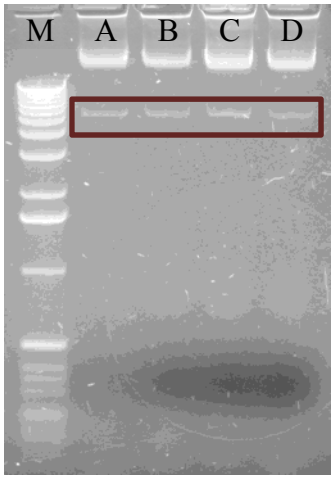

Figure 8.14. Confirmation of transformation of the TM1862 containing plasmid into *rimO*$^-$ cells was accomplished by extracting the DNA from the cells and running the extract on a 1% agarose gel to confirm the presence of the plasmid. Lane M is the DNA ladder, and lanes A, B, C, and D are DNA from four separate colonies. The boxed area indicates the location of the 6.6 kb vector, which runs at approximately 5 kb because it is circular and uncut.

modifies the ribosomal S12 protein) was examined by transforming the vector containing the gene expressing TM1862 into a *rimO*$^-$ cell line (Figure 8.14). The ribosomes from the transformed cells were isolated and submitted to the Montana State Mass Spectrometry Facility, however analysis was unable to be optimized before a paper was published by another group detailing the function of TM1862 [2].

Conclusions

The alignment of TM1862 with known MiaB and RimO enzymes suggested that it was a radical SAM enzyme, specifically a MTTase; it contains all three of the domains (UPF0004, radical SAM, and TRAM) used in imparting the methylthio modification. Radical SAM enzymes must also contain a [4Fe-4S] cluster capable of being reduced. EPR of the as-isolated protein indicated that TM1862 did indeed contain an Fe-S cluster in a [3Fe-4S] form, which is not unusual for radical SAM enzymes. It is upon reduction that the [3Fe-4S] cluster is converted to a $[4Fe\text{-}4S]^{1+}$ cluster, which is the case for TM1862 when reduced with either sodium dithionite or 5-deazariboflavin where EPR shows and axial signal indicative of a $[4Fe\text{-}4S]^{1+}$ cluster. This was also supported by the UV-Vis spectra showing a decrease in the absorbance at approximately 420 nm due to the lessened ligand to metal charge transfer upon reduction of the cluster.

In radical SAM enzymes the EPR signal is usually perturbed upon the addition of SAM indicating its binding to the cluster, and while this is not the case for TM1862, it did not exclude TM1862 from the superfamily. There are radical SAM enzymes, RimO from *E. coli* for one, whose EPR signal is not greatly perturbed when SAM is added;

instead the signal intensity may be decreased. As mentioned previously, the iron content of the protein must also be considered. Un-reconstituted TM1862 only contains approximately 1 Fe per protein while the sequence suggests two [4Fe-4S] clusters. It is possible that the use of reconstituted protein containing a better iron content would show a different EPR signal in the presence of SAM.

To further determine whether TM1862 was an MTTase, an attempt was made to restore activity to two different knockout cell lines. In the first case a *miaB*$^-$ cell line, which lacks the ms^{2}i^{6}A modification and builds up i^{6}A, was used. The HPLC separation and UV-Vis analysis of the nucleosides isolated from *miaB*$^-$ expressing TM1862 indicated that no ms^{2}i^{6}A was produced. The peak collected at 5.75 minutes showed a UV-Vis spectrum similar to i^{6}A. With the HPLC conditions used to separate the nucleosides the ms^{2}i^{6}A modified base would have eluted after i^{6}A, however no peaks were observed after 6 minutes for the entirety of the run. While the absence of ms^{2}i^{6}A was not completely conclusive of the lack of MiaB activity, it did indicate that this was not the most likely function of TM1862, so the use of a second knockout cell line, *rimO*$^-$ cells lacking the methylthioaspartic acid on the ribosomal S12 protein, was attempted. The ribosomal proteins from *rimO*$^-$ expressing TM1862 were isolated and submitted for mass spectrometry analysis, but the optimization of separation of all the ribosomal proteins was unable to be completed before a report was published [2] indicating that TM1862 was indeed a RimO protein from *T. maritima*. The function of TM1862 was determined using a 20-mer peptide containing the aspartate residue modified and the surrounding amino acids as a substrate for *in vitro* activity assays [2]. Mass spectrometry

was used to determine the state of modification on the peptide and demonstrated that a methylthio group was added to the aspartate, presumably at the β-carbon [2]. Interestingly the data also suggested the presence of a second methylthio modification, although its position on the peptide remains unresolved, that is possibly due to an incomplete substrate [2].

Although TM1862 has been established as RimO MTTase, there are still many uncertainties surrounding the mechanism by which RimO enzymes modify the aspartate residue of the ribosomal S12 protein. For example, when is the ribosomal S12 protein modified, after translation but before incorporation into the ribosomal complex or after assembly of the ribosome? Although not conclusive, evidence for the latter has been observed through the use of proteomics to identify proteins interacting with RimO [11]. Also the role of the second [4Fe-4S] cluster is presumed to be as a sulfur source for the methylthio modification, though this remains to be demonstrated. When EDTA was used on reconstituted protein, it appeared as though one cluster was stripped while the other remained. The ability to remove a select cluster and replace it with ^{57}Fe could prove to be a valuable tool in further characterization of the enzyme as well as dissecting the purpose of the second cluster.

References

1. Xiao R, Anderson S, Aramini J, Belote R, Buchwald WA, Ciccosanti C, Conover K, Everett JK, Hamilton K, Huang YJ, Janjua H, Jiang M, Kornhaber GJ, Lee DY, Locke JY, Ma LC, Maglaqui M, Mao L, Mitra S, Patel D, Rossi P, Sahdev S, Sharma S, Shastry R, Swapna GV, Tong SN, Wang D, Wang H, Zhao L, Montelione GT, and Acton TB (2010) J. Struct. Biol. 172: 21-33.

2. Arragain S, Garcia-Serres R, Blondin G, Douki T, Clemancey M, Latour J-M, Forouhar F, Neely H, Montelione GT, Hunt JF, Mulliez E, Fontecave M, and Atta M (2010) J. Biol. Chem. 285: 5792-5801.

3. Bradford MM (1976) Anal. Biochem. 72: 248-254.

4. Beinert H (1978) Methods Enzymol. 54: 435-445.

5. Larkin MA, Blackshields G, Brown NP, Chenna R, McGettigan PA, McWilliam H, Valentin F, Wallace IM, Wilm A, Lopez R, Thompson JD, Gibson TJ, and Higgins DG (2007) Bioinformatics 23: 2947-2948.

6. Gehrke CW, and Kuo KC. (1990) In Analytical Methods for Major and Modified Nucleosides (Gehrke CW, and Kuo KCT, Eds.), pp A3-A71, Elsevier Science Publishers, New York, NY.

7. Lee K-H, Saleh L, Anton BP, Madinger CL, Benner JS, Iwig DF, Roberts RJ, Krebs C, and Booker SJ (2009) Biochemistry 48: 10162-10174.

8. Hernández HL, Pierrel F, Elleingand E, Garcia-Serres R, Huynh BH, Johnson MK, Fontecave M, and Atta M (2007) Biochemistry 46: 5140-5147.

9. Anton BP, Saleh L, Benner JS, Raleigh EA, Kasif S, and Roberts RJ (2008) Proc. Natl. Acad. Sci. U.S.A. 105: 1826-1831.

10. Arragain S, Handelman SK, Forouhar F, Wei F-Y, Tomizawa K, Hunt JF, Douki T, Fontecave M, Mulliez E, and Atta M (2010) J. Biol. Chem. 285: 28425-28433.

11. Strader MB, Costantino N, Elkins CA, Chen CY, Patel I, Makusky AJ, Choy JS, Court DL, Markey SP, and Kowalak JA (2011) Mol. Cell. Proteomics 10: M110 005199.

REFERENCES CITED

Adams KL, Tsoi S, Yan J, Durbin SM, Ramdas AK, Cramer WA, Sturhahn W, Alp EE, and Schulz C (2006) J. Phys. Chem. B 110: 530-536.

Andersson CE, and Mowbray SL (2002) J. Mol. Biol. 315: 409-419.

Anton BP, Russell SP, Vertrees J, Kasif S, Raleigh EA, Limbach PA, and Roberts RJ (2010) Nucleic Acids Res. 38: 6195-6205.

Anton BP, Saleh L, Benner JS, Raleigh EA, Kasif S, and Roberts RJ (2008) Proc. Natl. Acad. Sci. U.S.A. 105: 1826-1831.

Arragain S, Garcia-Serres R, Blondin G, Douki T, Clemancey M, Latour J-M, Forouhar F, Neely H, Montelione GT, Hunt JF, Mulliez E, Fontecave M, and Atta M (2010) J. Biol. Chem. 285: 5792-5801.

Arragain S, Handelman SK, Forouhar F, Wei F-Y, Tomizawa K, Hunt JF, Douki T, Fontecave M, Mulliez E, and Atta M (2010) J. Biol. Chem. 285: 28425-28433.

Becker A, Fritz-Wolf K, Kabsch W, Knappe J, Schultz S, and Volker Wagner AF (1999) Nat. Struct. Biol. 6: 969-975.

Becker A, and Kabsch W (2002) J. Biol. Chem. 277: 40036-40042.

Beinert H (1978) Methods Enzymol. 54: 435-445.

Beinert H (2000) J. Biol. Inorg. Chem. 5: 2-15.

Beinert H, Holm RH, and Münck E (1997) Science 277: 653-659.

Benjdia A, Leprince J, Sandström C, Vaudry H, and Berteau O (2009) J. Am. Chem. Soc. 131: 8348-8349.

Berkovitch F, Nicolet Y, Wan JT, Jarrett JT, and Drennan CL (2004) Science 303: 76-79.

Boal AK, Grove TL, McLaughlin MI, Yennawar NH, Booker SJ, and Rosenzweig AC (2011) Science: 1089-1092.

Bradford MM (1976) Anal. Biochem. 72: 248-254.

Bray RC (1961) Biochem. J. 81: 189-193.

Broderick JB. (2003) In Comprehensive Coordination Chemistry II: From Biology to Nanotechnology (McCleverty J, and Meyer T, Eds.), pp 739-757, Elsevier Science.

Broderick JB (2010) Nature 465: 877-878.

Broderick JB, Duderstadt RE, Fernandez DC, Wojtuszewski K, Henshaw TF, and Johnson MK (1997) J. Am. Chem. Soc. 119: 7396-7397.

Broderick JB, Henshaw TF, Cheek J, Wojtuszewski K, Smith SR, Trojan MR, McGhan RM, Kopf A, Kibbey M, and Broderick WE (2000) Biochem. Biophys. Res. Commun. 269: 451-456.

Brush EJ, Lipsett KA, and Kozarich JW (1988) Biochemistry 27: 2217-2222.

Burdette SC, and Lippard SJ (2003) Proc. Natl. Acad. Sci. U.S.A. 100: 3605-3610.

Calzolai L, Zhou ZH, Adams MWW, and LaMar GN (1996) J. Am. Chem. Soc. 118: 2513-2514.

Challand MR, Ziegert T, Douglas P, Wood RJ, Kriek M, Shaw NM, and Roach PL (2009) FEBS Lett. 583: 1358-1362.

Chatgilialoglu C, Castelhano AL, and Griller D (1985) J. Org. Chem. 50: 2516-2518.

Chatterjee A, Li Y, Zhang Y, Grove TL, Lee M, Krebs C, Booker SJ, Begley TP, and Ealick SE (2008) Nat. Chem. Biol. 4: 758-765.

Cheek J, and Broderick JB (2001) J. Biol. Inorg. Chem. 6: 209-226.

Cheek J, and Broderick JB (2002) J. Am. Chem. Soc. 124: 2860-2861.

Chen D, Walsby C, Hoffman BM, and Frey PA (2003) J. Am. Chem. Soc. 125: 11788-11789.

Cicchillo RM, Iwig DF, Jones AD, Nesbitt NM, Baleanu-Gogonea C, Souder MG, Tu L, and Booker SJ (2004) Biochemistry 43: 6378-6386.

Cicchillo RM, Lee K-H, Baleanu-Gogonea C, Nesbitt NM, Krebs C, and Booker SJ (2004) Biochemistry 43: 11770-11781.

Clarke S, and Banfield K. (2001) In Homocysteine in Health and Disease (Carmel R, and Jacobsen DW, Eds.), pp 63-78, Cambridge University Press, Cambridge, UK.

Colichman EL, and Love DL (1953) J. Org. Chem. 18: 40-46.

Conradt H, Hohmann-Berger M, Hohmann HP, Blaschkowski HP, and Knappe J (1984) Arch. Biochem. Biophys. 228: 133-142.

Davoust CE, Doan PE, and Hoffman BM (1996) J. Magn. Reson., Ser. A 119: 38-44.

Demick JM, and Lanzilotta WN (2011) Biochemistry 50: 440-442.

Demple B, Ding H, and Jorgensen M (2002) Methods Enzymol. 348: 355-364.

Dey A, Peng Y, Broderick WE, Hedman B, Hodgson KO, Broderick JB, and Solomon EI (2011) J. Am. Chem. Soc. 133: 18656-18662.

Díaz I, and Ehrenberg M (1991) J. Mol. Biol. 222: 1161-1171.

Ding H, and Demple B (2000) Proc. Natl. Acad. Sci. U.S.A. 97: 5146-5150.

Dowling DP, Vey JL, Croft AK, and Drennan CL (2012) Biochim. Biophys. Acta.: 1178-1195.

Driesener RC, Challand MR, McGlynn SE, Shepard EM, Boyd ES, Broderick JB, Peters JW, and Roach PL (2010) Angewandte Chemie 49: 1687-1690.

Escalettes F, Florentin D, Bui BTS, Lesage D, and Marquet A (1999) J. Am. Chem. Soc. 121: 3571-3578.

Evans HJ, and Wildes RA. (1971) In Potassium in Biochemistry and Physiology, pp 13-39, International Potash Institute, Berne, Switzerland.

Frey PA, Hegeman AD, and Ruzicka FJ (2008) Crit. Rev. Biochem. Mol. Biol. 43: 63-88.

Frey PA, Rothe M, Wagner AFV, and Knappe J (1994) J. Biol. Chem. 269: 12432-12437.

Fu W, O'Handley S, Cunningham RP, and Johnson MK (1992) J. Biol. Chem. 267: 16135-16137.

Gambarelli S, Luttringer F, Padovani D, Mulliez E, and Fontecave M (2005) Chembiochem : a European journal of chemical biology 6: 1960-1962.

Gehrke CW, and Kuo KC. (1990) In Analytical Methods for Major and Modified Nucleosides (Gehrke CW, and Kuo KCT, Eds.), pp A3-A71, Elsevier Science Publishers, New York, NY.

Giessing AMB, Jensen SS, Rasmussen A, Hansen LH, Gondela A, Long K, Vester B, and Kirpekar F (2009) RNA 15: 327-336.

Green J, Scott C, and Guest JR (2001) Adv. Microb. Physiol. 44: 1-34.

Grimshaw J. (1981) In The Chemistry of the Sulphonium Group (Stirling CJM, and Patai S, Eds.), pp 141-155, Wiley & Sons Ltd.

Grove TL, Benner JS, Radle MI, Ahlum JH, Landgraf BJ, Krebs C, and Booker SJ (2011) Science 332: 604-607.

Grove TL, Radle MI, Krebs C, and Booker SJ (2011) J. Am. Chem. Soc. 133: 19586-19589.

Guianvarc'h D, Florentin D, Bui BTS, Nunzi F, and Marquet A (1997) Biochem. Biophys. Res. Commun. 236: 402-406.

Gustilo EM, Vendeix FA, and Agris PF (2008) Curr. Opin. Microbiol. 11: 134-140.

Haile DJ, Rouault TA, Harford JB, Kennedy MC, Blondin GA, Beinert H, and Klausner RD (1992) Proc. Natl. Acad. Sci. U.S.A. 89: 11735-11739.

Haile DJ, Rouault TA, Tang CK, Chin J, Harford JB, and Klausner RD (1992) Proc. Natl. Acad. Sci. U.S.A. 89: 7536-7540.

Hänzelmann P, and Schindelin H (2004) Proc. Natl. Acad. Sci. U.S.A. 101: 12870-12875.

Harding MM (2002) Acta. Crystallogr. D Biol. Crystallogr. 58: 872-874.

Henshaw TF, Cheek J, and Broderick JB (2000) J. Am. Chem. Soc. 122: 8331-8332.

Hernández HL, Pierrel F, Elleingand E, Garcia-Serres R, Huynh BH, Johnson MK, Fontecave M, and Atta M (2007) Biochemistry 46: 5140-5147.

Hinckley GT, and Frey PA (2006) Biochemistry 45: 3219-3225.

Hoffman BM, Derose VJ, Ong JL, and Davoust CE (1994) J. Magn. Reson., Ser. A 110: 52-57.

Hunsicker-Wang LM, Heine A, Chen Y, Luna EP, Todaro T, Zhang YM, Williams PA, McRee DE, Hirst J, Stout CD, and Fee JA (2003) Biochemistry 42: 7303-7317.

Ifuku O, Kishimoto J, Haze S, Yanagi M, and Fukushima S (1992) Biosci. Biotechnol. Biochem. 56: 1780-1785.

Kaczanowska M, and Rydén-Aulin M (2007) Microbiol. Mol. Biol. Rev. 71: 477-494.

Kaminska KH, Purta E, Hansen LH, Bujnicki JM, Vester B, and Long KS (2010) Nucleic Acids Res. 38: 1652-1663.

Kampmeier JA (2010) Biochemistry 49: 10770-10772.

Kennedy MC, Werst M, Telser J, Emptage MH, Beinert H, and Hoffman BM (1987) Proc. Natl. Acad. Sci. U.S.A. 84: 8854-8858.

Khoroshilova N, Popescu C, Munck E, Beinert H, and Kiley PJ (1997) Proc. Natl. Acad. Sci. U.S.A. 94: 6087-6092.

Kiley PJ, and Beinert H (1998) FEMS Microbiol. Rev. 22: 341-352.

Kilgore JL, and Aberhart DJ (1991) J. Chem. Soc., Perkin Trans. 1: 79-84.

Knappe J, Blaschkowski HP, Grobner P, and Schmitt T (1974) Eur. J. Biochem. 50: 253-263.

Knappe J, Elbert S, Frey M, and Wagner AFV (1993) Biochem. Soc. Trans. 21: 731-734.

Knappe J, Neugebauer FA, Blaschkowski HP, and Gänzler M (1984) Proc. Natl. Acad. Sci. U.S.A. 81: 1332-1335.

Knappe J, and Sawers G (1990) FEMS Microbiol. Rev. 6: 383-398.

Knappe J, Schacht J, Mockel W, Hopner T, Vetter H, Jr., and Edenharder R (1969) Eur. J. Biochem. 11: 316-327.

Knappe J, and Schmitt T (1976) Biochem. Biophys. Res. Commun. 71: 1110-1117.

Konevega AL, Soboleva NG, Makhno VI, Semenkov YP, Wintermeyer W, Rodnina MV, and Katunin VI (2004) RNA 10: 90-101.

Krebs C, Broderick WE, Henshaw TF, Broderick JB, and Huynh BH (2002) J. Am. Chem. Soc. 124: 912-913.

Krebs C, Henshaw TF, Cheek J, Huynh BH, and Broderick JB (2000) J. Am. Chem. Soc. 122: 12497-12506.

Külzer R, Pils T, Kappl R, Huttermann J, and Knappe J (1998) J. Biol. Chem. 273: 4897-4903.

Lah N, Lah J, Zegers I, Wyns L, and Messens J (2003) J. Biol. Chem. 278: 24673-24679.

Larkin MA, Blackshields G, Brown NP, Chenna R, McGettigan PA, McWilliam H, Valentin F, Wallace IM, Wilm A, Lopez R, Thompson JD, Gibson TJ, and Higgins DG (2007) Bioinformatics 23: 2947-2948.

Larsen TM, Benning MM, Rayment I, and Reed GH (1998) Biochemistry 37: 6247-6255.

Layer G, Moser J, Heinz DW, Jahn D, and Schubert W-D (2003) EMBO J. 22: 6214-6224.

Lee K-H, Saleh L, Anton BP, Madinger CL, Benner JS, Iwig DF, Roberts RJ, Krebs C, and Booker SJ (2009) Biochemistry 48: 10162-10174.

Lehtiö L, Leppänen VM, Kozarich JW, and Goldman A (2002) Acta Crystallogr. Sect. D 58: 2209-2212.

Lepore BW, Ruzicka FJ, Frey PA, and Ringe D (2005) Proc. Natl. Acad. Sci. U.S.A. 102: 13819-13824.

Leu BM, Zhang Y, Bu L, Straub JE, Zhao J, Sturhahn W, Alp EE, and Sage JT (2008) Biophys. J. 95: 5874-5889.

Liao DI, Dotson G, Turner I, Jr., Reiss L, and Emptage M (2003) J. Inorg. Biochem. 93: 84-91.

Lieder KW, Booker S, Ruzicka FJ, Beinert H, Reed GH, and Frey PA (1998) Biochemistry 37: 2578-2585.

Lin Y, Gerfen GJ, Rousseau DL, and Yeh SR (2003) Anal. Chem. 75: 5381-5386.

Link TA (1999) Adv. Inorg. Chem. 47: 83-157.

Lipkin HJ (1995) Phys. Rev. B. 52: 10073-10079.

Liu A, and Graslund A (2000) J. Biol. Chem. 275: 12367-12373.

Lukianova OA, and David SS (2005) Curr. Opin. Chem. Biol. 9: 145-151.

Magnusson OT, Reed GH, and Frey PA (1999) J. Am. Chem. Soc. 121: 9764-9765.

Magnusson OT, Reed GH, and Frey PA (2001) Biochemistry 40: 7773-7782.

Marsh EN, Patterson DP, and Li L (2010) Chembiochem : a European journal of chemical biology 11: 604-621.

McGlynn SE, Boyd ES, Shepard EM, Lange RK, Gerlach R, Broderick JB, and Peters JW (2010) J. Bacteriol. 192: 595-598.

Meyer J (2008) J. Biol. Inorg. Chem. 13: 157-170.

Miller DJ, Ouellette N, Evdokimova E, Savchenko A, Edwards A, and Anderson WF (2003) Protein Sci. 12: 1432-1442.

Miller JR, Busby RW, Jordan SW, Cheek J, Henshaw TF, Ashley GW, Broderick JB, Cronan JE, Jr., and Marletta MA (2000) Biochemistry 39: 15166-15178.

Mulder DW, Boyd ES, Sarma R, Lange RK, Endrizzi JA, Broderick JB, and Peters JW (2010) Nature 465: 248-251.

Nicolet Y, Amara P, Mouesca J-M, and Fontecilla-Camps JC (2009) Proc. Natl. Acad. Sci. U.S.A. 106: 14867-14871.

Nicolet Y, and Drennan CL (2004) Nucleic Acids Res. 32: 4015-4025.

Nnyepi MR, Peng Y, and Broderick JB (2007) Arch. Biochem. Biophys. 459: 1-9.

O'Brien JR, Raynaud C, Croux C, Girbal L, Soucaille P, and Lanzilotta WN (2004) Biochemistry 43: 4635-4645.

Ollagnier S, Mulliez E, Schmidt PP, Eliasson R, Gaillard J, Deronzier C, Bergman T, Graslund A, Reichard P, and Fontecave M (1997) J. Biol. Chem. 272: 24216-24223.

Page MJ, and Di Cera E (2006) Physiol. Rev. 86: 1049-1092.

Paraskevopoulou C, Fairhurst SA, Lowe DJ, Brick P, and Onesti S (2006) Mol. Microbiol. 59: 795-806.

Parast CV, Wong KK, Kozarich JW, Peisach J, and Magliozzo RS (1995) J. Am. Chem. Soc. 117: 10601-10602.

Parast CV, Wong KK, Lewisch SA, Kozarich JW, Peisach J, and Magliozzo RS (1995) Biochemistry 34: 2393-2399.

Peng Y, Veneziano SE, Gillispie GD, and Broderick JB (2010) J. Biol. Chem. 285: 27224-27231.

Perna AF, Ingrosso D, Zappia V, Galletti P, Capasso G, and De Santo NG (1993) J. Clin. Invest. 91: 2497-2503.

Peters JW, and Broderick JB (2012) Annu. Rev. Biochem. 81: 429-450.

Pierrel F, Björk GR, Fontecave M, and Atta M (2002) J. Biol. Chem. 277: 13367-13370.

Pierrel F, Douki T, Fontecave M, and Atta M (2004) J. Biol. Chem. 279: 47555-47563.

Plaga W, Frank R, and Knappe J (1988) Eur. J. Biochem. 178: 445-450.

Plaga W, Vielhaber G, Wallach J, and Knappe J (2000) FEBS Lett. 466: 45-48.

Popescu CV, Bates DM, Beinert H, Munck E, and Kiley PJ (1998) Proc. Natl. Acad. Sci. U.S.A. 95: 13431-13435.

Posewitz MC, King PW, Smolinski SL, Zhang L, Seibert M, and Ghirardi ML (2004) J. Biol. Chem. 279: 25711-25720.

Ramirez-Silva L, and Oria-Hernandez J. (2008) In Advances in Protein Physcial Chemistry (Garcia-Hernandez E, and Fernandez-Velasco DA, Eds.), pp 249-277, Transworld Research Network.

Rana S, Pozzi N, Pelc LA, and Di Cera E (2011) Proc. Natl. Acad. Sci. U.S.A. 108: 5221-5225.

Raynaud C, Sarçabal P, Meynial-Salles I, Croux C, and Soucaille P (2003) Proc. Natl. Acad. Sci. U.S.A. 100: 5010-5015.

Rouault TA, Haile DJ, Downey WE, Philpott CC, Tang C, Samaniego F, Chin J, Paul I, Orloff D, Harford JB, and Klausner RD (1992) Biometals 5: 131-140.

Ruszczycky MW, Choi S-h, and Liu H-w (2010) J. Am. Chem. Soc. 132: 2359-2369.

Saeva FD, and Morgan BP (1984) J. Am. Chem. Soc. 106: 4121-4125.

Sanyal I, Cohen G, and Flint DH (1994) Biochemistry 33: 3625-3631.

Scheidt WR, Durbin SM, and Sage JT (2005) J. Inorg. Biochem. 99: 60-71.

Schmidt B, Mahmud G, Soh S, Kim SH, Page T, O'Halloran TV, Grzybowski BA, and Hoffman BM (2011) Appl. Magn. Reson. 40: 415-425.

Schultz SG, and Solomon AK (1961) J. Gen. Physiol. 45: 355-369.

Schwartz CJ, Giel JL, Patschkowski T, Luther C, Ruzicka FJ, Beinert H, and Kiley PJ (2001) Proc. Natl. Acad. Sci. U.S.A. 98: 14895-14900.

Shao X, and Grishin NV (2000) Nucleic Acids Res. 28: 2643-2650.

Shepard EM, Boyd ES, Broderick JB, and Peters JW (2011) Curr. Opin. Chem. Biol. 15: 319-327.

Shepard EM, and Broderick JB. (2010) In Comprehensive Natural Products II: Chemistry and Biology (Mander L, and Liu H-W, Eds.), pp 625-661, Elsevier, Oxford.

Shepard EM, Duffus BR, George SJ, McGlynn SE, Challand MR, Swanson KD, Roach PL, Cramer SP, Peters JW, and Broderick JB (2010) J. Am. Chem. Soc. 132: 9247-9249.

Shepard EM, McGlynn SE, Bueling AL, Grady-Smith CS, George SJ, Winslow MA, Cramer SP, Peters JW, and Broderick JB (2010) Proc. Natl. Acad. Sci. U.S.A. 107: 10448-10453.

Shibata N, Masuda J, Tobimatsu T, Toraya T, Suto K, Morimoto Y, and Yasuoka N (1999) Structure 7: 997-1008.

Singwi KS, and Sjolander A (1960) Phys. Rev. 120: 1093-1102.

Sofia HJ, Chen G, Hetzler BG, Reyes-Spindola JF, and Miller NE (2001) Nucleic Acids Res. 29: 1097-1106.

Strader MB, Costantino N, Elkins CA, Chen CY, Patel I, Makusky AJ, Choy JS, Court DL, Markey SP, and Kowalak JA (2011) Mol. Cell. Proteomics 10: M110 005199.

Sturhahn W (2000) Hyperfine Interact. 125: 149-172.

Suelter CH, and Snell EE (1977) J. Biol. Chem. 252: 1852-1857.

Tan L, and Chi-lung Y (1970) Int. Geol. Rev. 12: 778-786.

Taylor AM, Stoll S, Britt RD, and Jarrett JT (2011) Biochemistry 50: 7953-7963.

Thayer MM, Ahern H, Xing D, Cunningham RP, and Tainer JA (1995) EMBO J. 14: 4108-4120.

Toellner TS (2000) Hyperfine Interact. 125: 3-28.

Toh S-M, Xiong L, Bae T, and Mankin AS (2008) RNA 14: 98-106.

Toraya T, Sugimoto Y, Tamao Y, Shimizu S, and Fukui S (1971) Biochemistry 10: 3475-3484.

Ugulava NB, Gibney BR, and Jarrett JT (2001) Biochemistry 40: 8343-8351.

Ugulava NB, Surerus KK, and Jarrett JT (2002) J. Am. Chem. Soc. 124: 9050-9051.

Unkrig V, Neugebauer FA, and Knappe J (1989) Eur. J. Biochem. 184: 723-728.

Urbonavičius J, Qian Q, Durand JMB, Hagervall TG, and Björk GR (2001) EMBO J. 20: 4863-4873.

Vey JL, and Drennan CL (2011) Chem. Rev. 111: 2487-2506.

Vey JL, Yang J, Li M, Broderick WE, Broderick JB, and Drennan CL (2008) Proc. Natl. Acad. Sci. U.S.A. 105: 16137-16141.

Visscher WM (1960) Ann. Phys. 9: 194-210.

Wagner AFV, Frey M, Neugebauer FA, Schafer W, and Knappe J (1992) Proc. Natl. Acad. Sci. U.S.A. 89: 996-1000.

Wagner AFV, Schultz S, Bomke J, Pils T, Lehmann WD, and Knappe J (2001) Biochem. Biophys. Res. Commun. 285: 456-462.

Walsby CJ, Hong W, Broderick WE, Cheek J, Ortillo D, Broderick JB, and Hoffman BM (2002) J. Am. Chem. Soc. 124: 3143-3151.

Walsby CJ, Ortillo D, Broderick WE, Broderick JB, and Hoffman BM (2002) J. Am. Chem. Soc. 124: 11270-11271.

Wang J, and Boisvert DC (2003) J Mol Biol 327: 843-855.

Wang SC, and Frey PA (2007) Biochemistry 46: 12889-12895.

Wei F-Y, Suzuki T, Watanabe S, Kimura S, Kaitsuka T, Fujimura A, Matsui H, Atta M, Michiue H, Fontecave M, Yamagata K, Suzuki T, and Tomizawa K (2011) J. Clin. Invest. 121: 3598-3608.

Wiig JA, Hu Y, Lee CC, and Ribbe MW (2012) Science 337: 1672-1675.

Wilson RH, and Evans HJ. (1968) In The Role of Potassium in Agriculture (Kilmer VJ, Younts SE, and Brady NC, Eds.), pp 189-202, ASA, CSSA, SSSA, Madison, WI.

Wong KK, Murray BW, Lewisch SA, Baxter MK, Ridky TW, Ulissi-DeMario L, and Kozarich JW (1993) Biochemistry 32: 14102-14110.

Xiao R, Anderson S, Aramini J, Belote R, Buchwald WA, Ciccosanti C, Conover K, Everett JK, Hamilton K, Huang YJ, Janjua H, Jiang M, Kornhaber GJ, Lee DY, Locke JY, Ma LC, Maglaqui M, Mao L, Mitra S, Patel D, Rossi P, Sahdev S, Sharma S, Shastry R, Swapna GV, Tong SN, Wang D, Wang H, Zhao L, Montelione GT, and Acton TB (2010) J. Struct. Biol. 172: 21-33.

Yan F, and Fujimori DG (2011) Proc. Natl. Acad. Sci. U.S.A. 108: 3930-3934.

Yan F, LaMarre JM, Rohrich R, Wiesner J, Jomaa H, Mankin AS, and Fujimori DG (2010) J. Am. Chem. Soc. 132: 3953-3964.

Yokoyama K, Numakura M, Kudo F, Ohmori D, and Eguchi T (2007) J. Am. Chem. Soc. 129: 15147-15155.

Zaccai G (2000) Science 288: 1604-1607.

Zappia V, Zydek-Cwick CR, and Schlenk F (1969) J. Biol. Chem. 244: 4499-4509.

Zeng W, Silvernail NJ, Scheidt WR, and Sage JT. (2008) In Encyclopedia of Inorganic Chemistry (Scott RA, and Lukehart CM, Eds.).

Zhang Y, Dougherty M, Downs DM, and Ealick SE (2004) Structure 12: 1809-1821.

Zhang Y, Zhu X, Torelli AT, Lee M, Dzikovski B, Koralewski RM, Wang E, Freed J, Krebs C, Ealick SE, and Lin H (2010) Nature 465: 891-896.

Zhu X, Dzikovski B, Su X, Torelli AT, Zhang Y, Ealick SE, Freed JH, and Lin H (2011) Mol. Biosyst. 7: 74-81.

APPENDIX A

SUPPORTING INFORMATION FOR CHAPTER 3

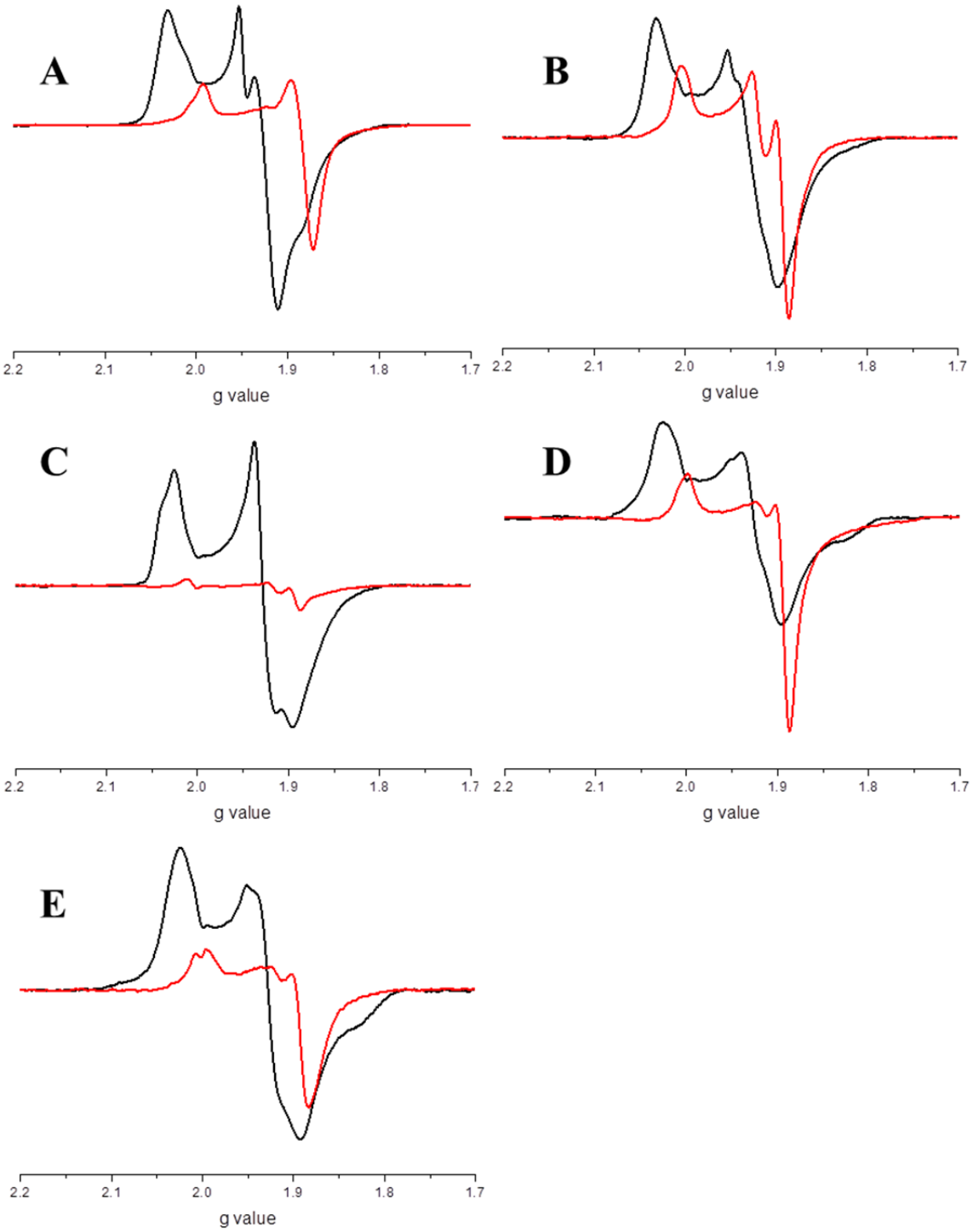

Figure S1. EPR spectra from Figure 3.7 shown with the cation with and without SAM overlaid. The black line represents the spectra of PFL-AE + cation and the red is PFL-AE + cation + SAM. The monovalent cations are (A) Na^+, (B) K^+, (C) NH_4^+, (D) Rb^+, and (E) Cs^+. The addition of SAM causes a decrease in signal intensity in all conditions.

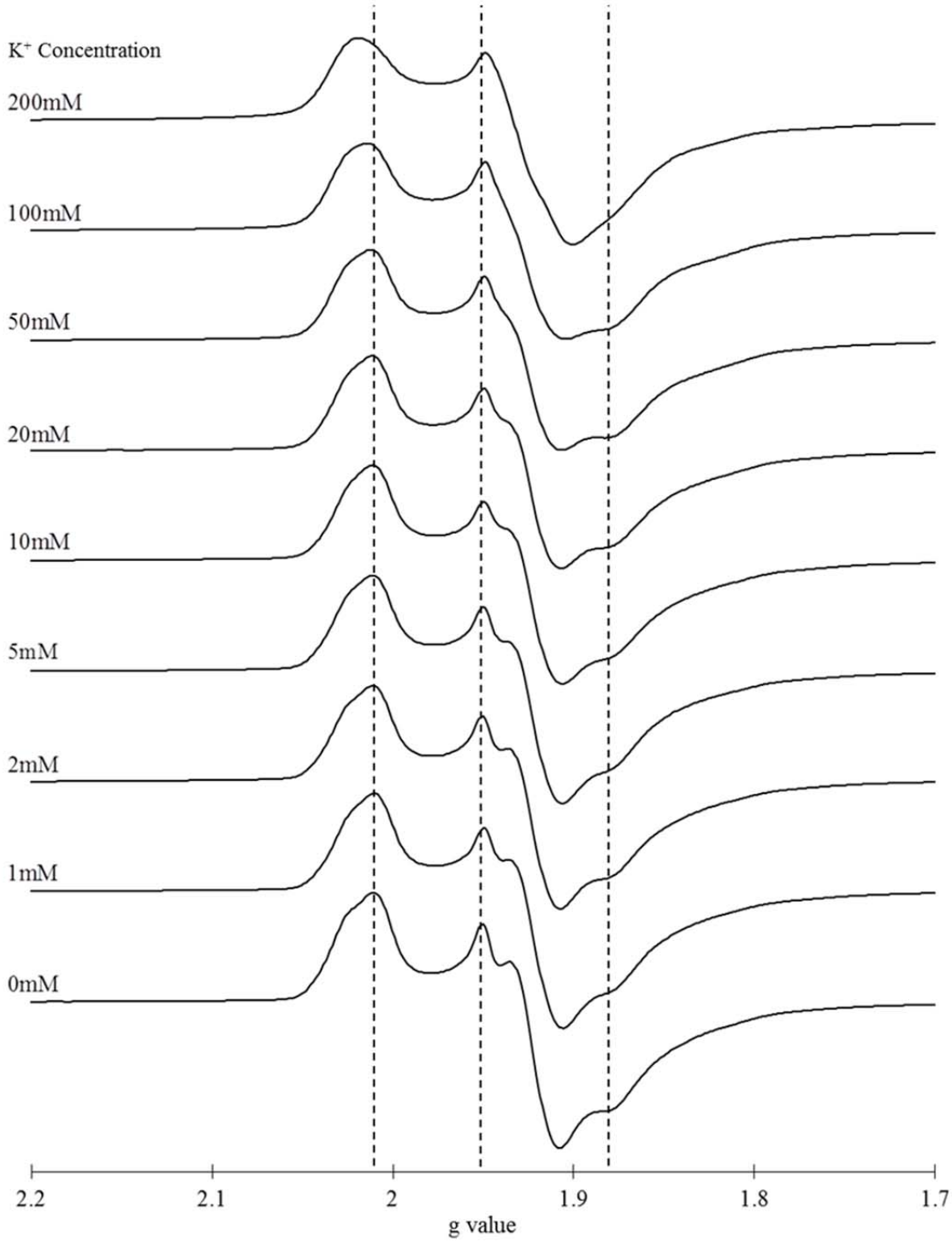

Figure S2. EPR spectra of 200 μM PFL-AE containing approximately 3.5 Fe per protein in the presence of different K^+ concentrations. The changes in intensity at different g values were not as drastic as when PFL-AE is in the presence of SAM as seen in Figure 3.8.